ABSTRACT

HOT-MELT MIXING OF PARTIALLY MISCIBLE ACTIVE PHARMACEUTICAL INGREDIENT-POLYMER MIXTURES

by
Min Yang

Solid dispersion/solution processes for producing pharmaceutical oral dosages such as hot-met extrusion (HME) have received increasing attention by industry and academe because they can enhance drugs' solubility and even bioavailability to a great extent by converting drugs from crystalline to amorphous form. HME can be carried out at two process temperature regimes: one where $T_{process} > T_m$ of the drug and the T_g of the polymer (or the T_m for the case of semi-crystalline polymers); the other at $T_m > T_{process} > T_g$ (T_m for the case of semi-crystalline polymer). Processing below the drug's melting point in the second case has the advantage of reducing potential for degradation.

Broader applications of HME are often limited by two technical challenges. One is that the active pharmaceutical ingredient (API) or the polymer may degrade at the elevated temperatures during extrusion processing. To avoid this problem and yet obtain a well-mixed solid dispersion/solution, HME needs to be carried out in an optimal processing window, where the temperature is kept safely below the degradation temperature but is high enough to enhance API's dissolution in the polymer. Another challenge is the possible physical instability of the extrudate during its shelf life. The API's solubility is decreased significantly once the temperature is dropped from the HME processing temperature to room temperature. As a result, the drug may recrystallize from the polymeric matrix. It is rather challenging to experimentally determine the API's solubility in the polymer and there are only few published articles in this area. In this

dissertation, solid dispersions of a model drug acetaminophen (APAP) and a pharmaceutical grade polymer poly(ethylene oxide) (PEO) were prepared by using hot-melt mixing (HMM), a process closely related to HME. APAP's solubility in PEO at HME processing temperature was measured utilizing a novel rheological characterization technique, hot-stage microscopy and differential scanning calorimetry (DSC). The results from the three methods were consistent and the solubility was found to increase from 14% at 80 ºC to 41% at 140 ºC. A "phase diagram" was constructed based on the experimental data and could be explored to design the HME process and formulation.

The apparent drug solubility at room temperature was estimated to be less than 10% via glass transition temperature (T_g) measurements using DSC and dynamic mechanical thermal analysis (DMTA), scanning electron microscopy (SEM), and X-ray diffraction (XRD). A model using the Flory-Huggins interaction parameter χ estimated from the "phase diagram" was utilized to predict the room temperature solubility. The drug's solubility in the amorphous portion of PEO was estimated to be 11.7% at 300 K. Since PEO is a semi-crystalline polymer with crystallinity of about 80%, the actual solubility is around 2.3%, consistent with apparent solubility estimation.

A new method to determine APAP's solubility at temperatures below the PEO's melting temperature was developed by observing the number of spherulitic nuclei, growth rate and the "quality" of the spherulites under polarized optical microscopy (POM). At 30 ^{o}C, the solubility was determined to be less than 1%, while at 50 ^{o}C the solubility was 10%. The nucleation constant K_g, fold surface free energy σ_e and work of chain folding q were calculated using the Hoffman-Lauritzen (HL) theory and it was found that the chain folding of PEO became more difficult in the presence of APAP.

HOT-MELT MIXING OF PARTIALLY MISCIBLE ACTIVE PHARMACEUTICAL INGREDIENT-POLYMER MIXTURES

by
Min Yang

A Dissertation
Submitted to the Faculty of
New Jersey Institute of Technology
in Partial Fulfillment of the Requirements for the Degree of
Doctor of Philosophy in Chemical Engineering

Otto H. York Department of Chemical, Biological and Pharmaceutical Engineering

January 2012

.

APPROVAL PAGE

HOT-MELT MIXING OF PARTIALLY MISCIBLE ACTIVE PHARMACEUTICAL INGREDIENT-POLYMER MIXTURES

Min Yang

Dr. Costas G. Gogos, Dissertation Co-Advisor — Date
Distinguished Research Professor of Chemical, Biological and Pharmaceutical Engineering, NJIT

Dr. Marino Xanthos, Dissertation Co-advisor — Date
Professor of Chemical, Biological and Pharmaceutical Engineering, NJIT

Dr. Peng Wang, Dissertation Co-advisor — Date
Assistant Professor of Chemical Engineering, University of Rhode Island

---

Dr. Laurent Simon, Committee Member — Date
Associate Professor of Chemical, Biological and Pharmaceutical Engineering, NJIT

Dr. Norman Loney, Committee Member — Date
Professor of Chemical, Biological and Pharmaceutical Engineering, NJIT

BIOGRAPHICAL SKETCH

Author: Min Yang

Degree: Doctor of Philosophy

Date: January 2012

Undergraduate and Graduate Education:

- Doctor of Philosophy in Chemical, Biological and Pharmaceutical Engineering, New Jersey Institute of Technology, Newark, NJ, 2011
- Master of Science in Chemical Engineering, Clarkson University, Potsdam, NY, 2007
- Bachelor of Science in Chemical Engineering, Tongji University, Shanghai, P. R. China, 2003

Major: Chemical Engineering

Presentations and Publications:

Min Yang, Peng Wang, Herman Suwardie, and Costas G. Gogos, "Determination of Acetaminophen's Solubility in Poly(ethylene oxide) by Rheological, Thermal and Microscopic Methods," International Journal of Pharmaceutics, 403, 83-89, 2011.

Min Yang, Peng Wang, Chien-Yeuh Huang, M. Sherry Ku, Huiju Liu, and Costas G. Gogos, "Solid Dispersion of Acetaminophen and Poly(ethylene oxide) Prepared by Hot-Melt Mixing," International Journal of Pharmaceutics, 395, 53-61, 2010.

Herman Suwardie, Peng Wang, David B. Todd, Viral Panchal, Min Yang, Costas G. Gogos, "Rheological Study of the Mixture of Acetaminophen and Poly(ethylene oxide) for Hot-melt Extrusion Application", European Journal of Pharmaceutics and Biopharmaceutics, 78, 506-512, 2011.

Min Yang, Peng Wang, Costas G. Gogos, "A New Systematic Methodology to Determine Drug's Solubility in Polymer", ANTEC™, Boston, MA, May 1-5, 2011.

Min Yang, Peng Wang, Costas G. Gogos, "Experimental Determination and Theoretical Prediction of Acetaminophen's Solubility in Poly(ethylene oxide)", APV Experts' Workshop on Hot-melt Extrusion and Its Use in the Manufacturing of Pharmaceutical Dosage Forms, Tarrytown, NY, April 12-13, 2011.

Min Yang, Firouz Asgarzadeh, Rima Jaber, Kathrin Nollenberger, Jian Li, Andreas Gryczke, "A Systematic and Predictive Approach for Formulation Development of Poorly Soluble Drugs via Solid Dispersions", AAPS, New Orleans, LA, Nov 14-18, 2010.

Min Yang, Peng Wang, Costas G. Gogos, "Crystallization of Acetaminophen-Incorporated Poly(ethylene oxide) Prepared by Hot-Melt Mixing", AAPS, New Orleans, LA, Nov 14-18, 2010.

Min Yang, Peng Wang, Costas G. Gogos, "Experimentally Determine the Phase Diagram of a Drug-Polymer Binary Mixture", AAPS, New Orleans, LA, Nov 14-18, 2010.

Min Yang, Herman Suwardie, Huiju Liu, Costas G. Gogos, Peng Wang, "Characterization of Drug-Polymer Mixtures", ANTEC^{TM}, Orlando, FL, May 16-20, 2010.

Min Yang, Peng Wang, Costas G. Gogos, "Solubility Prediction of Acetaminophen in Poly(ethylene oxide) by Utilizing Rheological, Microscopic and Thermal Analysis", ANTEC^{TM}, Orlando, FL, May 16-20, 2010.

Herman Suwardie, Min Yang, Peng Wang, Huiju Liu, Costas G. Gogos, "Rheological Study and Characterization of Acetaminophen and Poly(ethylene oxide) for Hot Melt Extrusion Process", ANTEC^{TM}, Orlando, FL, May 16-20, 2010.

Min Yang, Peng Wang, Costas G. Gogos, "Sustained-release and instant-release dosage forms prepared by hot-melt extrusion: solubility and stability", ISPE student poster contest, New Jersey chapter, April 26, 2010.

This dissertation is dedicated to my father, Guoqiang Yang, and my mother, Meili Chen, who always believe in me

ACKNOWLEDGMENT

The author would like to acknowledge Dr. Costas G. Gogos for both the research and life guidance. Dr. Gogos always encourages the students to read extensively in order to expand the knowledge and to discuss with people in order to solve questions and spark new ideas. He cultivates an innovative environment for any young scientists who are determined for academic achievement. Dr. Gogos is also very strict in science. Sometimes a little push helps a tremendous progress in research. Other times a small talk resolves the doubts in a young mind.

Details determine success. The author is very thankful to Dr. Peng Wang for spending so much time discussing data interpretation and paper writing. Dr. Wang is always patient and pays a great attention to details. He is also very generous in sharing new ideas, which really opens up the eyes of the students. The author went a long way from the first draft of a manuscript to all the published papers and conference presentations later on. Without the help and support of Dr. Wang, the author might not have been able to finish them all.

Dr. Marino Xanthos is acknowledged for his insightful discussions as well as his work in promoting hot-melt extrusion in the Society of Plastics Engineers. The author's work would not have been recognized in the polymer field without the strong recommendation of Dr. Xanthos. Dr. Xanthos is willing to listen to the students, which makes the tough PhD candidate life a little less lonely.

Dr. Laurent Simon and Dr. Norman Loney are thanked for their unique questions and suggestions on the dissertation proposal. The author is able to look at the same object from a different angle, thanks to both professors.

The author received support from the ongoing US Department of the Army, DAAE30-03-D1015 Advanced Cluster Energetics (ACE^{TM}) Program at New Jersey Institute of Technology (NJIT). This research was also partially supported by the National Science Foundation under Grant CMMI-0927142.

TABLE OF CONTENTS

TABLE OF CONTENTS
(Continued)

Chapter **Page**

TABLE OF CONTENTS
(Continued)

Chapter **Page**

LIST OF TABLES

LIST OF FIGURES

LIST OF FIGURES
(Continued)

Figure **Page**

LIST OF FIGURES
(Continued)

Figure **Page**

LIST OF FIGURES
(Continued)

Figure **Page**

LIST OF FIGURES
(Continued)

Figure **Page**

LIST OF FIGURES
(Continued)

Figure **Page**

LIST OF FIGURES
(Continued)

Figure **Page**

LIST OF FIGURES
(Continued)

Figure **Page**

LIST OF FIGURES
(Continued)

Figure **Page**

LIST OF SYMBOLS

®	Registered
$T_{process}$	Process Temperature of HME/HMM
T_g	Glass Transition Temperature
T_m	Melting Temperature
T_m^{mix}	Melting Temperature of Drug-Polymer Mixture
T_c	Crystallization Temperature in Isothermal DSC
T_x	Crystallization Temperature in POM
T_m^0	Equilibrium Melting Temperature
T_{cp}	Crystallization Temperature in Non-isothermal DSC
ΔG_m	Gibbs Free Energy of Mixing
ΔS	Mixing Entropy
ΔH	Mixing Enthalpy
$\dot{\gamma}$	Shear Rate
γ	Shear Strain
η	Viscosity
τ	Shear Stress
E	Modulus
δ	Phase Angle
ω	Frequency of Strain Oscillation
a	Activity Coefficient

LIST OF SYMBOLS
(Continued)

R	Universal Gas Constant
C_p	Heat Capacity
Φ	Volume Fraction
χ	Flory-Huggins Interaction Parameter
m	Molar Volume Ratio
x	Saturation Mole Fraction
N	Number of Moles
n’	Exponent in Dissolution Power Law Expression
m’	Diffusion Exponent
G	Spherulite Growth Rate
U^*	Activation Energy
k_g	Nucleation Constant
f	Temperature Correction Factor
σ_e	Surface Free Fold Energy
K	Boltzmann Constant
a_0	Stem Width
γ'	Lamellar Thickness Factor
n	Avrami Exponent
q	Work of Chain Folding
A	Molecular Cross-sectional Area

CHAPTER 1

INTRODUCTION

1.1 Background Information

One of the major challenges for the pharmaceutical industry is that more than 40% of marketed drugs are poorly water soluble[1] while the percentage of insoluble newly developed chemical entities in pharmaceutical chemical laboratories is up to 60% of the total.[2] As a result, solid dispersion technologies such as hot-met extrusion (HME) and spray drying have become more popular because they can enhance the drugs' solubility and even bioavailability to a great extent by converting drugs from crystalline to amorphous solution form.[3-5] An example of solubility enhancement is given in Figure 1.1, which shows the improvement of piroxicam dissolution rate after the spray-drying process.[6] Plasma concentration of a drug substance in beagle dogs demonstrates significant increase after hot-melt extrusion process (Figure 1.2).[7]

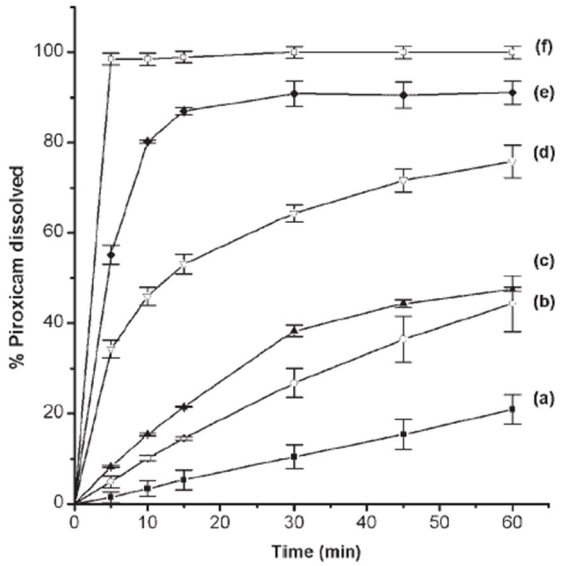

Figure 1.1 Dissolution profiles of (a) Piroxicam, (d) physical mixtures of piroxicam and PVP K25 (1:4), (e) spray-dried solid dispersion of piroxicam and PVP K25 (1:4).[6]

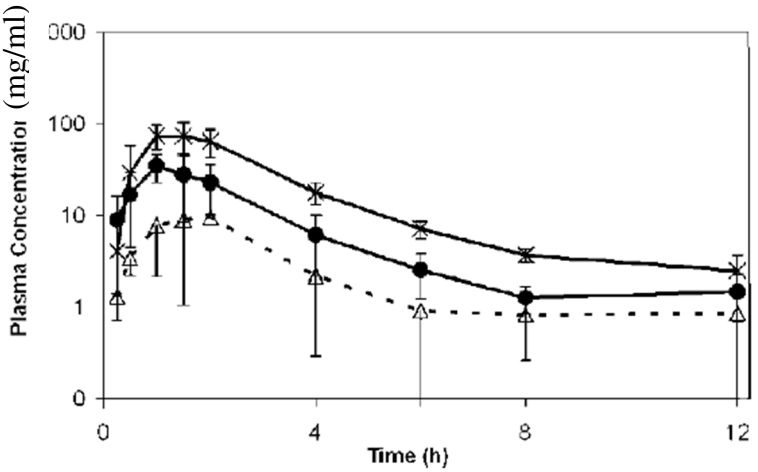

Figure 1.2 Mean plasma concentrations in dogs (n=4) after oral administration of 50 mg capsules. The samples from top to bottom are 20% melt-extruded drug-PVP K30 solid dispersion, 30% melt-extruded drug-PVP K30 solid dispersion and 20% crystalline drug triturated with 80% poloxamer 188 that served as the control.[7]

Chiou and Riegelman have defined solid dispersion as "a dispersion of one or more active ingredients in an inert carrier at the solid state, prepared by the melting, the solvent or the melting solvent method".[8] Formulation of poorly soluble compounds as solid dispersions might lead to particle size reduction, improved wetting, reduced agglomeration, changes in the physical state of the drug and desirably dispersion on a molecular level, according to the physical state of the solid dispersion. Nowadays, the term solid dispersion is mostly linked to glass solutions of poorly soluble compounds, using amorphous carriers with high glass transition temperatures. There are a large variety of pharmaceutically approved polymers available for solid dispersion purpose, including polyvinylpyrrolidone (PVP)[9, 10] and its co-polymers poly(ethylene-co-vinylacetate) (PVP/VA),[11, 12] polyethylene oxide (PEO),[13, 14] hydroxypropyl methylcellulose acetate succinate (HPMCAS),[15, 16] hydroxypropyl methylcellulose (HPMC),[17] acrylates[18, 19] etc. A list of carriers used for hot-melt extrusion dosage forms was summarized by Crowley et al. in the review paper (Table 1.1).[20]

Table 1.1 Carriers Used to Prepare Hot-melt Extrusion Dosage Forms[20]

Chemical Name	Trade Name	T_g (^oC)	T_m (^oC)
Ammonio methacrylate copolymer	Eudragit® RS/RL	64	-
Poly(dimethylaminoethylmethacrylate-co-methacrylic esters)	Eudragit® E	50	-
Poly(methyl acrylate-co-methyl methacrylate-co-methacrylic acid)	Eudragit® 4135F	48	-
Poly(methacrylic acid-co-methyl methacrylate) 1:2	Eudragit® S	160	-
Hydroxypropyl cellulose	Klucel®	130	-
Ethyl cellulose	Ethocel®	133	-
Cellulose acetate butyrate	CAB 381-0.5	125	157
Cellulose Acetate Phthalate	-	165	192
Poly(ethylene oxide)	Polyox® WSR	-67	65-80
Poly(ethylene glycol)	Carbowax®	-20	37-63
Poly(vinyl pyrrolidone)	Kollidon®	168	-
Poly(vinyl acetate)	Sentry® plus	35-40	-
Hydroxypropyl methylcellulose phthalate	-	137	150
Polyvinylpyrrolidone-co-vinyl acetate	Kollidon® VA64	-	-
Hydroxypropyl Methylcellulose	Methocel®	175	-
Hydroxypropyl Methylcellulose Acetate Succinate	Aqoat-AS®	-	-
Poly(lactide-co-glycolide)	PLGA	-	-
Polyvinyl Alcohol	Elvanol®	-	-
Chitosan Lactate	Sea-Cure®	-	-
Pectin	Obipektin®	-	-
Carbomer	Carbopol® 974P	-	-
Polycarbophil	Noveon® AA-1	-	-
Poly(ethylene-co-vinyl acetate)	Elvax® 40W	-36	45
Polyethylene	-	-125	140
Poly(vinyl acetate-co-methacrylic acid)	CIBA-I	-	84-145
Epoxy resin containing secondary amine	CIBA HI	80-100	-
Polycaprolactone	-	-	-
Carnauba Wax	-	-	82-85
Ethylene-vinyl acetate copolymer	Evatane®	-	-
Glyceryl Palmitostearate	Precirol® ATO 5	-	52-55
Hydrogenated Castor & Soybean Oil	Sterotex® K	-	-
Microcrystalline Wax	Lunacera®Paracera®	-	-
Corn Starch	-	-	-
Maltodextrin	-	-	-
Pregelatinized Starch	-	-	-
Isomalt	Palatinit®	-	145-150
Potato Starch	-	-	-
Citric Acid	-	-	153
Sodium Bicarbonate	-	-	-
Methacrylic acid copolymer type C	Eudragit® L100-55	-	104.4
Chitosan	-	203	-
Xanthan gum	-	-	-
Agar	-	-	-
Povidone	Plasdone® S-30	-	-
Lactose	-	-	201
Microcrystalline cellulose	Avicel® PH 101	-	-
Dibasic calcium phophate	Emcompress®		-

Recently, some new solid dispersion formulations have entered the market (Table 1.2): Kaletra (Abbott), Intelence (Tibotec), Certican (Novartis), Isoptin SR-E (Abbott), Nivadil, Prograf (Fujisawa Pharmaceutical Co., Ltd) and Rezulin (Sankyo). All of these new formulations utilize amorphous polymers as a carrier. A particular type of solid dispersion is solid solution, where the API is dispersed on a molecular level in the amorphous polymer.

Table 1.2 Examples of Commercially Available Solid Dispersions[21]

Brand Name	Manufacturer	Drug	Carrier
Gris-PEG	Pedinol Pharmacal Inc.	Griseofulvin	PEG6000
Cesamet	Valeant Pharmaceuticals	Nabilone	PVP
Kaletra	Abbott	Lopinavir, ritonavir	PVPVA (Copovidone)
Sporanox	Jassen Pharmaceutica	Itraconazole	HPMC
Intelence	Tibotec	Etravirin	HPMC
Certican	Novartis	Everolimus	HPMC
Isoptin SR-E	Abbott	Verapamil	HPC/HPMC
Nivadil	Fujisawa Pharmaceutical Co., Ltd	Nivaldipine	HPMC
Prograf	Fujisawa Pharmaceutical Co., Ltd	Tacrolimus	HPMC
Rezulin	Developed by Sankyo, manufactured by Parke-Davis division of Warner-Lambert	Troglitazone	PVP

HPC, hydroxypropyl cellulose

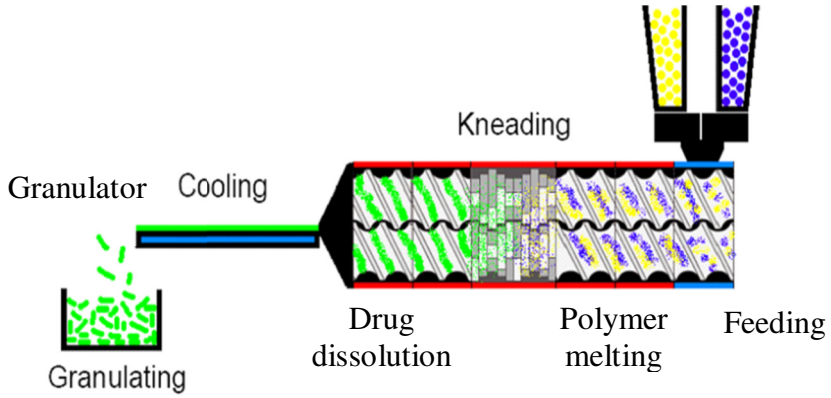

Figure 1.3 Schematic diagram of twin-screw extrusion followed by granulation.[22]

1.2 Mixing, Processing Temperature and Additives

Hot-melt extrusion (HME) is a process that involves mixing an active pharmaceutical ingredient (API) particulate with a molten, water soluble polymeric excipient in processing machines with one or more rotating screws. Figure 1.3 is a schematic diagram of twin-screw extrusion. As compared to spray drying (Figure 1.4), HME has the advantage of being continuous, solvent free, and easy to scale up. There are basically two laminar flow mixing mechanisms in the extrusion process.[23] The first is dispersive mixing, which involves the reduction of the size of a component having cohesive character, within the continuous molten excipient phase. The component in HME may be solid agglomerate if the processing temperature is below the melting point of the API, or a dispersed liquid phase if the processing temperature is above the melting point of the API. The cohesive character of the agglomerate is due to van der Waals forces between the particles of the agglomerate, to the surface tension and elastic properties of the liquid droplets, and to the surface tension of the gaseous bubbles. The second is distributive mixing of components through flow, which stretches the interfacial area elements between the components lacking a cohesive character and distributes them throughout the volume. In distributive mixing, one not only needs to stretch the interfacial area, but also to reorient it for effective mixing, as well as to randomize the interfacial elements throughout the volume. The mechanisms of mixing of miscible and immiscible liquids are depicted in Figure 1.5, and that of hard solid agglomerates with liquids in Figure 1.6. In the former, elongational and shear stretching is the dominant mechanism, while in the latter, shear stress dominates.

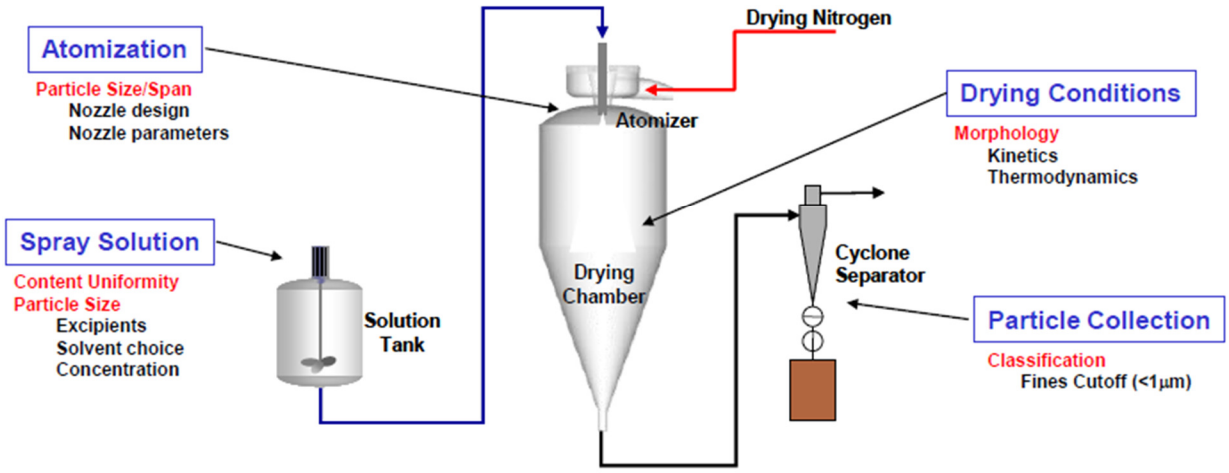

Figure 1.4 Schematic diagram of a spray-drying process.[24]

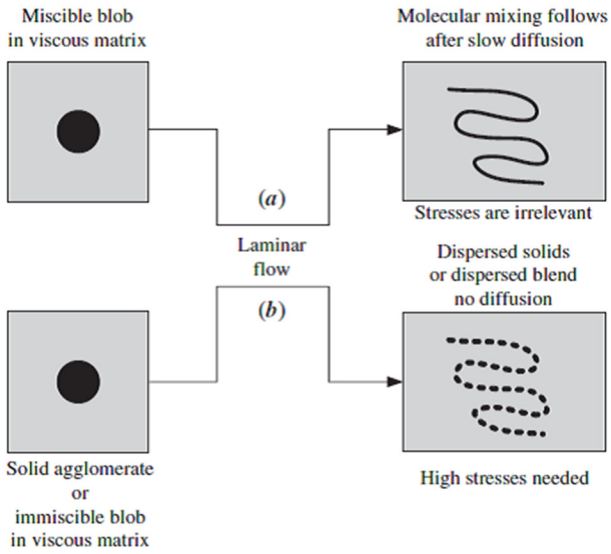

Figure 1.5 Schematic representation of (a) laminar distributive mixing where the miscible blob is stretched and deformed and distributed throughout the volume; (b) shows the same process as (a) but with an immiscible liquid where the stretching leads to a breakup process.[23]

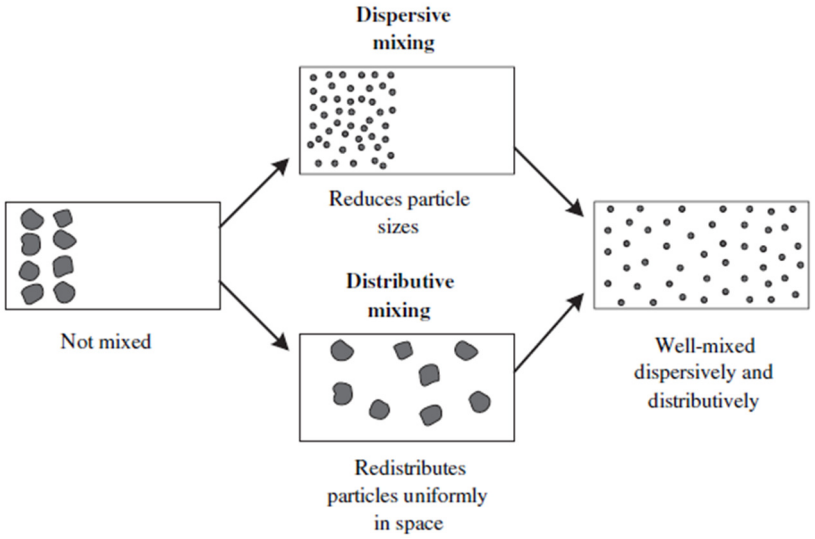

Figure 1.6 Dispersive mixing of hard solid agglomerates with liquids that, after breakup, are distributed throughout the volume.[23]

As mentioned above, the HME process can be conducted in two temperature regimes: one where $T_{process} > T_m$ of the drug and the T_g of the polymer (or the T_m of the polymer for the case of semi-crystalline polymers); the other is $T_m > T_{process} > T_g$ (or the T_m of the polymer for the case of semi-crystalline polymers). The first case is illustrated as Figure 1.5 and the second case is illustrated in more details as Figure 1.7. After the drug and polymer particles are fed into an extruder or a batch mixer, the polymer starts to melt due to the conductive heat from the barrel, and the frictional and plastic energy dissipation, resulting in a suspension with drug particles.[19] If the drug exhibits enhanced solubility in the water soluble polymeric excipient at the elevated processing temperature of the HME process, then the suspended API crystals will begin to dissolve. A dissolved liquid API layer is formed at the surface of the crystalline API. That layer is wiped away by the laminar flow of the HME process, promoting faster dissolution as the old polymer is replaced by fresh polymer melt. The drug molecules diffuse into the polymer melt via

the boundary layer, and the size of the suspended particles diminishes until the particles dissolved completely.

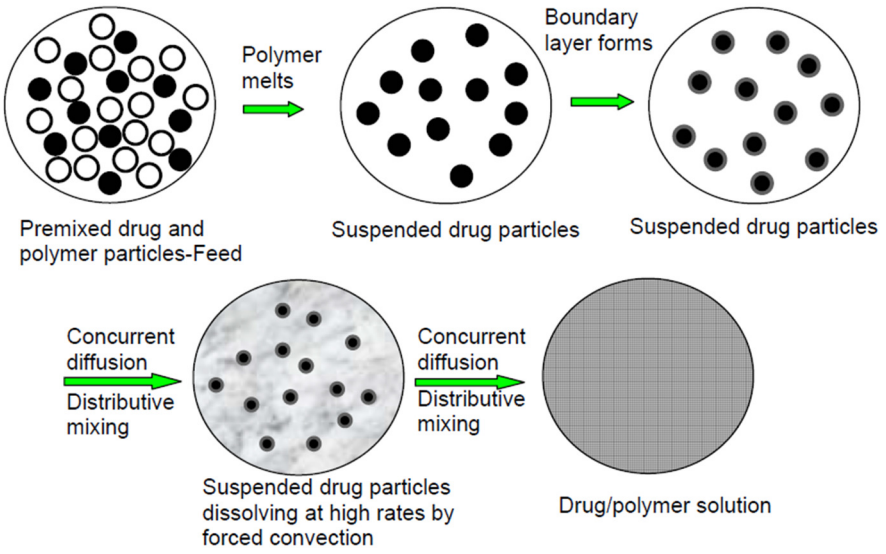

Figure 1.7 Schematic representation of the morphological changes of the drug and polymer system in the solution formation process.[19]

There are many literature papers that used the first case processing temperatures ($T_{process} > T_m$ and T_g).[25-29] The four heating zones in the twin-screw extruder that Patterson et al. used for carbamazepine (T_m of 190 °C) and PVP/VA 64 (T_g of 107 °C) or PVP/VA 37 (T_g of 55 °C) (1:2 w/w) are 80-100 °C (throat), 188 °C, 185 °C and 185 °C.[30] They used the zone temperatures 80-100 °C, 167 °C, 162 °C, 162 °C for dipyridamole (T_m of 163 °C) and polymers. All products were extruded at approximately 10 rpm. Qi et al. extruded felodipine (T_m of 145 °C) with Eudragit® E PO (T_g of 50 °C) at 160 °C and screw speed of 100 rpm.[31] Generally speaking, the risk of degradation is higher in the first case considering that many APIs have very high T_m. Processing below the APIs' melting temperatures in the second case above has the obvious advantage of reducing the potential for degradation. Albers et al. extruded celecoxib (T_m of 162 °C) with Eudragit® E PO (1:1 w/w) and found that the extrudates changed from opaque to transparent when

the processing temperature increased from 152 to 157 ^{o}C, indicating the complete dissolution of crystalline drug at higher processing temperature.[18] Nevertheless, 157 ^{o}C was still 5 ^{o}C below the drug's melting point. Besides, one could lower the temperature even more for smaller drug loading samples. DiNunzio et al. were able to achieve amorphous dispersion of hydrocortisone (T_m of 218 ^{o}C) in PVP/VA 64 (1:9 w/w) at the extrusion temperature of 160 ^{o}C.[12] Qi et al. extruded acetaminophen (T_m of 170 ^{o}C) with Eudragit® E PO at 140 ^{o}C with the speed of 200 rpm.[32] The extrudate strands produced containing 10% of API were clear while the strands produced containing 20% were opaque. When $T_{process} < T_m$ of the drug, drug's solubility at that temperature determines if one can achieve a miscible melt-mixed product. The solubility topic will be discussed in more details below.

Sometimes it is unavoidable to use plasticizers in order to reduce the T_g of a polymer (if $T_{degradation} < T_g$), and therefore reduce the extrusion processing temperatures. Plasticizers also lower the melt viscosity and thus, lower the shear forces needed to extrude a polymer, thereby improving the process of certain high molecular weight (high viscosity) polymers.[33, 34] Plasticization of the polymer is generally attributed to the intermolecular secondary forces between the plasticizer and the polymer. The free volume between polymer chains is increased by plasticizers, which leads to T_g and melt viscosity reduction. Plasticizers used for pharmaceutical dosage forms must have good stability, polymer-plasticizer compatibility and permanence, avoiding shelf life migration.[20] Triethyl citrate (TEC),[35-37] and low molecular weight polyethylene glycols[34, 38, 39] are the common plasticizers used for pharmaceutical extrusion. The physical and mechanical properties and drug release rate of pharmaceutical dosage forms

are dependent on the permanence of the plasticizers. Permanence of a plasticizer during processing and storage is very important and the evaporation of highly volatile plasticizers from the dosage form during storage has been studied and reported. Repka and McGinity demonstrated that the amount of plasticizer remaining in hot-melt extruded films over time was a function of the plasticizer type and storage conditions.[34] In transdermal films, the addition of a plasticizer can improve the film's flexibility.[34] It is interesting that several drug substances have been reported to function as plasticizers in the hot-melt extrusion process.[40-42] CO_2 has been injected into the extruder at supercritical pressures, dissolved in the melt, and used as a temporary plasticizer in the HME.[43] At the die of the extruder, expansion occurs to atmospheric pressure which results in a transformation of CO_2 to the gaseous phase. As a consequence, CO_2 escapes from the extrudate and is not present in the final product.

The elevated temperatures needed to process unplasticized or plasticized polymers may lead to polymer degradation. The stability of polymers that are susceptible to degradation can be improved with the addition of antioxidants, acid receptors and or light absorbers during HME. One manufacturer of these materials recommends the incorporation of an antioxidant into formulations containing low molecular weight hydroxypropylcellulose.[44] Similarly, poly(ethylene oxide) has been reported to be protected from free radical and oxidative degradation by the incorporation of one or more antioxidants.[45] This will be discussed in greater detail in the next chapter on material properties.

Antioxidants are classified as preventive antioxidants or chain-breaking antioxidants based upon their mechanism. Preventive antioxidants include materials that

act to prevent initiation of free radical chain reactions. Reducing agents, such as ascorbic acid, are able to interfere with autoxidation in a preventive manner since they preferentially undergo oxidation. The preferential oxidation of reducing agents protects drugs and polymers from attack by oxygen molecules. These antioxidants are sometimes referred to as oxygen scavengers. They are most effective when used in a closed system where oxygen cannot be replaced once it is consumed. Chelating agents such as edetate disodium (EDTA) and citric acid are another type of preventive antioxidant that decrease the rate of free radical formation by forming a stable complex with metal ions that catalyze these reduction reactions.[20]

Hindered phenols and aromatic amines are the two major groups of chain breaking antioxidants that inhibit free radical chain reactions. Commonly used antioxidants such as butylated hydroxyanisole, butylated hydroxytoluene and vitamin E are hindered phenols. Because the O-H bonds of phenols and the N-H bonds of aromatic amines are very weak, the rate of oxidation is generally higher with the antioxidant than with the polymer. Other materials have been used to facilitate HME processing. Waxy materials like glyceryl monostearate have been reported to function as a thermal lubricant during hot-melt processing. Vitamin E TPGS has been reported to plasticize polymers and enhance drug absorption.[45, 46]

The efficiency of the HME process does not depend only on the API and polymer material properties mentioned above. It also depends on extruder design variables and process variables, such as screw rpm, barrel set temperature profiles, residence time distribution and flow rate. Researchers have used very low rotating speeds such as 10 rpm[30] to high speeds such as 200 rpm[32], all of which worked well for the particular

materials processed. Qian et al. extruded a model drug (T_m of 160 ^oC) with PVP/VA 64 (T_g of 107 ^oC) (4:6 w/w) at 150 ^oC, and they compared the speed between 50 and 225 rpm.[47] A micro phase-separation of the drug and polymer was observed under the Raman mapping after the samples were stored for 2 months (Figure 1.8). Liu et al. melt-mixed indomethacin (T_m of 163 ^oC) and Eudagit® E PO (T_g of 53 ^oC) (3:7 w/w) at different rotating speed and temperatures.[19] It was found that at 140 ^oC, indomethacin was able to totally dissolve in E PO at 20 rpm. At 100 and 110 ^oC, however, a screw speed of 100 rpm was needed for a full dissolution. In the work of this dissertation, only the results from 50 rpm are presented. The reason is that when $T_{process} > T_m^{mix}$ (drug's dissolution temperature, details will be discussed in Chapter 3.1), melt-mixed samples were transparent, indicating the drug was well-mixed and completely dissolved in the polymer. The other reason why only one rotating speed was used in this dissertation is that for the particular API-excipient system, acetaminophen and poly(ethylene oxide), material properties are the main determining factor on miscibility and shelf-life stability. The processing conditions are far less important compared to the thermodynamics of mixing and therefore, the focus is placed on the latter.

In practice, the mean residence time in the twin-screw extruder ranges from one to 10 minutes.[48-50] It is desirable to shorten the residence time during processing to reduce the risk of degradation.[12] A long residence time of 10 minutes was used in this work for sample preparation to secure a well-mixed, homogeneous and dissolved state.

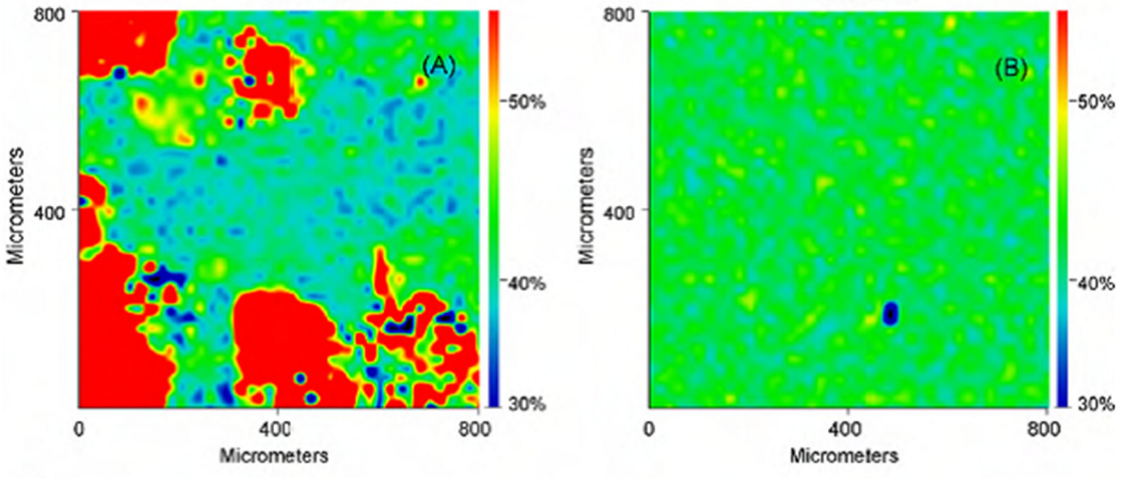

Figure 1.8 Raman mapping of drug-PVP/VA processed at (a) 50 rpm; and (b) 225 rpm. Red color represents higher concentration of the model drug.[47]

1.3 Challenges of HME

Solid dispersions/solutions with a wide range of API release profiles can be manufactured via HME, considering the richness of the polymer chemistry and the powerful mixing and shaping capability of the extrusion process. A new graft copolymer Soluplus® has been developed specifically for the purpose of pharmaceutical HME.[51] Besides instant-release oral formulations,[10, 18, 19, 52, 53] HME-prepared solid dispersions/solutions can also be used as sustained-release oral formulations,[33, 54-57] biodegradable implants,[58] and mucoadhesive films.[38, 59, 60] With the same formulation, the release rate of chlorpheniramine maleate (CPM) is lower for HME samples as compared to powder compressed samples (Figure 1.9).[61]

Although the extrusion technology has been realized by the pharmaceutical industry since 1971 (Figure 1.10), broader applications of HME are often limited by two common technical challenges. One is that the APIs may degrade at the elevated processing temperatures during the extrusion process. To avoid this problem and yet

obtain a well-mixed dispersion of API and polymer, the extrusion needs to be carried out in an optimal processing window, where the temperature is kept safely below the API's degradation temperature and kept in the HME equipment for a short time. Another challenge is the potential physical instablility of extrudate during its shelf life, which involves the API's recrystallization from the amorphous solid solution achieved at the $T_{process}$ through HME. The API's solubility can decrease significantly once the temperature is dropped from the HME processing temperature to the storage temperature, e.g., ambient temperature. As a result, the API may phase separate from the polymeric matrix and recrystallize.[47, 62] Different strategies can be applied to address this issue depending on the specific application and the material system. One common way to prevent recrystallization is to select a suitable polymer for a given API.[9, 63-65] However, considerable development time is needed to identify the appropriate formulations experimentally. Other methods such as utilizing polymer blends[66, 67] and additives[68] might also help to inhibit API's recrystallization.

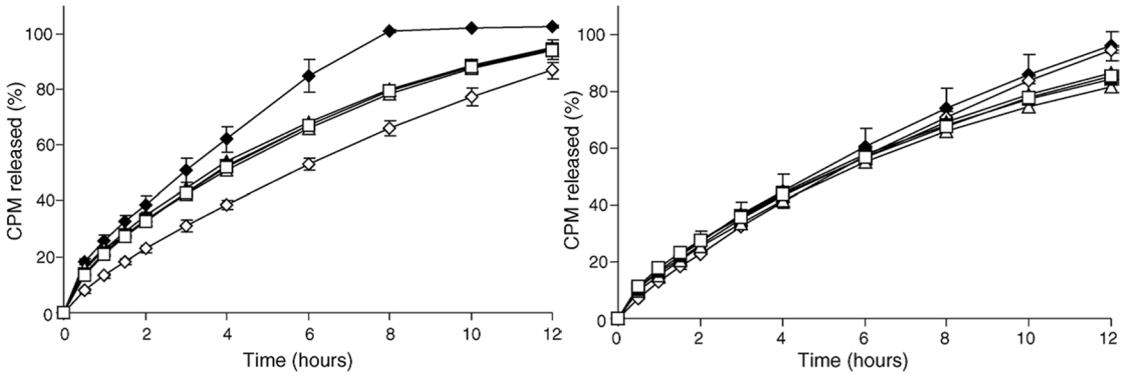

Figure 1.9 Chlorpheniramine maleate (CPM) release profiles from directly compressed (left) and HME (right) samples in 900 ml of 0.1N HCl (♦), pH 4.0 acetate buffer (◊), pH 4.0 citrate buffer (▲), pH 4.0 phosphate buffer (Δ), pH 6.8 phosphate buffer (■) and pH 7.4 phosphate buffer (□).[61]

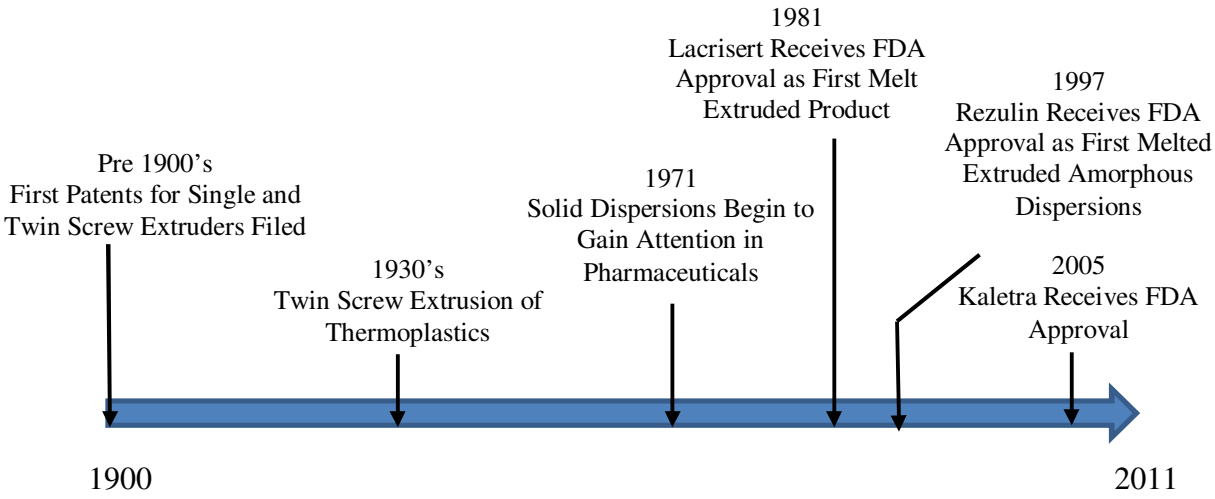

Figure 1.10 Historical perspective of pharmaceutical hot-melt extrusion.[69]

To address the aforementioned two challenges, it is critical to determine experimentally the API's solubility in a polymeric excipient at both processing and storage temperatures. There are very few publications devoted to such solubility studies, all of which utilized only amorphous polymers with high glass transition temperature (T_g) such as PVP, PVP/VA, PVAc (polyvinyl acetate) and Eudragit® E.[70-74] API-polymer powder mixtures were heated at very slow rates using a differential scanning calorimeter (DSC) to determine the depressed melting points (T_m^{mix}) of the APIs. Phase diagrams were plotted between the T_g of the polymer and the melting point (T_m) of the pure API, from which the API's solubility at HME processing temperature could be read (Figure 1.11-1.13). The method requires an "appreciable" thermal effect associated with the API dissolution process in order to determine T_m^{mix}. None of the studies provide direct experimental data regarding the solubility in highly viscous PVP and PVP/VA at room temperature. The difficulty lies in the fact that the kinetics of reaching the drug-polymer equilibrium are extremely slow.

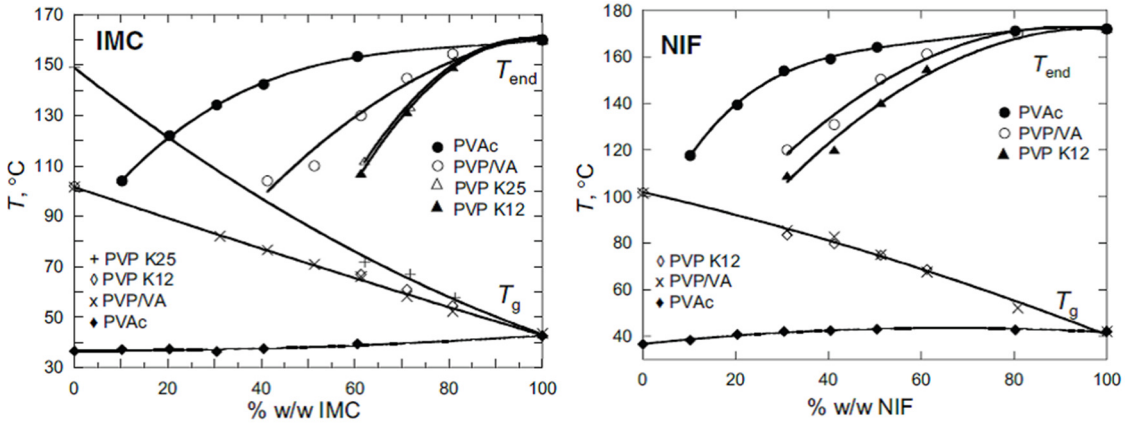

Figure 1.11 Melting point (T_{end}) and glass transition (T_g) of (a) indomethacin (IMC) and (b) nifedipine (NIF) - polymer mixtures at various drug loading.[70]

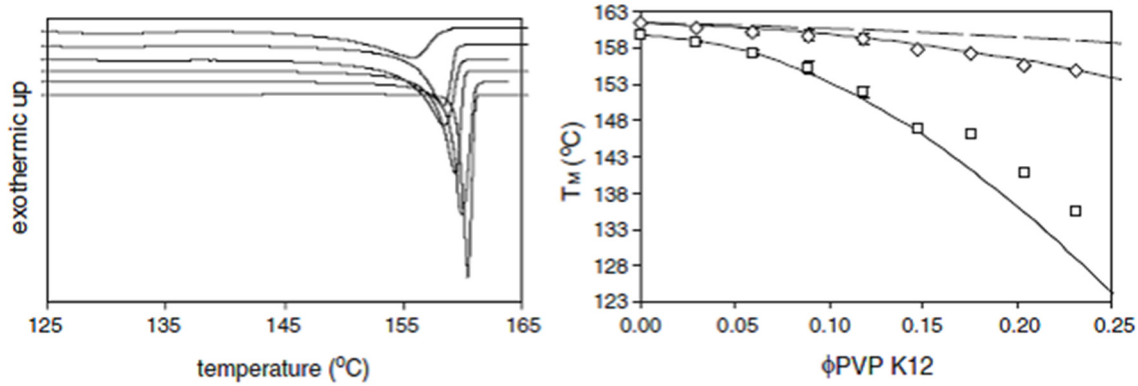

Figure 1.12 DSC thermograms of physical mixtures of indomethacin with increasing volume fraction of PVP K12 measured at a heating rate of 1 °C/minute. Onset of the melting (□), offset of melting (◊) and predicted melting point depression for an athermal mixture (enthalpy of mixing ΔH is zero, dashed line).[71]

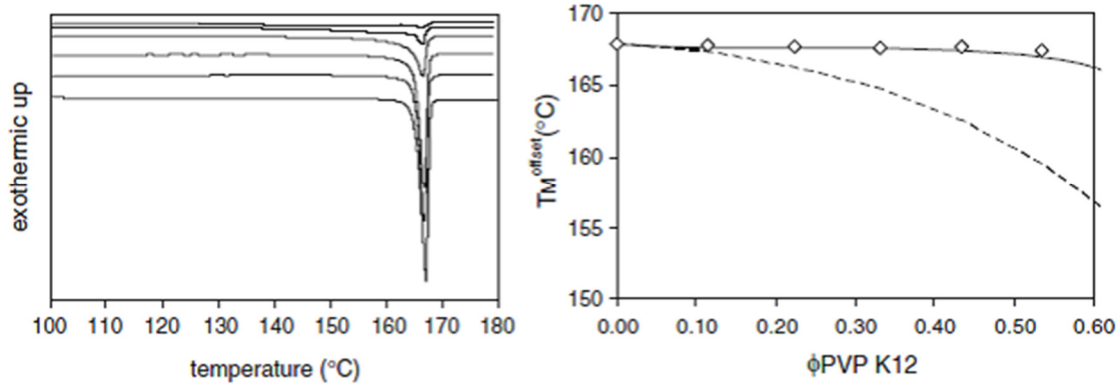

Figure 1.13 DSC thermograms of physical mixtures of itraconazole with increasing volume fraction of Eudragit® E measured at a heating rate of 1 °C/minute. Onset of the melting (□), offset of melting (◊) and predicted melting point depression for an athermal mixture (enthalpy of mixing ΔH is zero, dashed line).[71]

A more fundamental understanding of the miscibility of API-polymer mixtures is much needed for the pharmaceutical industry to embrace solid dispersion/solution technologies such as HME. Theoretically, the miscibility of any two components is governed by their Gibbs free energy of mixing (ΔG_m).

$$\Delta G_m = \Delta H - T\Delta S \quad (1.1)$$

The entropy of mixing (ΔS) is usually larger than zero and favors the mixing. Negative enthalpy of mixing ΔH is beneficial for miscibility and solid dispersion stabilization.[65, 75-77] ΔS is represented by the molecule size difference between the API and the polymer. The larger the difference is, the larger the ΔS. ΔH is represented by the intermolecular interaction between API and the polymer. The stronger the interaction is, the more negative the ΔH. The entropic and enthalpic effects on ΔG_m will be discussed in greater detail in Chapter 4.3.3. Based on this simple understanding of the thermodynamics, much effort has been devoted to understand the role of API-polymer molecular interactions and how they affect the drug's solubility in the polymer and its stability. However, beyond the above basic understanding, very limited literature references have discussed theoretical methods that can be applied to predict API's solubility in polymers and the stability of the solid dispersions/solutions. The studies that determined the APIs' phase diagram at high temperatures use the Flory-Huggins model to calculate APIs' activities or solubilities in polymers with the interaction parameter χ estimated from the melting point depression.[70-74] Theoretical treatment of polymer solutions was initiated independently by Flory[78] and Huggins[79] in 1942. The Flory-Huggins theory is based on the lattice model shown in Figure 1.14. In the case of the low molecular weight solvent (Figure 1.14a), it is assumed that the solute and solvent

molecules have roughly the same volumes, each occupies one lattice site. With the polymeric solvent, Figure 1.14b, a segment of the polymer molecule has the same volume as a solute molecule and also occupies one lattice site.

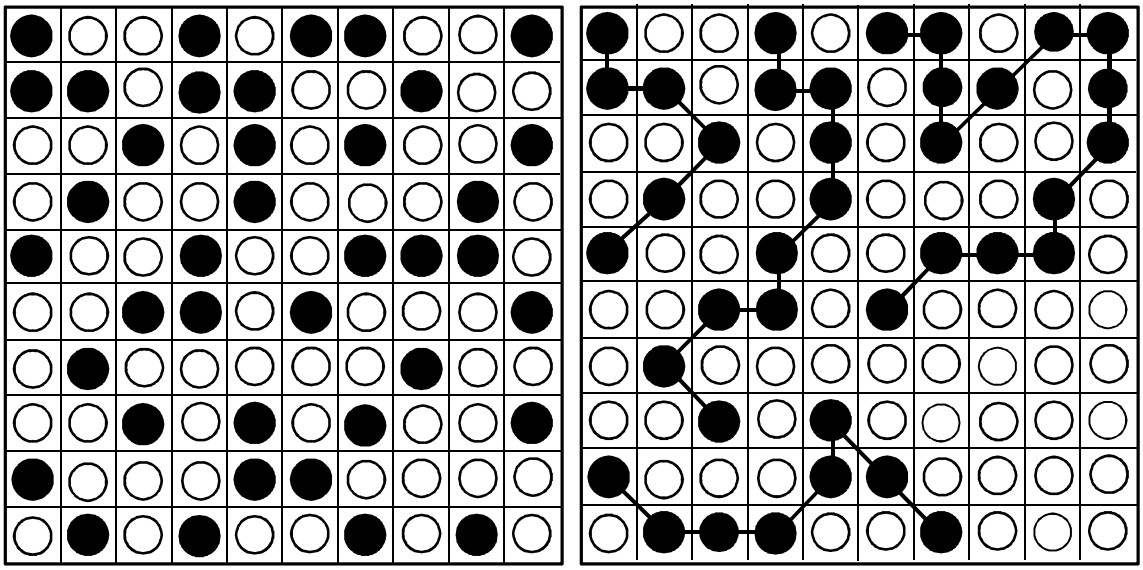

(a) (b)

Figure 1.14 Lattice model of solubility: (a) low molecular weight solvent; (b) polymeric solvent. ○, Solute; ●, Solvent.

By statistically evaluating the number of arrangements possible on the lattice, Flory and Huggins obtained an expression for the entropy of mixing in forming a solution from N_1 moles of solute and N_2 moles of solvent:

$$\Delta S = -R(N_1 \ln \phi_1 + N_2 \ln \phi_2) \tag{1.2}$$

where the φ_1 and φ_2 are volume fractions of solute and solvent, respectively.

An expression for the enthalpy of mixing was obtained by considering the change in the adjacent-neighbor (molecules or segments) interactions on the lattice:

$$\Delta H = RT\chi N_1 \varphi_2 \tag{1.3}$$

where χ is the Flory-Huggins interaction parameter.

The activity coefficient of a drug in a polymer a_1 is expressed as

$$\ln a_1 = \ln \frac{\phi_1}{x_1} + (1 - \frac{1}{m})\phi_2 + \chi\phi_2^2 \qquad (1.4)$$

where ϕ_1 is the volume fraction of the drug, ϕ_2 is the volume fraction of the polymer, m is the molar volume ratio of a polymer molecule to a drug molecule, and χ is the Flory-Huggins interaction parameter. The theoretical background on how to calculate activity and solubility can be found in Chapter 4.3.1.

It was found that the model fits reasonably well the activities of indomethacin and nifedipine dissolved in PVP, PVP/VA and polyvinyl acetate (PVAc) (Figure 1.15), but works poorly with D-mannitol in PVP.[70] Two studies conducted by the same group show that often predicted drug solubility in PVP and its derivatives is lower than the experimentally obtained values.[71, 73] To explain the discrepancy, the authors postulated that the kinetic factor also contributes to the inhibition of drug recrystallization, which is not included in the Flory-Huggins model.

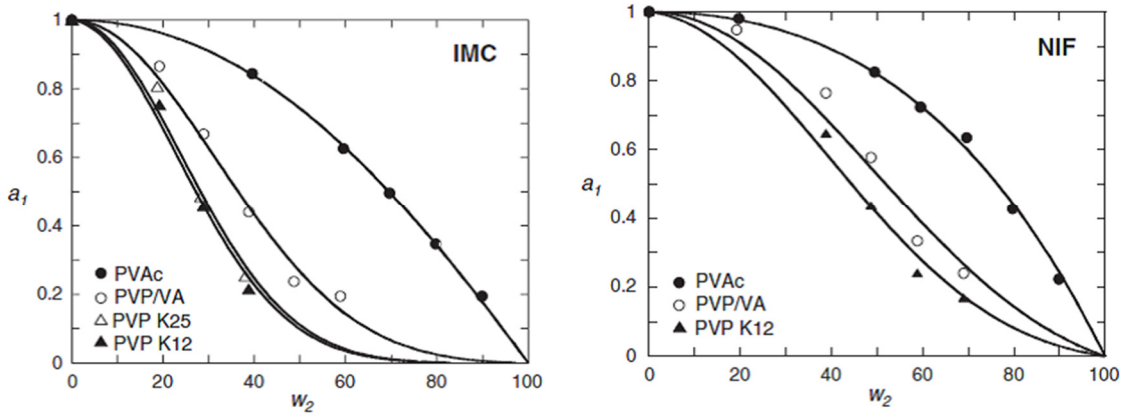

Figure 1.15 Activity a_1 of (a) indomethacin (IMC) and (b) nifedipine (NIF) versus polymer weight fraction w_2. The solid curves are Flory-Huggins predictions.[70]

1.4 Semi-crystalline Polymers

All previous literature studies address only few selected amorphous polymers. Not only it is necessary to test the melting point depression methodology on more polymers to understand its applicability, it is also of considerable fundamental and practical interest to find out whether this widely used model can be used to understand the drug's solubility in semi-crystalline polymers. This is a more complicated topic because true solutions are formed between the API and the molten polymer (above T_m^{mix}), and during cooling of the extrudate the dissolved API may interfere with the polymer chain folding involved in the crystallization process.

Semi-crystalline polymers such as poly(lactic acid) (PLA), poly(vinylidene fluoride) (PVDF) and poly(ester amide) (PEA) are often used in medical devices and biodegradable implants.[80-82] Poly(ethylene oxide)s (PEOs) with molecular weight (MW) of 1,500-20,000 g/mol, often referred as polyethylene glycol (PEG), are widely used for the preparation of oral solid dispersions for dissolution rate and bioavailability improvement.[14, 83, 84] High MW (>100,000 g/mol) PEOs, on the other hand, are often chosen for the HME process because of their broad processing window[13] and they have been used in applications such as sustained-release matrix systems, transdermal drug delivery systems, and mucosal bioadhesives.[33, 38, 59, 67] In semi-crystalline polymers, drug diffusion can be hindered due to the presence of crystallites.[85] The volume fraction and the size of the crystallites may affect the diffusion coefficient, and the influence of these parameters is expressed in terms of tortuosity factors.[86-88]

The semi-crystalline polymer excipient used in this thesis is a relatively high MW PEO, exhibiting spherulitic morphology under normal quenching. The crystallization of

PEO,[89-93] its blends with other polymers,[94-99] nanocomposites[100, 101] and block copolymers[102] has been extensively studied over the past decades. In the miscible blend system of poly(acetoxystyrene)(PAS)/PEO, the presence of the amorphous PAS phase reduced the spherulitic growth rate of PEO (Figure 1.16).[94] The crystallization ability of PEO increased with increasing PAS content as indicated by the decreasing nucleation constant k_g and surface free energy of the chain folding of PEO σ_e. Details on how to measure these kinetic parameters can be found in Chapter 4.5.1. In other miscible blend systems, however, the crystallization rate of PEO was found to decrease more significantly in the presence of strongly interacting polymers as compared to weakly interacting polymers.[95, 99] Figure 1.17 demonstrates that at the same crystallization temperature, PEO blends with the strongly interacting random copolymers of ethylene and methacrylic acid (EMAA, 55wt% acid units) and styrene and hydroxystyrene (SHS, 50wt% hydroxystyrene) crystallize much slower than PEO blends with weakly interacting poly(methyl methacrylate) (PMMA).[95] The long period of PEO, which is the sum of the thickness of the crystalline lamellae and amorphous layer, increased by 2-4 nm for the PMMA/PEO blends, an effect associated with interlamellar diluent placement. In the immiscible poly(ε-caprolactone) (PCL)/PEO blends, where both polymers are semicrystalline, the crystallization rate of PEO decreased with increasing amount of PCL.[97] The authors considered the slow-down of the crystallization rate to be caused by the physical restriction to the growth of crystalline PCL domains. In the silica-PEO nanocomposite system, the distribution of particle spacings in the semicrystalline state is always significantly broader than in the melt, even though the mean particle spacing is unchanged.[100] At low silica loading (<20 wt%), the crystallization polymer chains

"force" the nanoparticles "defects" out of their way to crystallize in a minimally perturbed form (Figure 1.18). Reversible de-intercalation and intercalation processes were detected in PEO-Cloisite 15A (material properties will be discussed in Chapter 2.3) nanocomposites during secondary crystallization and subsequent melting of the secondary crystals (Figure 1.19).[101]

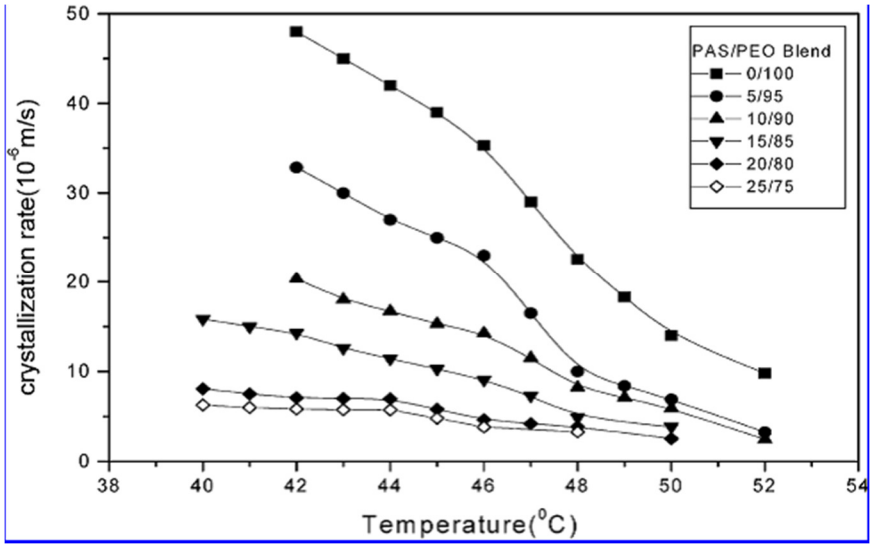

Figure 1.16 Spherulite growth rate (G) as a function of crystallization temperature (T_c) for PAS/PEO blends.[94]

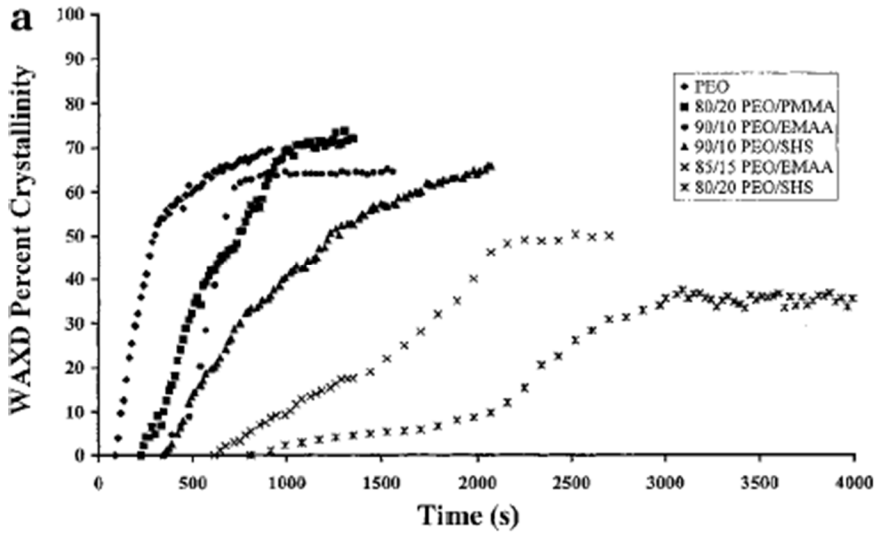

Figure 1.17 Wide angle X-ray diffraction (WAXD) measured crystallinity as a function of crystallization time for PEO and blends crystallized at 48 ^{o}C.[95]

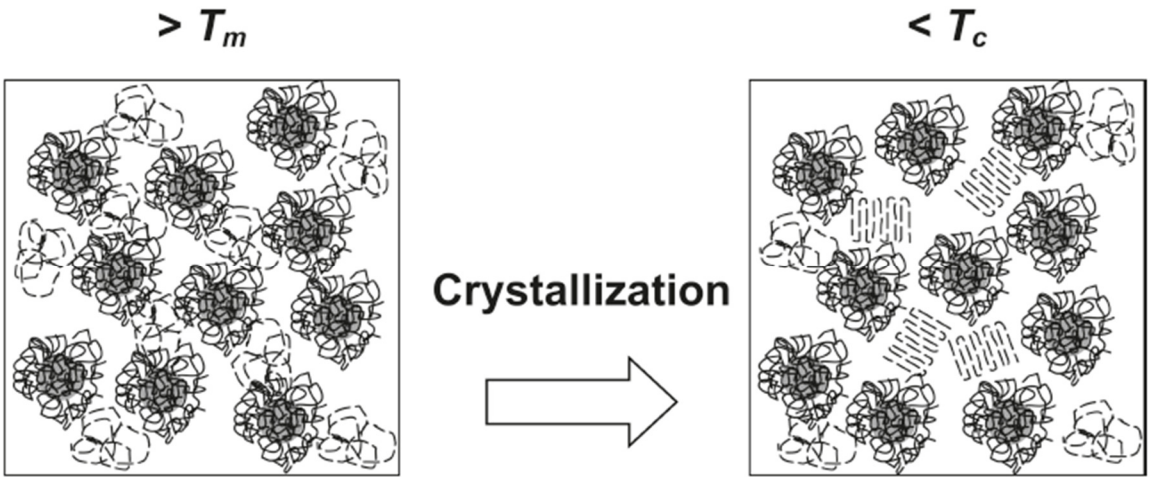

Figure 1.18 Crystallization in the presence of brush-coated nanoparticles. In well-dispersed nanocomposites, the growing lamellae can maneuver the nanoparticles, thereby broadening interstitials to allow bulk-like lamellae to form.[100]

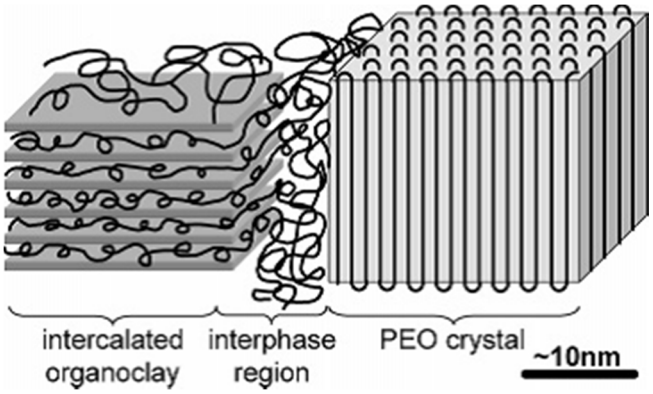

Figure 1.19 Schematic representation of the morphology in the PEO/Cloisite® 15A nanocomposite after PEO primary crystallization.[101]

The drug-PEO system studied in this thesis is more complicated than the miscible polymer blends, immiscible blends and nanocomposite systems. The drug's physical state, size, and miscibility with PEO, all play important roles in PEO's crystalline morphology, spherulite growth rate, and nucleation. One may be able to determine the APIs' solubility by observing the morphological change, spherulitic growth rate and number of nuclei.

CHAPTER 2

MATERIALS

2.1 Acetaminophen

Acetaminophen (APAP), also called paracetamol, is the active ingredient in Tylenol® (Figure 2.1). It is used to relieve mild to moderate pain from headaches, muscle aches, menstrual periods, colds and sore throats, toothaches, backaches, and reactions to vaccinations (shots), and to reduce fever. Acetaminophen may also be used to relieve the pain of osteoarthritis (arthritis caused by the breakdown of the lining of the joints). Acetaminophen is in a class of medications called analgesics (pain relievers) and antipyretics (fever reducers). It works by changing the way the body senses pain and by cooling the body.[103] When taken at recommended doses, APAP has an excellent safety profile, notably lacking the gastrointestinal (GI) side effects of aspirin and ibuprofen.[104] However, acute overdosaging with acetaminophen, whether accidental or deliberate, is relatively common and can be very serious. Ingestion of 10-15 g of acetaminophen by adults can cause severe hepatocellular necrosis and doses of 20-25 g are potentially fatal.[74, 105]

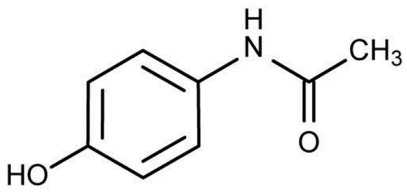

Figure 2.1 Chemical structure of acetaminophen.

Crystalline APAP has two common polymorphs, which are the monoclinic (form I)[106] and the orthorhombic (form II).[107] Monoclinic APAP is thermodynamically more stable at room temperature with respect to the orthorhombic modification.[108] The APAP synthesized by the manufacturers is in form I. Form II was shown to be more soluble[109] and directly compressible into tablets.[110] Despite considerable effort by researchers, its production in pure form from solution has remained elusive.[111] Figure 2.2 shows microscope pictures of monoclinic and orthorhombic APAP growing from different polymer solutions.[112] Their X-ray diffraction (XRD) patterns also exhibit distinct differences shown in Figure 2.3.[112] The melting point of the monoclinic form is 170 ºC and of the orthorhombic form is 158 ºC based on the DSC results (Figure 2.4). The raw crystalline and the recrystallized APAP in this thesis is in the monoclinic form and therefore the polymorphism will not be further discussed.

Figure 2.2 Monoclinic APAP growing from beads of butyl methacrylate/isobutyl methacrylate copolymer (left); and orthorhombic APAP growing from powdered poly(tetrafluoroethylene) (right).[112]

Raw acetaminophen was purchased from Spectrum Chemicals (Gardena, CA) and was used without further purification. It is a white powder and the crystals are of rod shape, with the length of one particle about 100 μm (Figure 2.5a). Since the particles are quite brittle, the powder also includes a significant amount of fine particles, ~5 μm in size

(Figure 2.5b). The molecular weight of APAP is 151.19 g/mol and the density is 1.293 g/cm^3. The glass transition temperature of amorphous acetaminophen is 24.5 ºC (Figure 2.6).

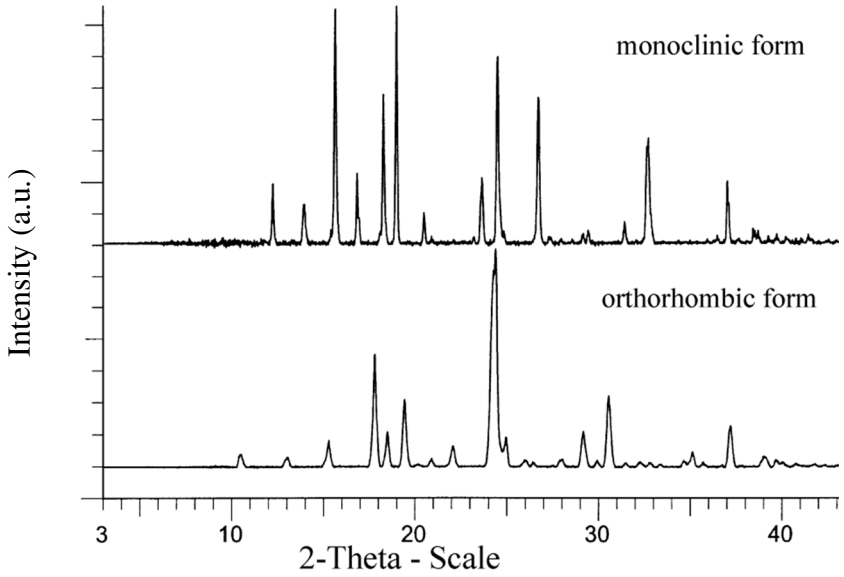

Figure 2.3 Powder X-ray diffraction (XRD) patterns of APAP polymorphs grown from aqueous solution.[112]

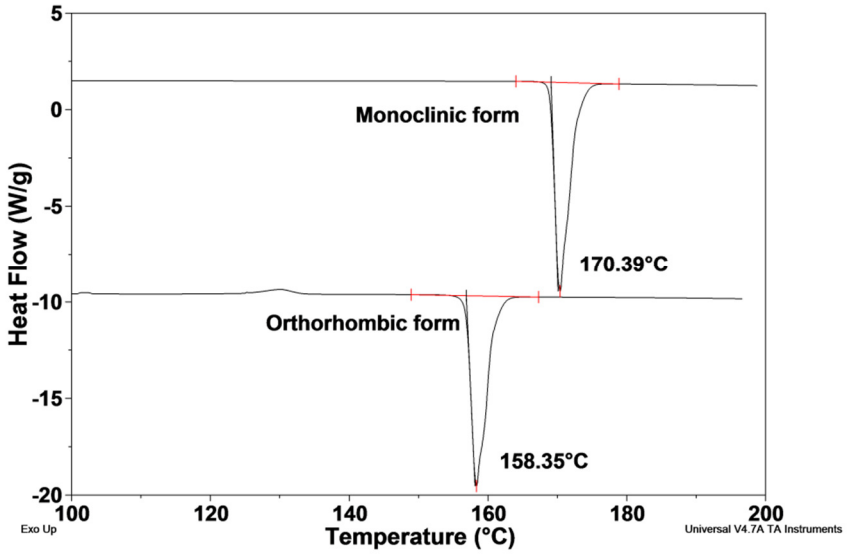

Figure 2.4 Melting peaks of monoclinic (top) and orthorhombic (bottom) acetaminophen in DSC at a heating rate of 10 ºC/minute.

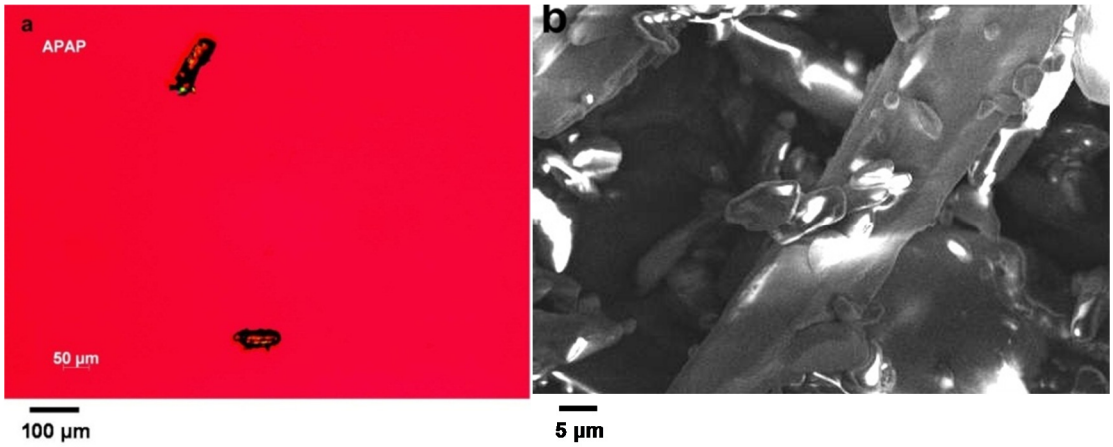

Figure 2.5 APAP particles under (a) polarized microscope, and (b) scanning electron microscope (SEM).

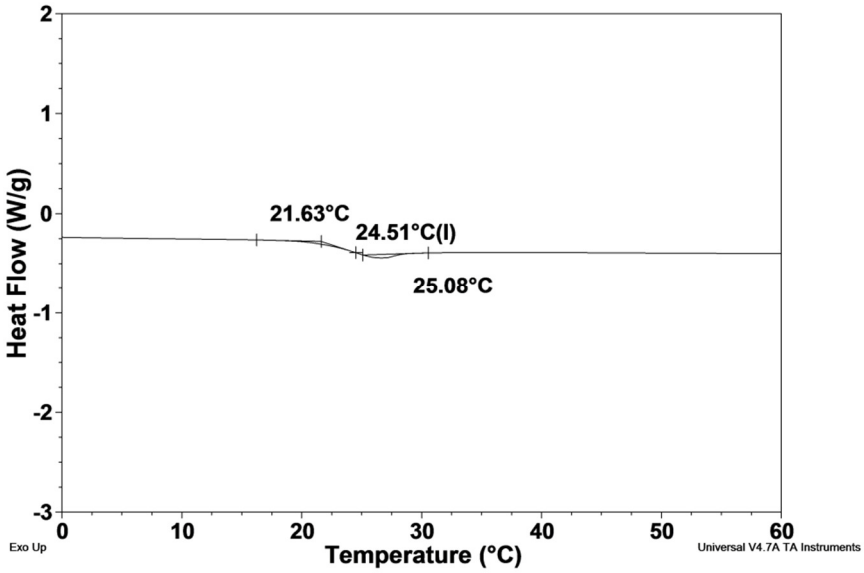

Figure 2.6 Glass transition of amorphous APAP determined from 2nd heating of crystalline APAP in DSC.

APAP's solubility in water is 14.9 mg/g at 25 ºC[113] and 23.7 mg/g at 37 ºC.[114] According to the biopharmaceutical classification system (BCS),[115] acetaminophen is a BCS class III drug,[116] which has high solubility in the aqueous medias over the pH range of 1 to 7.5 but low intestinal permeability. Grattan et al. showed that the addition of sodium bicarbonate to APAP formulation produced a faster and higher peak

concentration in plasma even though the dissolution profiles were similar.[117] This example shows that even though formulation change may seem completely innocuous, it may very well alter the plasma profile if the new excipient alters GI physiology.

Thermogravimetric analysis (TGA) of APAP was performed in air and N_2 environments (Figure 2.7). Degradation onsets of the two curves are very close, and APAP is thermally stable until 177 ^{o}C (higher than its T_m of 170 ^{o}C) in N_2 environment. The hot-melt mixing temperature of 120 ^{o}C used in this thesis (Chapter 3.1) is well below the 177 ^{o}C and, thus, safe for APAP processing.

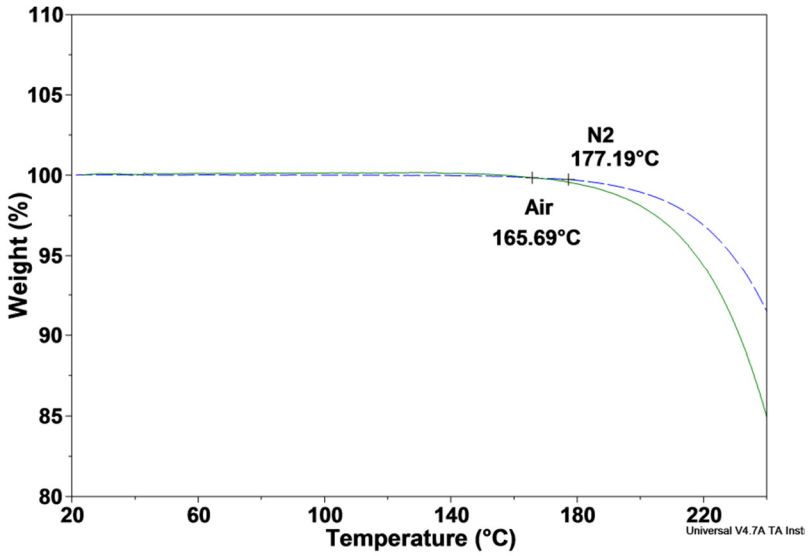

Figure 2.7 Weight loss of APAP during TGA at 10 ^{o}C/minute heating rate in air (solid) and N_2 (dashed).

2.2 Poly(ethylene oxide)

Poly(ethylene oxide) (PEO) is a semi-crystalline polymer and is often chosen as the solid dispersion excipient for HME because of its broad processing window.[13] Polyethylene glycols (PEGs) with molecular weight of 1,500-20,000 g/mol, which are smaller molecular weight analogues but have the same molecular structure as PEO (Figure 2.8),

are often used for the preparation of oral solid dispersion for dissolution rate and bioavailability improvement.[14, 83, 84] PEG 300 (MW of 280-320 g/mol) and PEG 400 (MW of 380-420 g/mol) are widely used in injectable formulations when pH adjustment alone is insufficient in achieving the desired solution concentrations.[118] High MW PEO has been used in applications such as sustained-release matrix systems, transdermal drug delivery systems, and mucosal bioadhesives.[33, 38, 59, 67] The influence of PEO molecular weight on the dissolution profiles are illustrated in Figure 2.9, showing that the drug release rate is slower by using higher MW PEO.[56] The PEO used in this thesis is in powder form and is kindly donated by the Dow Chemical Co. (Midland, MI). It is a POLYOX^{TM} Water-Soluble resin and is a nonionic polymer. The company markets different PEO grades with molecular weights ranging from 100,000 to about 8,000,000 g/mol. WSR N10 is the one used in this thesis, whose weight average molecular weight M_w is 100,000 g/mol and its density ρ is 1.13 g/cm^3.

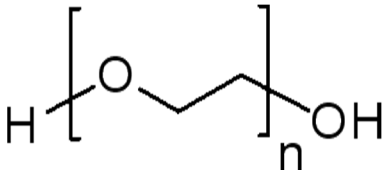

Figure 2.8 Chemical structure of PEO.

The melting and glass transition temperatures of PEO are 62.5 ºC (Figure 2.10) and -56.6 ^{o}C (Figure 2.11), respectively. The degree of crystallinity is about 80%, based on the heat of fusion of the "perfectly" 100% crystalline PEO being 203 J/g.[119] TGA of PEO was performed in air and N_2 environments (Figure 2.12). Unlike APAP, PEO is susceptible to oxidation as well as thermal degradation and its weight loss in air is much

more severe than that in N_2. To prevent PEO from such degradation, N_2 purge was used during the hot-melt mixing in this work (Chapter 3.1).

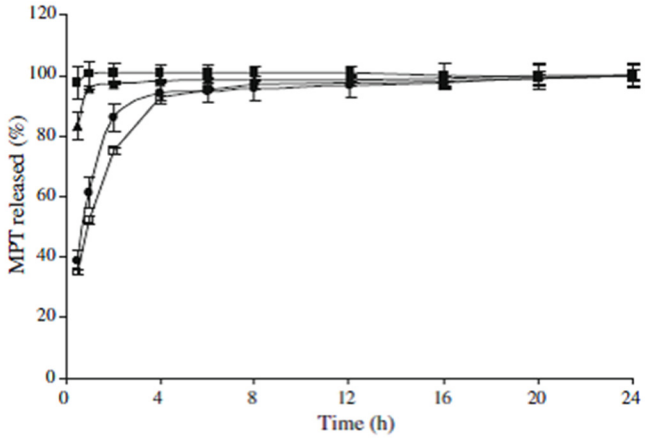

Figure 2.9 Dissolution profiles of hot-melt extruded mini-matrices containing 30% metroprolol tartrate (MPT) and 70% hydrophilic polymer: PEG 6000 (■), PEO 100,000 (▲), PEO 1,000,000 (●) and PEO 7,000,000 (□).[56]

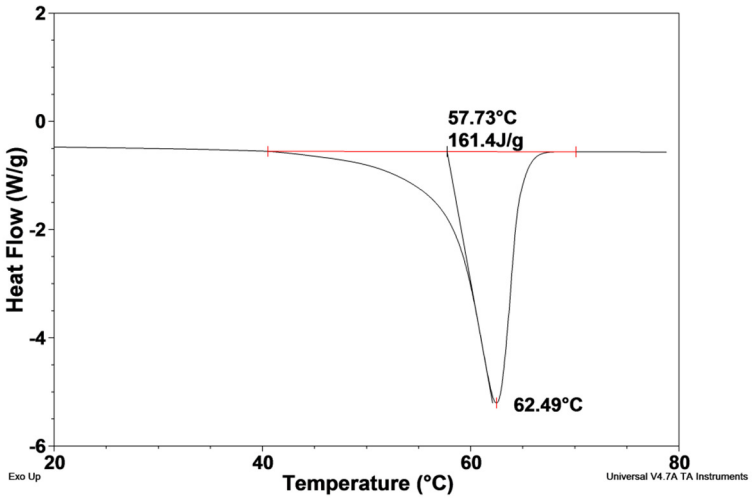

Figure 2.10 Melting peak and heat of fusion of PEO N10 in DSC at heating rate of 10 ºC/minute.

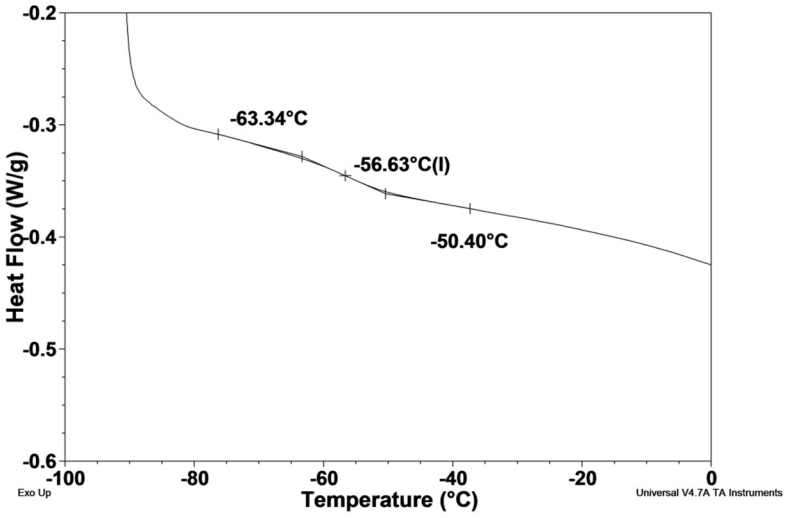

Figure 2.11 Glass transition of amorphous PEO N10 in DSC at a heating rate of 10 ºC/minute.

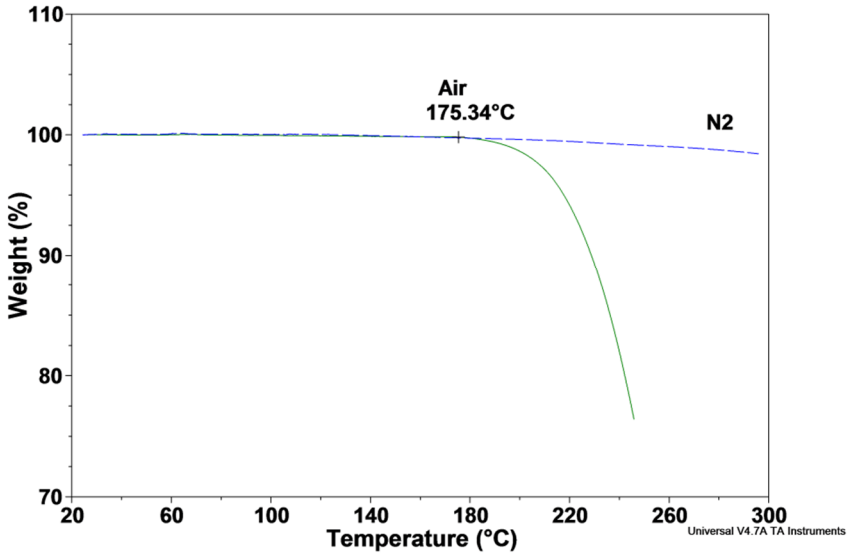

Figure 2.12 Weight loss of PEO during TGA at 10 ^{o}C/minute heating rate in air (solid) and N_2 (dashed).

The oxidative degradation of powdered PEO resin was studied by Scheirs et al.[120] Powdered PEO readily oxidizes under mild ageing conditions (60°C) owing to its large surface area, its weak crystalline lattice and the weak carbon-oxygen bonds in its backbone. As a result, its physical properties deteriorate after an induction period of

about 23 days and, in the extreme cases, the free-flowing powder is transformed into a soft wax. With increasing oxidation, there is also a pronounced change in the morphology of PEO from a spherulitic to an axialitic structure. This transition is due to oxidatively induced changes in molecular weight and dispersity that affect the crystallization conditions. The emergence of multiple DSC melting peaks after oxidation indicates that a number of low-melting, low-molecular-weight fractions are formed as a result of chain scission processes. Such degradation was not observed in the current study because all powdered PEO was stored in a sealed container at room temperature, supported by the evidence of a single DSC melting peak (Figure 2.10) and the fact that the powder remained free-flowing. N_2 purge was used during hot-melt mixing (HMM) to reduce the chance of oxidation degradation. The morphology of quenched HMM-prepared PEO is spherulitic with spherulite size, depending on crystallization temperature T_c, as large as 1mm, indicating a pure, not degraded sample (Figure 2.13). In practice, antioxidants such as Vitamin E and its derivatives, Vitamin C (ascorbic acid) and butylated hydroxyanisole (BHA) have been used in pharmaceutical preparations and these compounds have been found to suppress free radical production in photoirradiated phenol-melamine.[121]

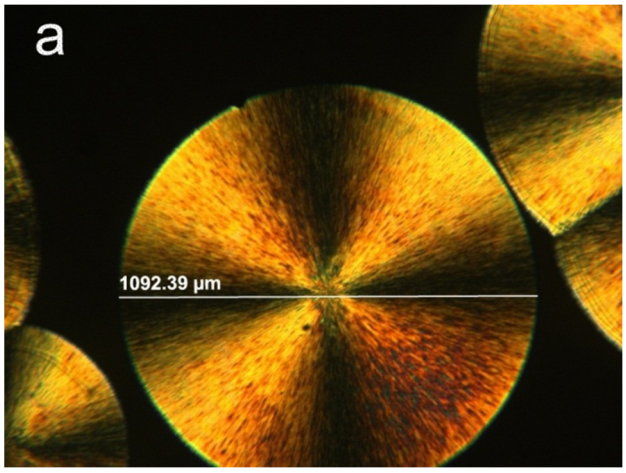

Figure 2.13 Typical polarized micrographs of PEO spherulites.

2.3 Nanoclays

Two commercial nanoclays, Cloisite® 15A and 30B were received as samples from Southern Clay Products (Gonzales, TX). Cloisite® 15A is a natural montmorillonite (MMT) modified with dimethyl, dehydrogenated tallow and quaternary ammonium cations, while Cloisite® 30B is a montmorillonite modified with bis-(2-hydroxyethyl) methyl tallowalkyl ammonium cations (Figure 2.14). Cloisite® nanoclays are surface treated to be compatible with a whole host of systems. Cloisite® 15A is the most hydrophobic and Cloisite® 30B is the most hydrophilic member in the surface treated Cloisite® family (Figure 2.15). A Cloisite® particle of 8 microns contains over 1,000,000 platelets stacked together. Extremely large interfacial area between the clay and the polymer can be obtained if the platelets can be separated, that is exfoliated, from each other after the clay is processed together with a polymer. Because of this unique property, nanoclays have the potential of being used in the polymer industry to slow down the diffusion of gaseous molecules through various polymers, creating "barrier" films or enclosure structures.

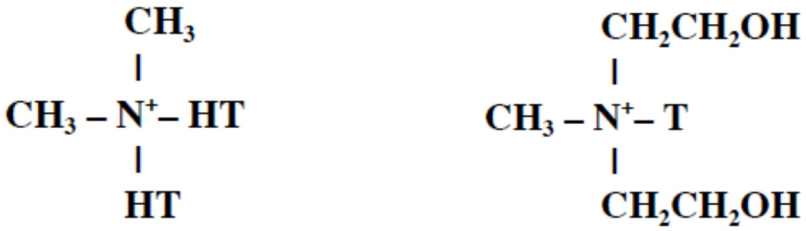

HT: hydrogenated tallow (~65% C18; ~30% C16; ~5% C14)

T: tallow (~65% C18; ~30% C16; ~5% C14)

Figure 2.14 Chemical structures of Cloisite® 15A (left) and Cloisite 30B® (right).

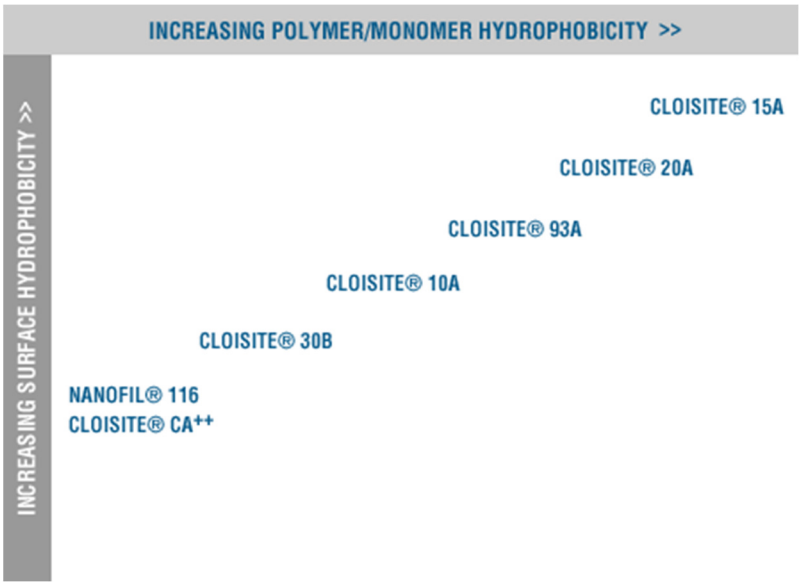

Figure 2.15 Cloisite® Selection Chart Based on Polymer/Monomer Chemistry.[122]

Three types of polymer layered silicate nanocomposites may be obtained while nanoclays are incorporated into the polymer, as illustrated in Figure 2.16.[123] When the polymer is unable to intercalate between the silicate sheets, a phase-separated composite is obtained, whose properties stay in the same range as that of traditional microcomposites. On the other hand, in intercalated nanocomposites, the insertion of a polymer matrix into the layered silicate structure occurs in a crystallographically regular fashion, regardless of the clay to polymer ratio. In such structures, a well-ordered multilayer morphology built up with alternating polymeric and inorganic layers is generated. Normally, only a few molecular layers of polymer can be intercalated in these materials.[124] Small angle X-ray scattering (SAXS) results show that at 2% Cloisite® 15A loading, the silicate nanoparticles entered into the PEO lamellae, increased the lamellae thickness while decreasing the distance between two lamellae (Figure 2.17).[125] At 4% loading, however, nanoparticles gathered in the amorphous regions between lamellae, possibly because the crystal lamellae cannot “include” so many particles, and increased

the amorphous layer thickness. The crystallization rate of PEO was accelerated by the addition of Cloisite® 15A.

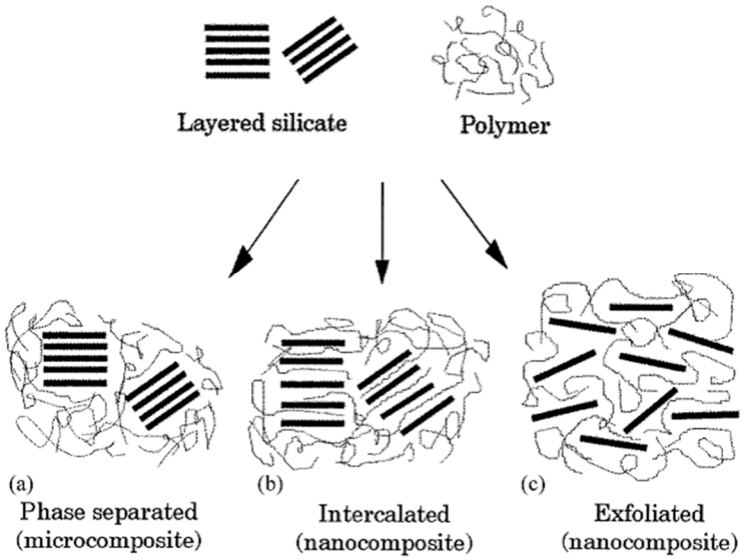

Figure 2.16 Different types of composites from the interaction of layered silicates and polymers: (a) phase-separated microcomposite; (b) intercalated nanocomposite and (c) exfoliated nanocomposite.[123]

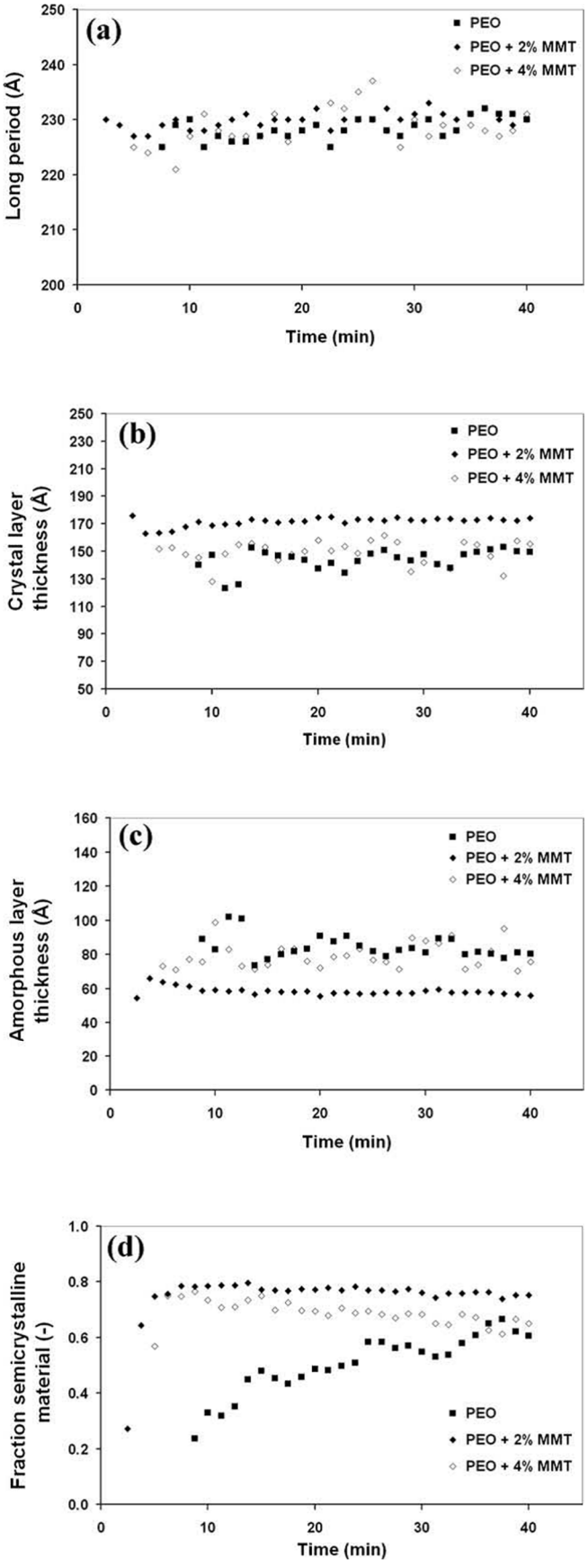

Figure 2.17 Small angle X-ray scattering (SAXS) measured (a) The long period, (b) lamellae layer thickness, (c) amorphous layer thickness and (d) the volume fraction of semi-crystalline material of pure PEO and the PEO/montmorillonite (MMT) nanocomposites with 2 and 4%MMT during isothermal crystallization of 48 ^{o}C.[125]

Homminga et al. found some very interesting results on poly(ε-caprolactone)(PCL)/Cloisite® 15A nanocomposites.[126] First of all, there is significant morphological difference between PCL/Cloisite® 15A samples (Figure 2.18) and PCL/Cloisite® Na^+ unmodified sample (Figure 2.19). The observed black lines in Figure 2.18 cannot be interpreted as individual silicate layers as they are too large and thick. The size and shape of the lines in the TEMs supports the view of intercalated stacks. In contrast, Cloisite® type MMT without surfactants cannot be intercalated and the original MMT stack is fully preserved even after mixing with PCL. These clay aggregates are larger, less diffuse and darker as compared to the intercalated, and most likely partially broken-up stacks seen in Figure 2.19. The second finding is that all nanocomposites display a pronounced decrease in amorphous layer thickness as shown in Figure 2.20, which is a signature of secondary crystallization via the insertion of new crystals in between already existing ones. Primary crystallization is defined as the growth of spherulites, involving primary crystals in rather open "primary stacks". Behind the spherulitic growth front another one follows much slower, involving further and delayed conversion of amorphous material that was left amorphous in the primary stacks by the insertion of new crystals. The overall crystallinity is significantly improved in the presence of MMT as well.

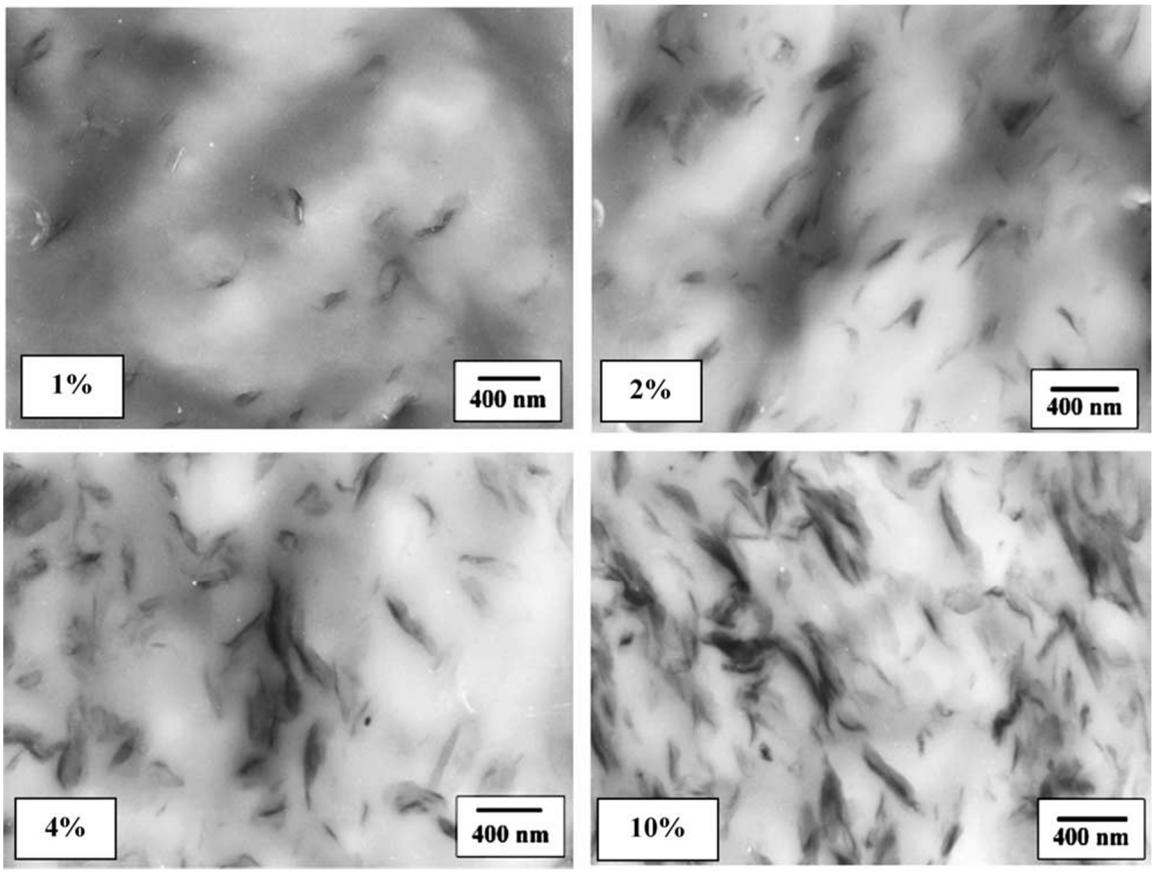

Figure 2.18 Transmission electron micrographs (TEMs) of poly(ε-caprolactone) and its Cloisite® 15A composites.[126]

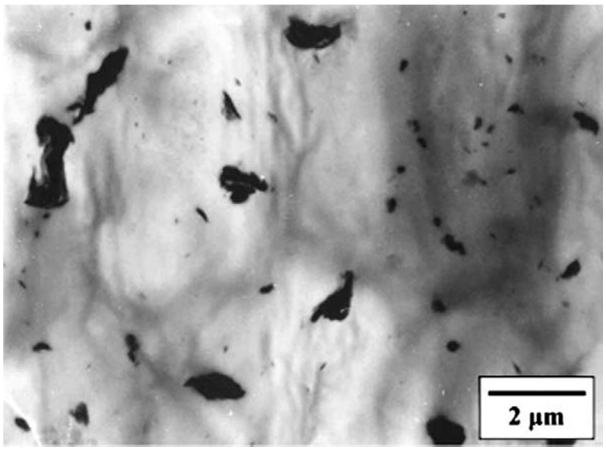

Figure 2.19 TEM of poly(ε-caprolactone) +8% Cloisite® type MMT without surface modification.[126]

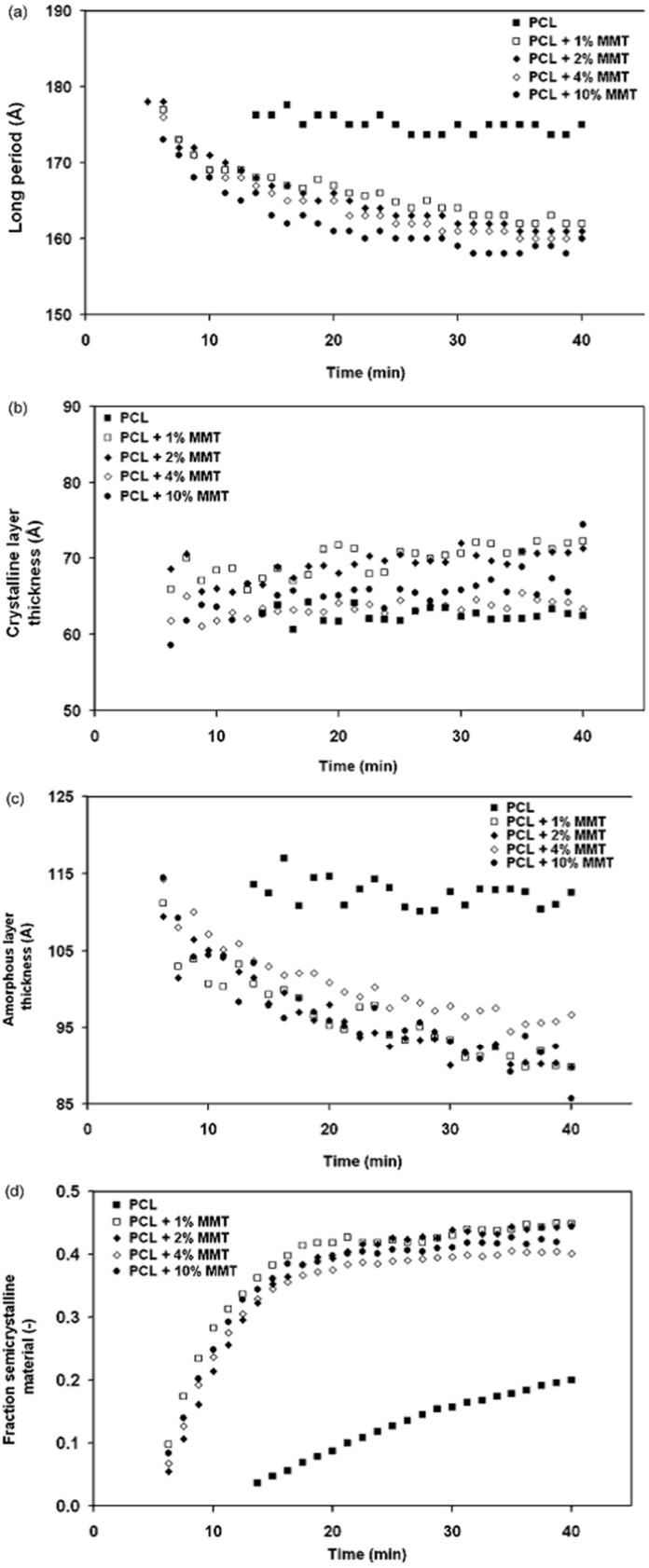

Figure 2.20 Small angle X-ray scattering (SAXS) measured (a) The long period, (b) lamellae layer thickness, (c) amorphous layer thickness and (d) the volume fraction of semi-crystalline material of pure PCL and the PCL/MMT nanocomposites during isothermal crystallization of 47 ^{o}C.[126]

Melt-mixed PEO/Cloisite® 30B, on the other hand, formed exfoliated nanocomposites with no clear SAXS peaks of PEO (MW 100,000) (Figure 2.21) and lower PEO crystallinity.[127] Park et al. have developed a method of inserting and stabilizing donepezil molecules in the interlayer space of clay via mono or double layer stacking (Figure 2.22).[128] The nanoclays they used were Na^+-MMT, Na^+-saponite (SA) and Na^+-laponite (LA), whose chemical formulae can be found in their paper.[128] By making hybrids where donepezil molecules intercalated into the smectite clays, controlled release drug delivery systems were achieved (Figure 2.23).

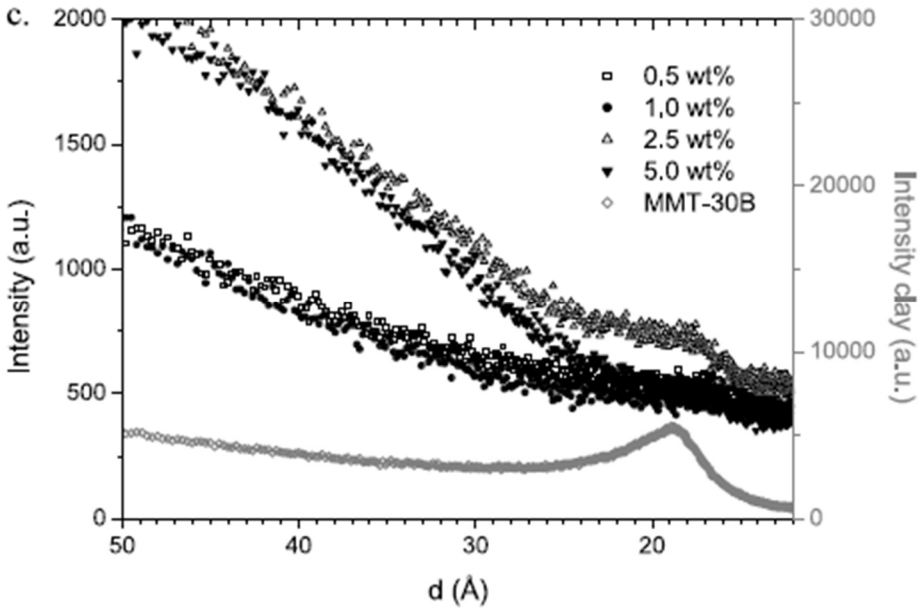

Figure 2.21 SAXS spectra of PEO/Cloisite® 30B nanocomposites.[127]

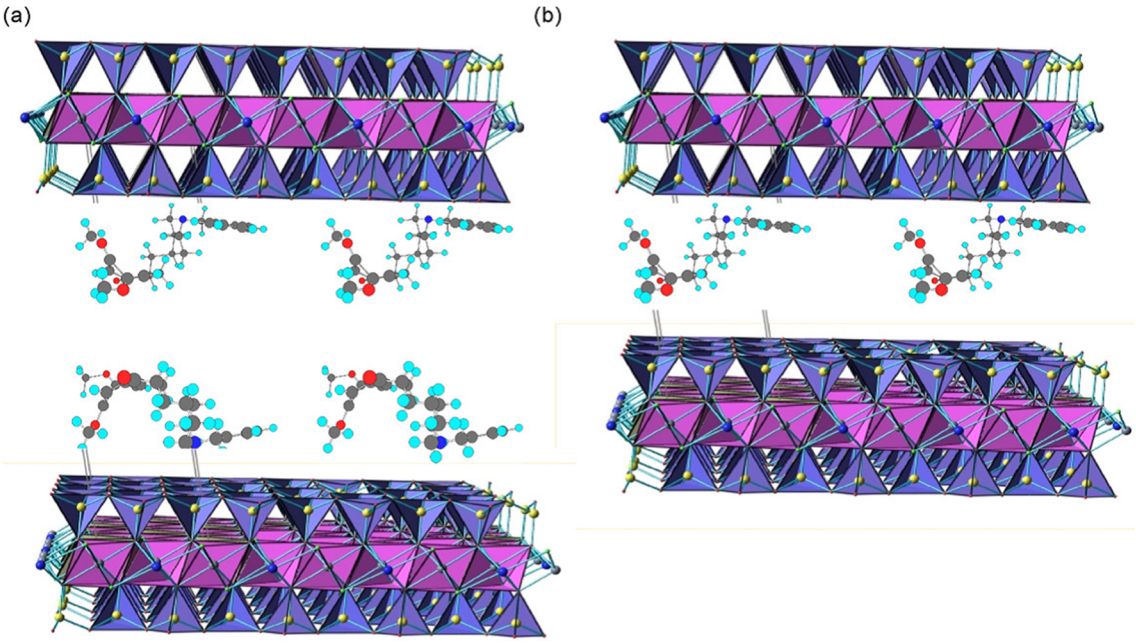

Figure 2.22 Schematic diagrams of the arrangement of the intercalated donepezil in nanoclay materials: (a) double layer arrangement in donepezile-MMT and (b) monolayer arrangement in donepezile-LA.[128]

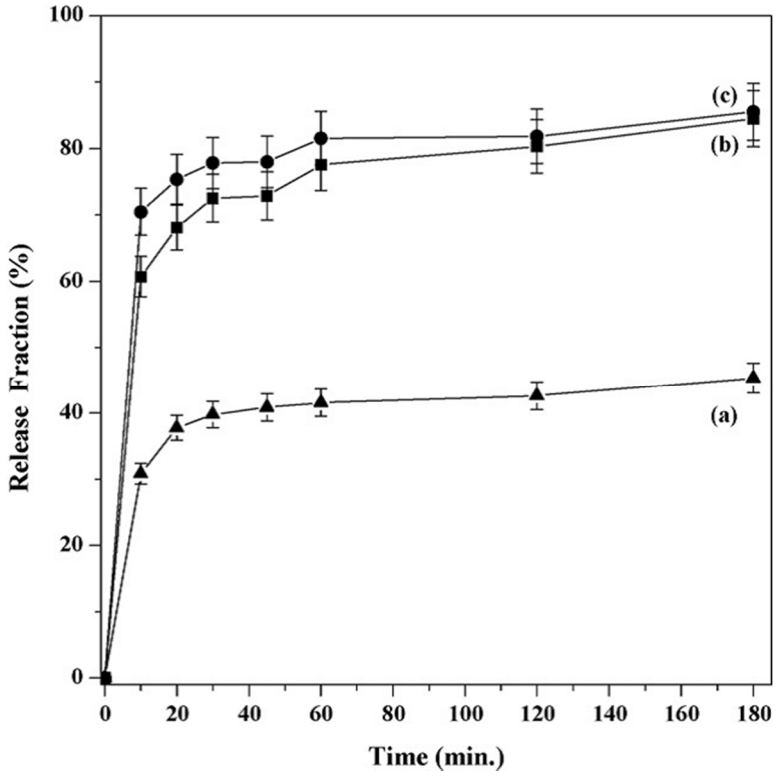

Figure 2.23 Release profiles of donepezil in pH 1.2 HCl from the Eudragit® E coated hybrids. The hybrids are (a) donepezil-MMT, (b) donepezil-SA and (c) donepezil-LA.[128]

CHAPTER 3

EXPERIMENTAL

3.1 High Temperature Solubility Measurement

3.1.1 Sample Preparation – Hot-melt Mixing (HMM)

The APAP-PEO mixture samples with twelve APAP weight percentages of 0, 1, 2, 3, 4, 5, 10, 20, 25, 30, 40, 50 and 60% were prepared by hot-melt mixing under a N_2 purge blanket using a Brabender FE-2000 batch intensive mixer with two counter rotating screw melting/mixing elements (Figure 3.1). 50 g of pre-mixed powders was processed for each batch at a mixer temperature of 120 ºC and rotor speed of 50 rpm. After 10 minutes of mixing, the melt was removed from the mixer and compression molded at 120 ºC into 25 mm diameter × 1 mm thickness discs as well as 14 × 10 × 2.7 mm bars separately. The evolution of the torque during mixing of 30%APAP-PEO is given as an example in Figure 3.2. The increase of the torque value at the beginning represents the feeding surge. After that, the torque value decreases until it reaches a plateau. It takes about 5 minutes for the torque to reach a constant value. The drop of the torque is due to the viscosity decrease of the mixture, which is caused not only by the melting of PEO, but also by the dissolution of the APAP molecules into the highly viscous polymer melt. Detailed rheological results are presented in Chapter 4.1.1. Simply put, the dissolved APAP acts as a plasticizer and lowers the viscosity of the mixture. A constant torque value indicates that 10 minutes is sufficient time for complete mixing. All samples were cooled down to 25 ºC with cooling water circulated in the compression mold. They were stored at room temperature in a vacuum desiccator with silica gel before further testing.

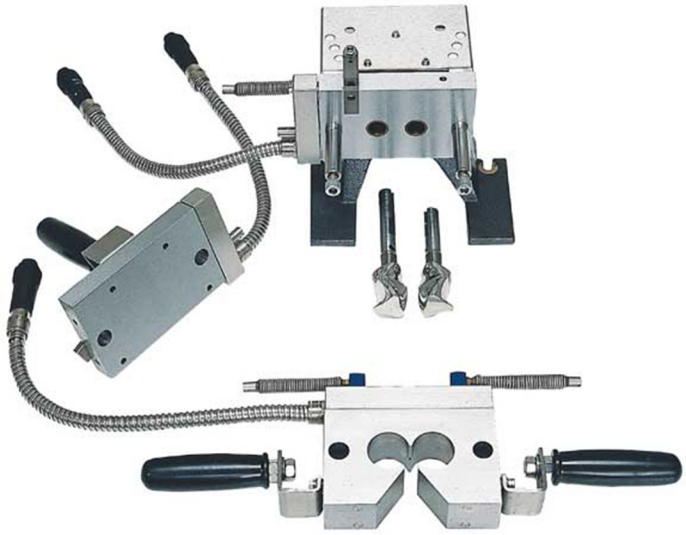

Figure 3.1 Brabender FE-2000 batch mixer with two counter rotating screws.

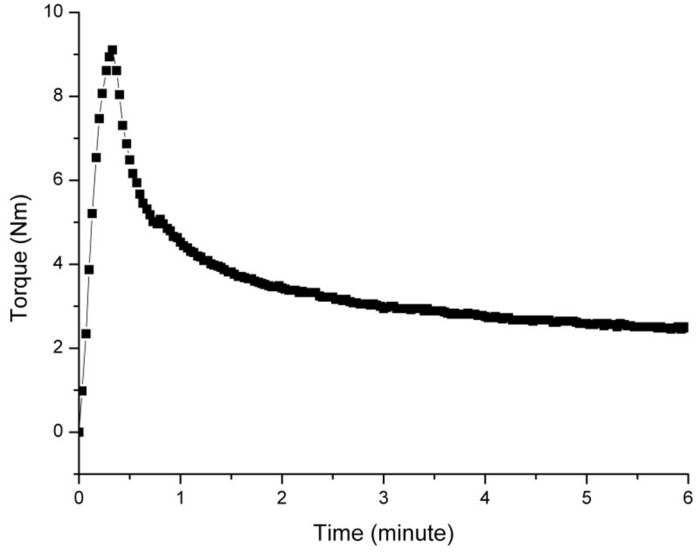

Figure 3.2 The evolution of torque during melt mixing for 30%APAP-PEO.

As mentioned in Chapter 1, the rotation speed and the residence time have been optimized to achieve a well-mixed and homogeneous mixture. 120 ^{o}C is a safe temperature for both APAP and PEO (Figures 2.7 and 2.12). For drug loadings ≤ 30%, APAP could completely dissolve in PEO at 120 ^{o}C (results in Chapter 4.1). For higher drug loading samples (APAP ≥ 40%), the purpose of the batch mixing is to prepare well-

distributed mixtures and suspensions for the solubility studies. As mentioned earlier, N_2 purge was used to prevent PEO from oxidative degradation (Chapters 1 and 2). All processing conditions are fixed as the focus of this thesis is the experimental and thermodynamic study of drug-polymer miscibility in HMM-prepared APAP-PEO systems of a wide range of APAP concentrations, determined over a wide range of temperatures from ambient to processing.

3.1.2 Rheological Experiments

The Rheometrics Mechanical Spectrometer RMS-800 from Rheometrics Scientific (now TA Instruments, New Castle, DE) was used to determine the steady viscosity of PEO and its mixtures with APAP. A step rate rotational flow test was conducted at a constant shear rate ($\dot{\gamma}$) of 0.5/s using 25 mm parallel plates. The PEO and APAP-PEO could achieve a steady-state stress and thus, viscosity, at this shear rate. A sample disc (25 mm diameter × 1 mm thickness) was loaded between the plates at 140 °C but was quenched to the testing temperatures (T_f) in less than 2 minutes. It was held isothermally at T_f for 15 minutes to reach equilibrium before testing. Each sample was tested individually at T_f values of 80, 100, 120 and 140 °C for 10 minutes.

A schematic drawing of a parallel plate set-up is presented in Figure 3.3.[129] The viscosity η is calculated by measuring experimentally the shear stress τ at a constant longitudinal shear rate $\dot{\gamma}$.

$$\eta = \tau / \dot{\gamma} \tag{3.1}$$

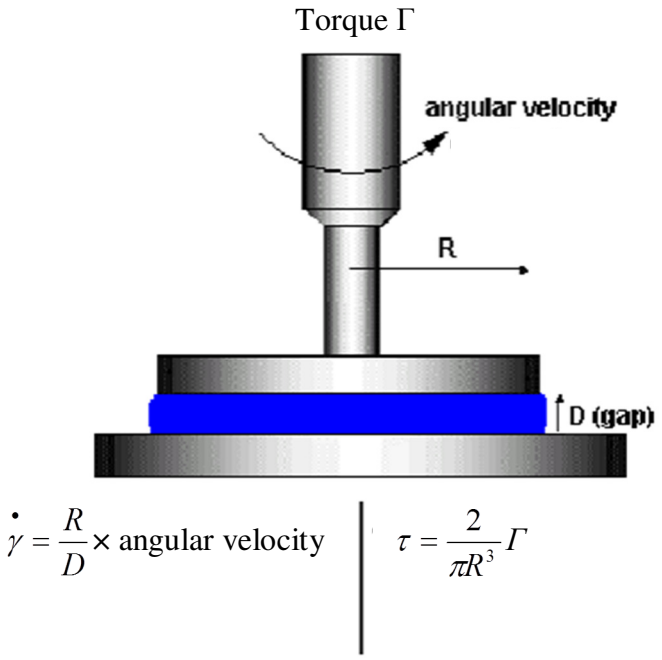

Figure 3.3 A schematic drawing of a parallel plate set-up.[129]

3.1.3 Hot-stage Microscopy (HSM)

Mixtures of 10, 20, 30, 40 and 50 wt% of APAP in PEO were examined by hot-stage microscopy using an optical microscope (Carl Zeiss Universal Research Microscope) equipped with a Zeiss AxioCam MRc5 (5MB-pixel resolution) digital camera and coupled with a Mettler FP82HT hot stage and Mettler FP90 temperature controller (Mettler-Toledo Inc., Columbus, OH, USA). Samples were heated between two glass slides from room temperature to a final temperature (T_f) of 80, 100, 120, and 140 ºC at a heating rate of 10 ºC/minute and kept isothermally at T_f for 15 minutes. Images were taken during and at the end of the experiment.

3.1.4 Differential Scanning Calorimetry (DSC)

DSC measurements were carried out using a TA Instruments Q100 (New Castle, DE) equipped with a refrigerated cooling system. The chamber was flushed with N_2 at a flow rate of 40 ml/minute during testing. A sample of about 4 mg was weighed and placed in an aluminum pan with lid and crimp sealed. The glass transition temperatures (T_gs) of PEO and APAP were measured in the 2nd heating cycle of a heat-cool-heat loop. Pure PEO was heated from 30 ºC to 80 ºC at 10 ºC/minute, quenched to -80 ºC and reheated to 80 ºC at 10 ºC/minute. Pure APAP powder was heated from 30 ºC to 180 ºC at 10 ºC/minute, quenched to -25 ºC and reheated to 180 ºC at 10 ºC/minute.

Binary mixture samples, with 10, 20, 25, 30, 40, 50 and 60 wt% of APAP, were examined using the following heat-cool-heat cycle for determination of the glass transition temperature T_g of the mixture, which were further utilized to estimate APAP's solubility at high temperatures, i.e., above the PEO's melting point, and the melting temperature T_m of the mixture.

1: A sample was heated from 30 ºC at 10 ºC/minute to a final temperature (T_f) of 80, 100, 120 or 140 ºC, at which temperature it was held isothermally for 15 minutes.

2: The sample was quenched from T_f to -80 ºC at 20 ºC/minute.

3: The sample was reheated from -80 ºC to 80 ºC at 10 ºC/minute to measure T_g and T_m.

3.2 Apparent Room Temperature Solubility Measurement

3.2.1 Sample Preparation - HMM

The same APAP-PEO mixture samples as in Chapter 3.1.1 were used for the determination of the apparent room temperature solubility. APAP-nanoclay-PEO mixtures, with APAP concentrations ranging from 10, 20 and 30wt%, and nanoclay Cloisite® 15A and 30B concentration kept constant at 10wt%, were prepared by using the same hot-melt mixing procedure.

3.2.2 DSC

APAP's apparent solubility in PEO at room temperature was estimated by T_g measurement in a single heating ramp. Samples were stored at room temperature for four weeks. APAP-PEO mixtures with APAP concentration varying from 1 to 50% were quenched to -80 ºC and then heated to 80 ºC at 10 ºC/minute. The melting temperature onset T_m was also recorded in the same cycle.

3.2.3 Dynamic Mechanical Thermal Analysis (DMTA)

Dynamic Mechanical Thermal Analyzer DMTA-IV from Rheometrics Scientific (now TA Instruments, New Castle, DE) was used to determine the T_gs of pure PEO and its mixtures with APAP that were stored at room temperature for four weeks after hot-melt mixing. The experiment was conducted using a dual cantilever with a small frame. A sample bar (14 × 10 × 2.7 mm) was first quenched to -70 °C and then ramped to 30 °C at a heating rate of 2 °C/min using liquid nitrogen as a cooling medium and 5 ml/minute N_2 gas to prevent the build-up of moisture during the experiment. A strain of 0.02%, within the linear viscoelastic region of the material (that is below the strain limit of linear

viscoelastic response), and a frequency of 1 Hz were applied for each sample. The elastic (in-phase) modulus (*E'*), viscous (out-of-phase) modulus (*E"*) and tan δ (*E"/E'*) were recorded during the experiment. T_g was determined from the peak of the tan δ curve in the glass transition region.

The modulus of a material *E* is defined as:

$$E = \frac{\tau}{\gamma} \tag{3.2}$$

where τ is the stress and γ is the strain. The viscoelastic properties of the APAP-PEO systems were studied by dynamic mechanical analysis where a sinusoidal strain was applied and the resulting stress was measured. For an ideally elastic solid, the resulting stress and the strain will be perfectly in phase. For a purely viscous fluid, there will be a 90^o phase lag of stress with respect to strain.[130] In the dynamic mechanical test, stress and strain are expressed as:

$$\tau = \tau_0 \sin(t\omega + \delta) \tag{3.3}$$

$$\gamma = \gamma_0 \cos(t\omega) \tag{3.4}$$

where ω is the frequency of strain oscillation, *t* is the time and δ is the phase lag between stress and strain. By definition, the elastic (in-phase) modulus *E*', viscous (out-of-phase) modulus *E*" and phase angle δ are described as:

$$E' = \frac{\tau_0}{\gamma_0} \cos\delta \tag{3.5}$$

$$E'' = \frac{\tau_0}{\gamma_0} \sin\delta \tag{3.6}$$

$$\tan\delta = \frac{E''}{E'} \tag{3.7}$$

3.2.4 Scanning Electron Microscopy (SEM)

Morphologies of binary and ternary mixture samples were examined using a LEO 1530 Field Emission Scanning Electron Microscope (Carl Zeiss SMT Inc., Peabody, MA) at 2 keV. Both the surfaces and cryo-fractured surfaces of the samples were characterized. The cryo-fractures were prepared by snapping a sample disc that had been soaked in liquid nitrogen for 5 minutes. All samples were sputtered with a thin layer of carbon to improve the electrical conductivity prior to imaging.

3.2.5 X-ray Diffraction (XRD)

A Philips PW3040 X-ray diffractometer (PANalytical Inc., Westborough, MA) was controlled by X'Pert software with Cu Kα radiation (λ = 1.54 Å) generated from a copper source operating at a power level of 40 KV and 40 mA. The sample discs were held directly for XRD analysis and scanned over the 2θ range of 5–30º at the step size of 0.03º/step and the scan rate of 1 second/step. The slit configuration was 1.0º, 1.0º and 0.1mm for divergence, anti-scatter and receiving slit, respectively.

3.3 Determination of Flory-Huggins χ Parameter from Melting Point Depression

3.3.1 Melting Point Determination

The melting point T_m and heat of fusion $\Delta_{fus}H$ of crystalline APAP were measured by heating APAP from 298.15 K to 473.15 K at a heating rate of 10 K/minute in DSC. The polymer-depressed drug's melting points at different PEO weight percentage, namely 100, 90, 80, 75, 70, 60, 50 and 40%, were determined from high temperature solubility in Chapter 3.1.

3.3.2 Determination of Acetaminophen's Solubility in PEG 400

APAP's solubility in PEG 400, a small molecular weight analogue of PEO N10, was measured using an Agilent 8453 UV Spectrophotomer (Foster City, CA) at wavelength of 243 nm. An excess amount of APAP was added to a capped glass bottle containing PEG 400 maintained at 300 K and was stirred vigorously for 48 hours. The resulting suspension was filtered using a Millipore 0.2 μm PVDF syringe filter (Millipore Corp., Billerica, MA). Samples were diluted with DI water and the UV readings were compared to a calibration curve.

3.4 Dissolution Testing

Dissolution tests on binary and ternary mixture samples were performed under the sink condition using a Distek 2100A USP standard dissolution apparatus with a basket stirrer. The dissolution medium (900ml of aqueous buffer solution with pH=7) was maintained at 37±0.5ºC and stirred at 50 rpm. At predetermined intervals, 5 ml of solution was withdrawn and the volume change was corrected in the calculation. The liquid was filtered with a Millipore 0.45μm PVDF filter and analyzed using 10mm quartz cells and an Agilent 8453 UV Spectrophotometer (Foster City, CA) at 243nm. Each of the tests were performed three times to check repeatability.

3.5 Crystallization of PEO and APAP-PEO

3.5.1 Sample Preparation – Solvent Evaporation

The APAP-PEO mixtures containing 0, 0.1, 1, 2, 10 and 20% by wt. APAP were prepared by dissolving both materials in acetone/water and drying the solution in a vacuum oven at room temperature for 24 hours. The dry films were about 140 μm thick and were stored in a vacuum desiccator with silica gel before further testing.

3.5.2 Polarized Optical Microscopy (POM)

Pure PEO or APAP-PEO mixtures were placed on a glass slide and left on a hot plate at 130 ºC, when both PEO and APAP were fully melted based on results of the solubility study at that temperature (Figure 4.8). Since the films were very thin (140 μm), it took less than 30 seconds for complete melting (confirmed under polarized light) and ready for optical microscope observation. After 30 seconds of heating, the sample was quickly transferred to a Mettler FP82HT hot stage (Mettler-Toledo Inc., Columbus, OH, USA) that was equilibrated at different crystallization temperature (T_x) (Table 3.1). The morphology, number and size of the spherulites were monitored under a polarized optical microscope (Carl Zeiss MicroImaging, LLC, Thornwood, NY, USA). The growth of the spherulites as a function of time was recorded until spherulite impingement and the diameter of the spherulites was measured directly from the monitor screen using the length measurement function in AxioVision software. Reported spherulitic growth rates (G) were determined as the average rates from 6-12 spherulites of three to six samples. The standard deviation on the average growth rates was less than 5% of the magnitude of G.

Table 3.1 Crystallization Temperatures T_x Used in POM and T_c Used in DSC

PEO									
T_x	51	50	49	48	47	46	45	40	30
T_c	50	48	46	44	42	40			
0.1%APAP-PEO									
T_x	50	40	30						
T_c	52	50	48	46	44	42			
1%APAP-PEO									
T_x	50	40	30						
T_c	52	50	48	46	44	42			
2%APAP-PEO									
T_x	50	49	48	47	46	45	44		
T_c	52	50	48	46	44	42			
10%APAP-PEO									
T_x	50	49	48	47	46	45	44	40	30
T_c	52	50	48	46	44	42			
20%APAP-PEO									
T_x	46	45	44	43	42	41	40		
T_c	46	44	42	40	38	36			

All values in ºC

3.5.3 DSC

DSC measurements were carried out using a TA Instruments Q100 (New Castle, DE) equipped with a refrigerated cooling system. The chamber was flushed with N_2 at a flow rate of 40 ml/minute during testing. Samples were cut to nearly identical shape, and the sample weight was kept low (1.000 ± 0.050 mg) to minimize thermal lag during heating. During the isothermal crystallization experiment, a sample was first heated to 130 ºC and kept isothermally for 1 minute. It was then quenched to a specific crystallization temperature T_c (Table 3.1) and was kept isothermally for a sufficient period to allow complete crystallization. The sample was then heated to 90 ºC at 10 ºC/minute to determine the melting temperature T_m (offset).

Non-isothermal crystallization was carried out by using DSC to determine the crystallization temperature (T_{cp}) and enthalpy (ΔH_c). A sample was heated from 25 ºC to 130 ºC at 10 ºC/minute and kept isothermally for 1 minute to remove the thermal history. It was then cooled to 25 ^{o}C at the rate of 10 ºC/minute and the T_{cp} was taken as the maximum point of the exothermic peak.

CHAPTER 4

RESULTS AND DISCUSSION

4.1 High Temperature Solubility Measurements

4.1.1 Determination of Drug Solubility at Elevated Temperatures by Rheological Analysis

The objective of the rheological study is to find drug's solubility at different temperatures within the extrusion processing window by tracking the viscosity change of the binary mixtures with different drug loadings. The selected testing temperatures are above the melting temperature of PEO (~62 ºC) and below the melting point of APAP (~170 ºC). In this temperature range, if the APAP is not dissolved in the PEO, it will form a suspension.

In general, steady viscosity (η) of PEO and APAP-PEO mixtures decrease with increase in temperature due to increase of polymer chain mobility and reduction of intermolecular forces. The viscosity results are plotted against APAP concentration in Figure 4.1. The four viscosity curves at different T_f exhibit a similar trend, namely the viscosity value drops first with increasing drug loading, and then increases after reaching a certain concentration. The viscosity curve at T_f= 140 ºC, as an example, decreases from 6110 Pa·s for pure PEO to 430 Pa·s for 40 wt% of APAP, after which it climbs up to 691 Pa·s for 60 wt% of APAP. The initial decrease of viscosity indicates intermolecular force weakening due to the drug dissolution.[131-133] That is, the dissolved APAP acts as a plasticizer in this case, which leads to decrease of the viscosity with the increase of drug concentration. On the other hand, the rise of the viscosity at higher drug concentrations

occurs when the drug solubility limit is exceeded and the undissolved solid drug particles act as suspended fillers. Extensive previous studies, starting with Einstein,[134] have shown that the viscosity of a filler-polymer melt suspension system depends on the interfacial energy as well as the filler's concentration and shape.[135-138] Generally speaking, the viscosity increases with the filler's concentration,[139-141] which can be explained by the increased viscous "drag" and dissipation due to the suspension and particle/particle interactions at high concentrations. An example of the solid filler effect is presented in Figure 4.2, where the zero-shear viscosity of PP(polypropylene) increases appreciably with $CaCO_3$ concentration.[141]

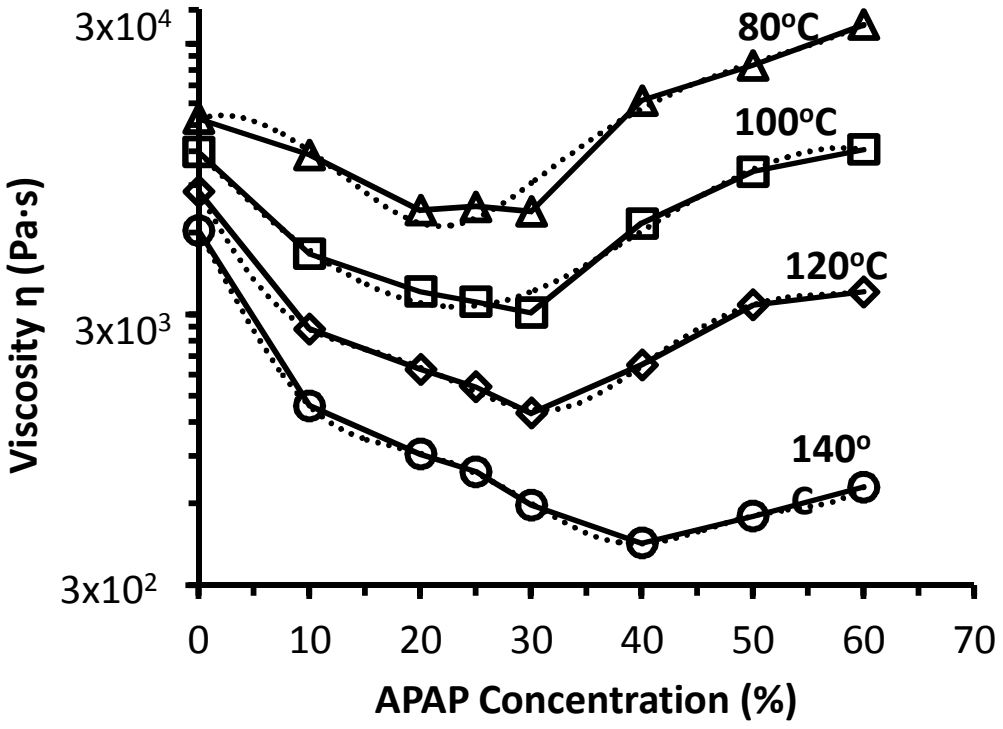

Figure 4.1 Viscosity η curves of 0, 10, 20, 25, 30, 40, 50 and 60% APAP in PEO at temperatures (T_f) of 80 ºC (Δ), 100 ºC (□), 120 ºC (◊) and 140 ºC (○).

The viscosity data are further fitted with fifth-degree polynomial only to determine the minimum value. Theoretically, the drug concentration with the lowest η is the drug solubility at the specific temperature T_f. Dotted curves in Figure 4.1 were obtained from polynomial fitting with R^2>0.99 and the drug solubility values determined from the fitting curves are listed in Table 4.1. The result shows that the drug solubility increases steadily with temperature. It should be mentioned that the predicted solubility at 80 ºC (22%) may be slightly higher than the real value because the viscosity values of 20, 25 and 30 wt% of APAP are very close to each other, which makes it more difficult to identify the critical point. These solubility data obtained by such a simple rheological experiment is an original contribution of this thesis work and is of great value for determining the processing window of HME. For example, to prepare a fully miscible APAP-PEO system with drug loading of 20%, the lowest processing temperature is 100 ºC. Otherwise, the drug crystals will not fully dissolve into the polymer melt no matter how intensive or how long the mixing is.

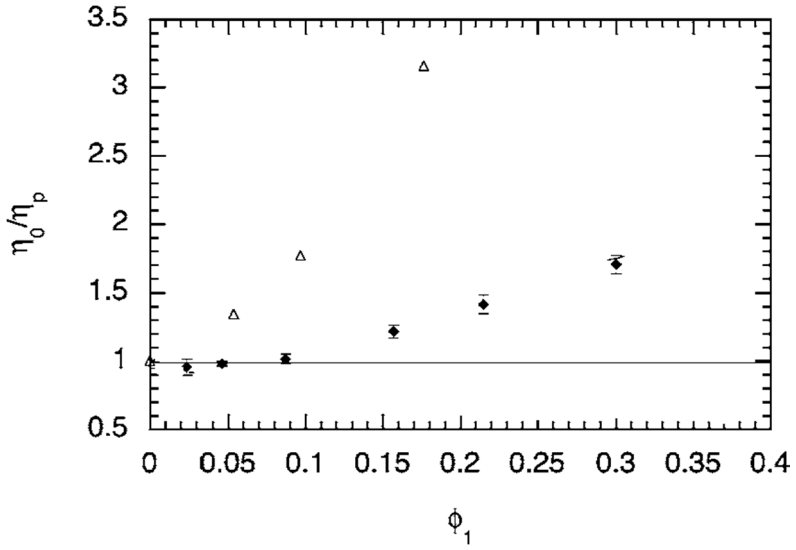

Figure 4.2 Zero-shear viscosity η_0/η_p vs. filler volume fraction φ_1. The solid data points represent the simulation results based on Einstein's theory. The open triangles represent the experimental results using PP (polypropylene) and $CaCO_3$ treated with stearic acid. The horizontal line indicates mixture viscosity η_0= pure polymer viscosity η_p.[141]

Table 4.1 Summary of APAP Solubility in PEO at Elevated Temperatures Measured with The Rheometrics Mechanical Spectrometer, Hot-Stage Microscope and DSC

Temperature	Solubility by rheological evaluation (%)	Solubility by hot-stage microscopy (%)	Solubility by DSC (%)
80 ºC	22	10 - 20	14
100 ºC	24	20 - 30	20
120 ºC	31	30 - 40	30
140 ºC	41	40 - 50	n.a.

A low shear rate (0.5 s^{-1}) was used in the rheological study so that the materials remained as Newtonian flows under the testing conditions. If a high shear rate was used, the materials would exhibit non-Newtonian behavior such as shear thinning, where the viscosity would decrease with increasing shear rate. Shear thinning would diminish the viscosity difference between samples with different APAP concentrations, which would make it difficult to determine the minim on the viscosity curves in Figure 4.1.

4.1.2 Optical Determination of Drug Solubility at Elevated Temperatures

To check the solubility data obtained from the rheological test, a hot-stage microscope (HSM) was used to directly observe the physical state of the drug particles in the molten polymer mixtures. The same temperatures (T_f) as those in rheological experiments were used. To facilitate observation and assure intimate contact between two materials, PEO and APAP were first hot-melt mixed. The sample was placed on a glass slide, slightly heated on the hot stage, and pressed carefully with a cover glass. The mixture was further equilibrated at the temperature of interest. At T_f of 80 ºC and APAP loading of 10% (Figure 4.3a), crystalline APAP fully dissolves in the molten PEO with no visible particles observed. In contrast, at a drug loading of 20%, APAP crystals can be found even after 15 minutes of heating at 80 ºC (Figure 4.3b). Therefore, APAP solubility at

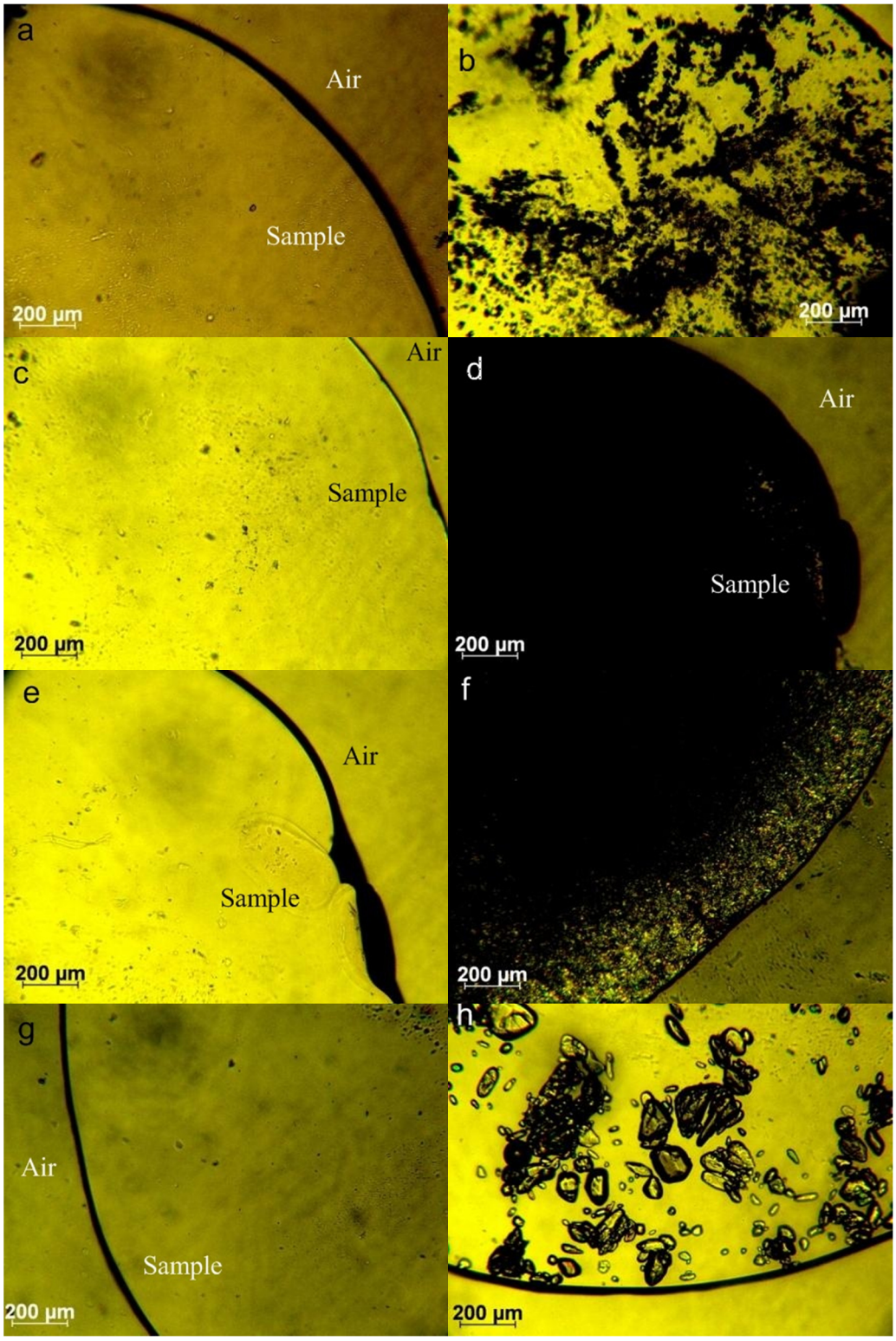

Figure 4.3 Hot-stage microscopic images of samples after being kept isothermally at different temperatures for 15 minutes. a) 10% APAP-PEO at 80 ºC; b) 20% APAP-PEO at 80 ºC; c) 20% APAP-PEO at 100 ºC; d) 30% APAP-PEO at 100 ºC; e) 30% APAP-PEO at 120 ºC; f) 40% APAP-PEO at 120 ºC; g) 40% APAP-PEO at 140 ºC; h) 50% APAP-PEO at 140 ºC.

80ºC should fall between 10 and 20%. Experiments were also conducted at 100, 120 and 140 ºC (Figure 4.3c-h) and the results are summarized in Table 4.1. Clearly, most solubility data obtained from rheological tests fall into the range determined by HSM. The only slight mismatch was found at 80 ºC. As discussed in the previous section, the critical point on the curve of viscosity versus drug loading cannot be accurately determined at 80 ºC because the transition is not sharp enough. It should be mentioned that the optical microscopy method is an approximate method and cannot be applied to accurately identify the solubility value. Nevertheless it is quite straightforward, readily accessible, and can be applied to obtain an "engineering" estimate of the solubility. Another advantage is that the microscopy method, being straightforward, can be applied to a wide range of drug-polymer systems compared to other analytical methods.

4.1.3 Determination of Drug Solubility at Elevated Temperatures Using DSC

A third approach using DSC was explored to determine the drug solubility at high temperatures. The method is based on the assumption that the glass transition temperature should vary with APAP's concentration in the APAP-PEO solution. Similarly to the rheological and microscopic analyses, temperatures within the HME processing window were selected, namely 80, 100, 120 and 140 ºC. In the 1st heating cycle, the sample was heated to a final temperature T_f and then held at the temperature for 15 minutes. Depending on the drug loading and the temperature, the crystalline drug may be partially or fully dissolved in the molten polymer at T_f. The sample was then quenched to -80ºC, a temperature below the glass transition temperatures of both PEO and APAP. In the 2nd heating scan, T_g of the APAP-PEO mixture was determined.

T_g of PEO and APAP are -56.6 ºC and 24.5 ºC, respectively. Glass transition temperatures of amorphous APAP-PEO from the 2nd heating cycle are plotted in Figure 4.4. One interesting finding is that the T_g behavior for T_f = 80, 100 and 120 ºC shows quite a similar trend. T_g increases with APAP concentration but the glass transition temperature stops rising after a certain drug loading. When the APAP concentration is less than the critical value, APAP particles fully dissolve in the molten polymer at T_f during the first heating scan. Beyond that limit, no more crystalline APAP can dissolve in PEO and, thus, the curve reaches a plateau (in the case of 140 ºC, T_g dips at the region of high drug loading, which will be discussed later). Hence, the critical concentration is taken to be the drug's solubility at T_f. The solubility data were summarized in Table 4.1. It should be mentioned in this juncture that one assumption for the DSC method is that the drug does not recrystallize during the quench and the second heating scan. The fact that the solubility values predicted by all three methods are very close to each other in this temperature range seems to support this assumption. Overall, the data show that the solubility increases from 14% at 80 ºC to 41% at 140 ºC.

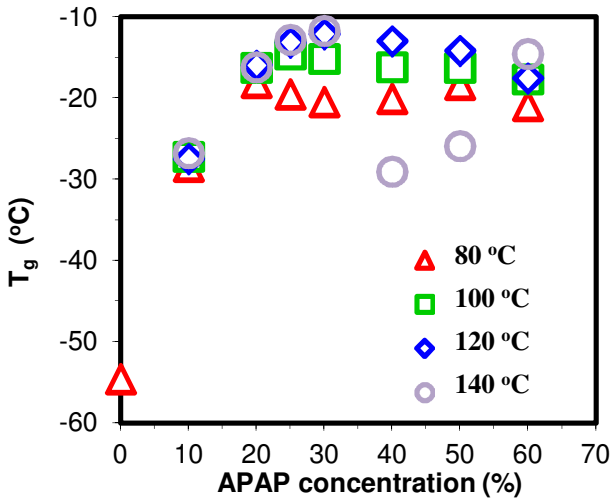

Figure 4.4 Glass transition temperatures of mixtures at different drug loading determined from the 2nd heating cycle in DSC with the ending temperatures (T_f) in the 1st heating cycle of 80 ºC (Δ), 100 ºC (□), 120 ºC (◊) and 140 ºC (○), respectively.

The following peculiar phenomenon is found on the curve corresponding to T_f of 140 ºC: the T_g drops as much as 17 ºC when the drug loading increases from 30% to 40%. It is known from the rheological and microscopic analysis that drug solubility is around 41% at 140 ºC. Thus, the sharp T_g decrease is not caused by drug recrystallization or phase separation. To further investigate this issue, the Fox equation[142] was used to calculate the theoretical glass transition temperatures for APAP-PEO with different drug concentrations and is expressed as:

$$\frac{1}{T_g} = \frac{w_1}{T_{g1}} + \frac{w_2}{T_{g2}} \tag{4.1}$$

where w_1 and w_2 refer to the weight fraction and T_{g1} and T_{g2} refer to the glass transition temperatures of the drug and polymer, respectively.

The Fox equation, as well as the Gordon Taylor (GT) equation expressed as Equation (4.2),[143] are often applied to predict the glass transition temperature of random copolymers[144-146] and plasticized polymers[147-149] based on compositions of two components.

$$T_g = \frac{w_1 T_{g1} + K w_2 T_{g2}}{w_1 + K w_2} \tag{4.2}$$

where w_i is the weight fraction and T_{gi} the glass transition temperature of the blend component i and K is an arbitrary fitted parameter. Ideal volume additivity was assumed for the repeat units in the copolymer and the plasticizer-polymer blend for both of the two original equations. Under that assumption, K is defined as the ratio of the differences of the coefficients of expansion at T_g of the glassy state and rubbery state. Unlike the Flory-Huggins theory as discussed in Chapter 1, neither the Fox nor the GT equation takes intermolecular interactions into consideration.

These two semi-empirical equations have been applied to drug-polymer and drug-salt systems to study the miscibility of the binary components.[76, 150-153] The T_g values of these systems often do not agree with the GT predictions made on the assumption of ideal mixing. A positive deviation was observed in the sodium indomethacin (NaIMC) and indomethacin (IMC) system as shown in Figure 4.5.[152] The influence of molecular interactions on the T_g of nonideal binary polymer blends has been explained in terms of the relative magnitude of two different interaction energies: the interactions between like molecules, or homo-contacts, and those between unlike molecules, or hetero-contacts.[154] When the interaction between the hetero-contacts dominates the overall energies of the system, the nonideally mixed system will have a T_g that is greater than that which would be expected from the GT prediction. This appears to be the case for the NaIMC and IMC solid solution. Because the GT prediction for an ideally mixed system is based on the assumption that the free volume of the individual components is additive, a nonideal system with a T_g value greater than that predicted from the ideal system would be expected to have a free volume that is smaller than that of the ideal system. This is supported by the increased true density values in the NaIMC and IMC solid solution.[152]

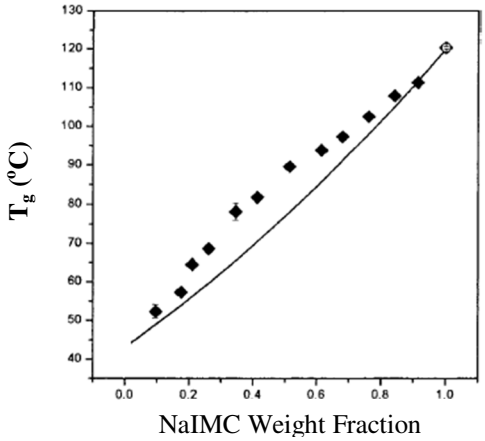

Figure 4.5 T_g of coprecipitated sodium indomethacin (NaIMC) and indomethacin (IMC) measured by DSC (♦) and predicted by the GT equation (solid line).[152]

Similar positive T_g deviation was observed in the indomethacin-Eudragit® E system (Figure 4.6),[153] which was most likely to be caused by the strong intermolecular interactions between the indomethacin and Eudragit® E molecules.[19]

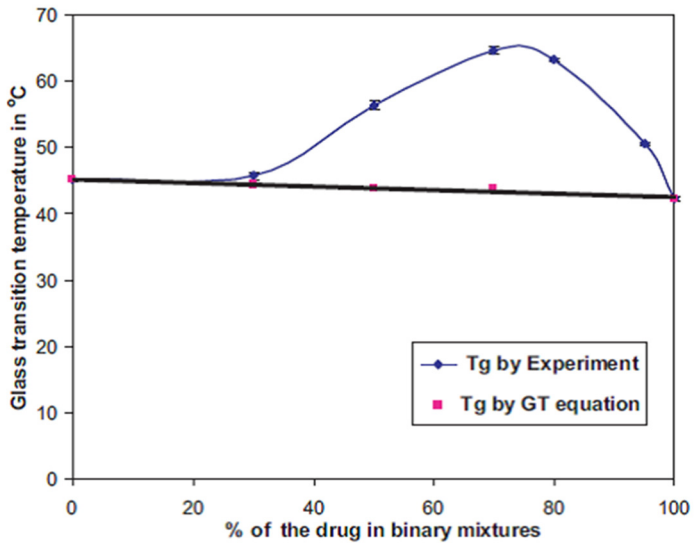

Figure 4.6 T_g of HME-prepared indomethacin and Eudragit® E measured by DSC (●) and predicted by the GT equation (■).[153]

Since the APAP solubility is about 41% at 140 ºC, T_g is only calculated for samples having less than 40% APAP loading. As shown in Figure 4.7, most experimental T_g values are significantly higher than the theoretical values, suggesting possible specific physical interactions between APAP and PEO. When APAP concentration is 40%, however, the theoretical T_g is able to match the experimental value. The hydroxyl group of acetaminophen is a good proton donor and can form strong hydrogen bonds with the oxygen acceptor on the PEO chain,[155, 156] which is capable of leading to a nonlinear relationship between T_g and the composition. Strong intermolecular interaction is usually beneficial for miscibility and solid solution stabilization,[65, 75, 77] but the H-bonding in the current case does not seem to prevent APAP from recrystallizing at room temperature.

According to Wen et al., the high flexibility of PEG and the high mobility of the functional groups involved in the H-bonds is the reason why the crystallization of APAP cannot be inhibited.[157, 158] The unusual drop of T_g at drug concentration between 30 and 40% may be due to the saturation of hydrogen bond at high drug concentration.

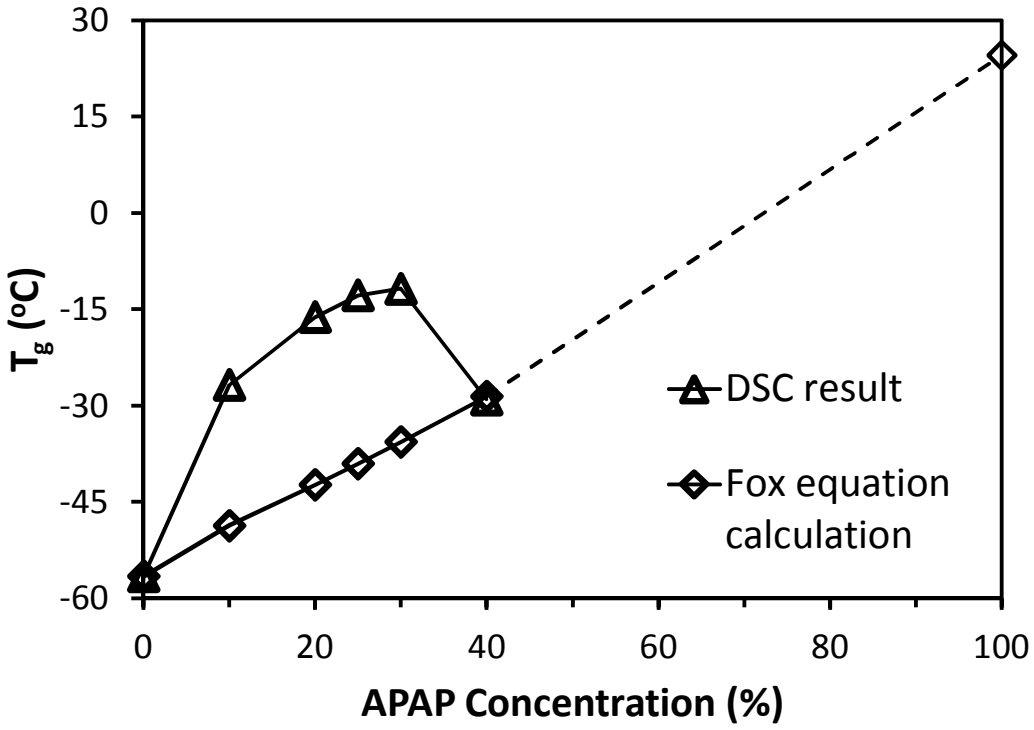

Figure 4.7 Calculated (◊) and DSC determined (Δ) glass transition temperatures of APAP-PEO. Experimental data were obtained from the 2nd heating cycle in DSC with the final temperature (T_f) in the 1st heating cycle of 140 ºC.

4.1.4 Phase Diagram of the APAP-PEO System

Figure 4.8 shows the relationships of polymer-depressed melting point of APAP T_m^{mix} and melting point of PEO T_m(PEO) with different APAP concentrations. APAP's solubility in the range of 80 to 120 ºC was determined by DSC analysis, while the solubility at 140 ºC was estimated to be 41% based on the rheological evaluation method. T_m(PEO) values were acquired from the 2nd DSC heating.

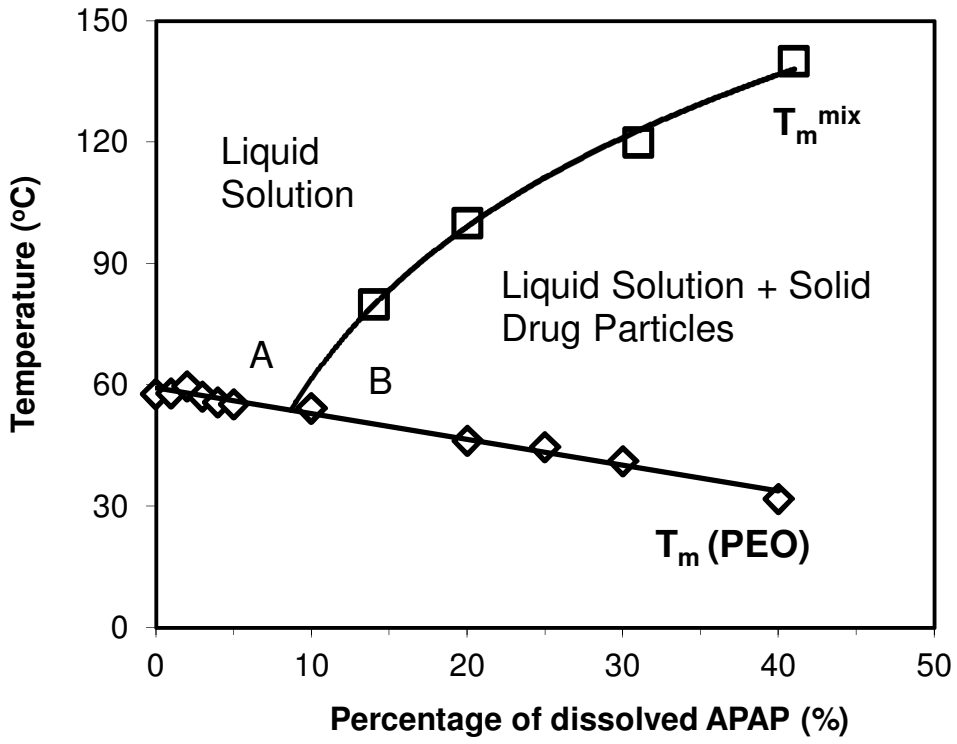

Figure 4.8 Dissolution temperature T_m^{mix} (□) and PEO melting point T_m (◊) of APAP-PEO with different percentage of APAP dissolved.

The composite figure of T_m^{mix}/T_m(PEO) *vs.* drug loading (Figure 4.8) is, in essence, a "phase diagram". Such "phase diagram" may provide valuable information for API-excipient formulation and HME process development. HME is often processed at temperatures above the T_m(PEO) curve where PEO is in the molten state. APAP and PEO are fully miscible and form a liquid solution in region A. In region B, however, APAP does not totally dissolve in PEO, and thus the system contains solid suspended drug particles. In order to obtain a true solution, it is more favorable to process the mixture in region A as compared to region B. Of course, other factors such as the potential of thermal degradation need to be taken into consideration.

Insightful information regarding the mixture's physical state can be obtained by using the above three methods, i.e., rheological, microscopic and thermal analysis.

Understandably, each method has its own limitations. The rheological method can only be applied to study the upper range of the processing temperature due to the instrument's toque limitations. More specifically, rheometers generally can only be applied to study the system at a temperature higher or significantly higher than the melting temperature of the polymer excipient. For solubility determination, the temperature also needs to be lower than the melting point of the pure drug. Otherwise, the drug will exist as a liquid and increase of drug loading will lead to decrease of the viscosity of the mixture even if the drug liquid is not fully miscible with the molten polymer. On the other hand, the advantage of the rheological method lies in the relative simple relationship between the viscosity and the mixture composition, which makes easy to identify the critical point in the viscosity *vs.* composition curve, i.e., the solubility point range, compared to the DSC method. The rheological data themselves are of great interest for process optimization as well. The microscopic method allows for a straightforward observation of the physical state of the materials. However, it is almost impossible to determine the exact solubility due to resolution limitations. The solubility data can also be determined from the shift of the glass transition temperature measured via DSC. The DSC method also provides other valuable information, such as the melting point of the mixture. However, one has to be careful when using the trend of the glass transition temperature to determine the drug's solubility because it is not uncommon for a drug-polymer mixture to have a complicated and non-monotonic relationship between the T_g and the composition, such as the one at the 140 ºC case described above.

4.2 Apparent Room Temperature Solubility Measurements

4.2.1 Estimation of Apparent Drug Solubility at Room Temperature via DSC and DMTA

Apparent APAP solubility in PEO at room temperature was estimated with similar T_g evaluation method described in the previous DSC Section 4.1.3. The difference is that samples were stored at room temperature for four weeks before testing, and the T_g was determined during the first heating scan. In other words, the T_g value reflects the mixtures' physical state at room temperature instead of the state at elevated temperatures. Glass transition temperatures were determined by using both DSC and Dynamic Mechanical Thermal Analysis (DMTA) methods. It should be mentioned that the system has probably not reached thermodynamic equilibrium after four weeks at room temperature, although the recrystallization does drop to an almost undetectably slow rate by that time. Hence, the solubility obtained is an "apparent" solubility, which may be higher than the thermodynamic solubility. In real application though, it is required by the FDA to perform the long-term stability testing in order to examine the shelf-life of any pharmaceutical products. Therefore, the experimentally measured "apparent" solubility at room temperature can provide sufficient information.

DMTA is a thermo-analytical technique. While DSC detects the change in heat capacity when a polymer changes from the glassy to the rubbery state, DMTA detects the temperature when a change of modulus occurs. T_g is determined from the peak of the mechanical loss tanδ, which is responsible for dissipation of energy during deformation and is defined as:

$$\tan \delta = E''/E' \tag{3.7}$$

where *E'* is the elastic modulus and represents how much energy the polymer stores, and *E"* is the viscous modulus and indicates the polymer's ability to dissipate energy as heat. These moduli relate to the stiffness of the material and to its damping capacity (energy dissipation).

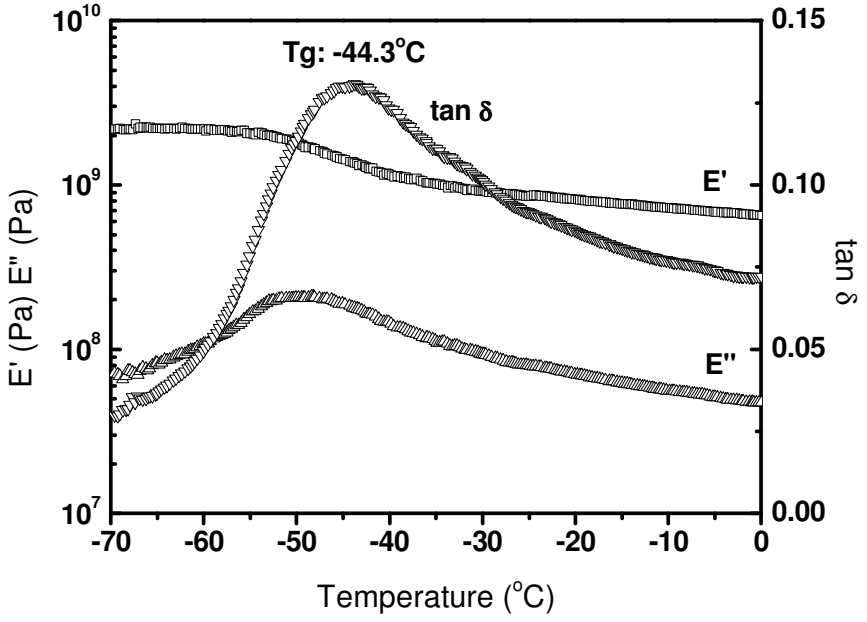

Figure 4.9 DMTA measured elastic modulus (E'), viscous modulus (E") and tan δ of PEO.

The peak of the tan δ is the center of the T_g relaxation while in DSC the onset temperature of the T_g relaxation is usually reported. In such a case the DSC T_g will be lower than that obtained from DMTA. In addition, a "frequency effect" puts the mechanical (ca. 1 Hz) T_g higher than that for a DSC measurement (0.0001 Hz).[159] The DMTA determined T_g of pure PEO is -44.3 ºC (Figure 4.9), while the T_g from the DSC measurements is -56.6 ºC. Despite of the difference in absolute numbers, both methods show similar T_g evolution trends with increasing drug concentration. Only one T_g in each

APAP-PEO sample is observed. For DSC, T_g increases from -51.2 ºC for 1 wt% of APAP to -38.7 ºC for 10 wt% of APAP and basically remains constant afterwards. DMTA data show a similar trend: T_g first increases with APAP loading, but then reaches a plateau at the concentration around 5%. As presented in Figure 4.10, the critical turning point is around 10% for DSC and 5% for DMTA. More evidence of APAP recrystallization after the sample is cooled from the HME processing temperature to room temperature will be presented in the next few sections.

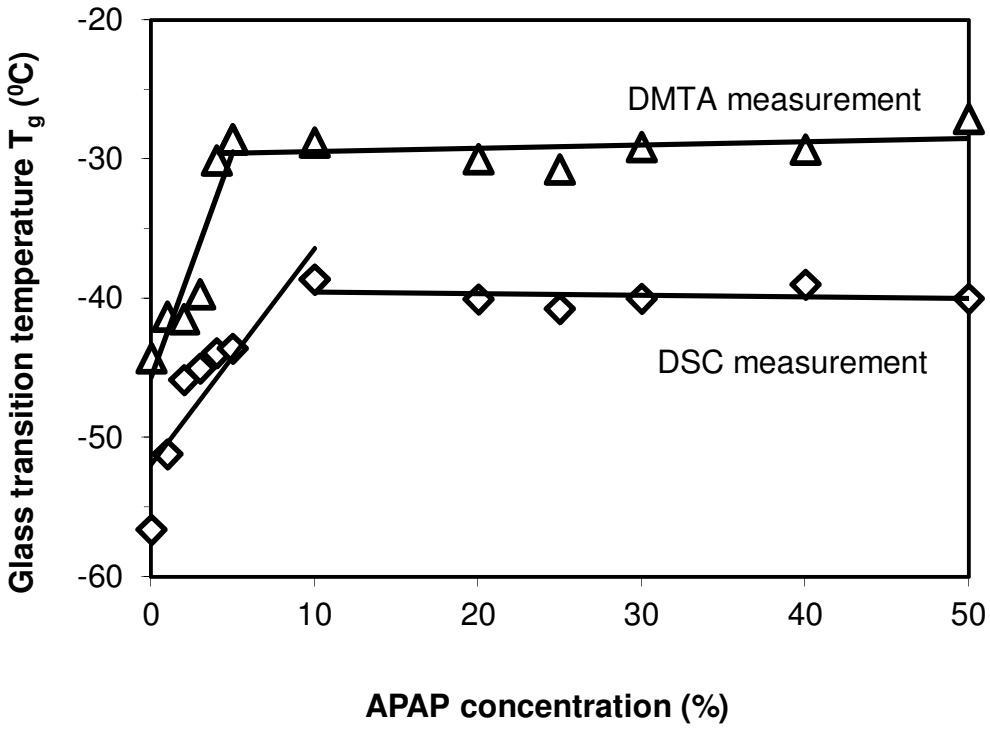

Figure 4.10 Glass transition temperatures of 4-week old melt-mixed APAP-PEO samples measured by using DSC (◊) and DMTA (Δ).

4.2.2 APAP Recrystallization Observed under Scanning Electron Microscopy (SEM)

Freshly made disc samples with APAP $\leq 30\%$ have a light yellow color, the same as pure PEO processed under the same conditions. However, unlike the pure PEO, the color of APAP-PEO mixtures (where APAP >10 wt%) will gradually change to milky white at room temperature, suggesting the occurrence of APAP's recrystallization after processing. The rate of the color change is dependent on the APAP concentration: the appearance of 20-60% APAP-PEO changes appreciably within several hours, whereas it takes several days for 10%APAP-PEO samples to exhibit appreciable visual changes. SEM photos reveal what happens at the micro scale. Freshly made 10%APAP-PEO has a relatively smooth and APAP particle-free surface (Figure 4.11a). On the contrary, drug particles, about 1-3 μm in size, are found on the surfaces of 20%APAP-PEO (Figure 4.11b-c) after the same storage time. SEM images of cryo-fractured surface samples suggest that APAP also recrystallizes at the interior bulk of all samples (Figure 4.12). It should be mentioned that after 18 days of storage, drug particles appear also at the surface of 10%APAP-PEO (Figure 4.13). The size of the recrystallized APAP particles does not change over time (Figure 4.14).

The recrystallization of APAP from a solid dispersion or solid solution formed at the processing temperature following quenching occurs in two stages as indicated by the recrystallization rate. For samples with APAP concentration > 20%, the first stage takes only several hours, whereas for 10%APAP-PEO, the first stage takes weeks. After the first stage, the systems still have not reached thermodynamic equilibrium. Furthermore, the recrystallization rate drops significantly in the second stage.

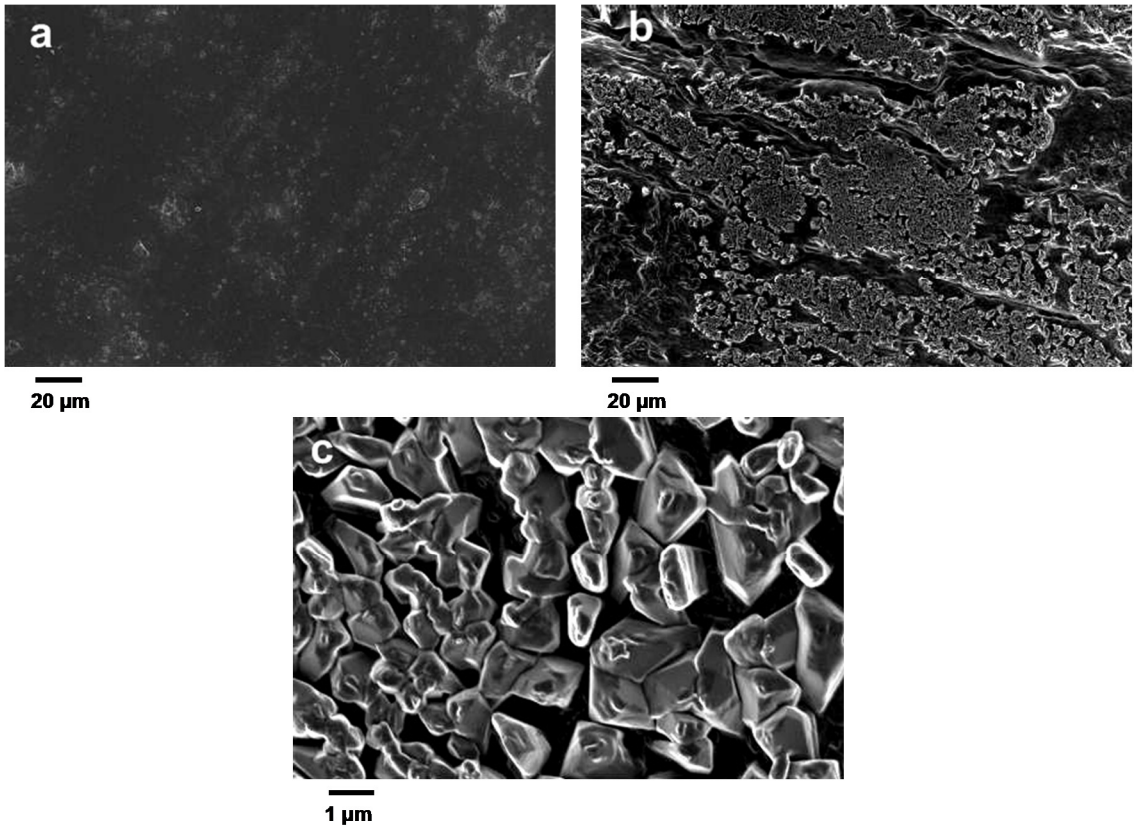

Figure 4.11 SEM images of freshly-made samples (3 hours after melt mixing) (a) 10%APAP-PEO; (b) 20%APAP-PEO; (c) 20%APAP-PEO.

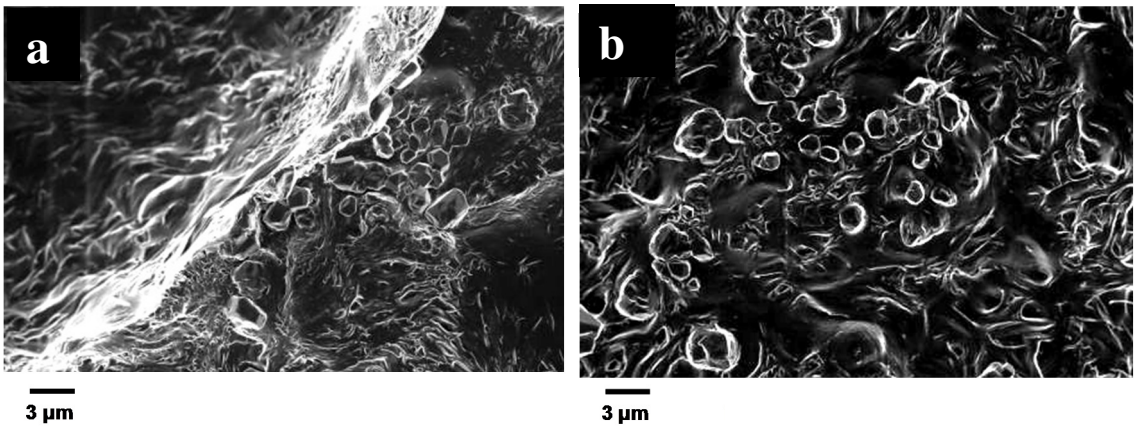

Figure 4.12 SEM images of cryo-fractured samples: (a) 20%APAP-PEO; (b) 30%APAP-PEO.

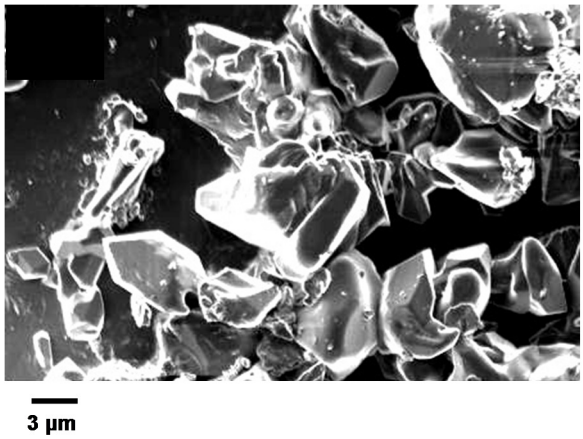

Figure 4.13 SEM images of 10%APAP-PEO after being stored for 18 days.

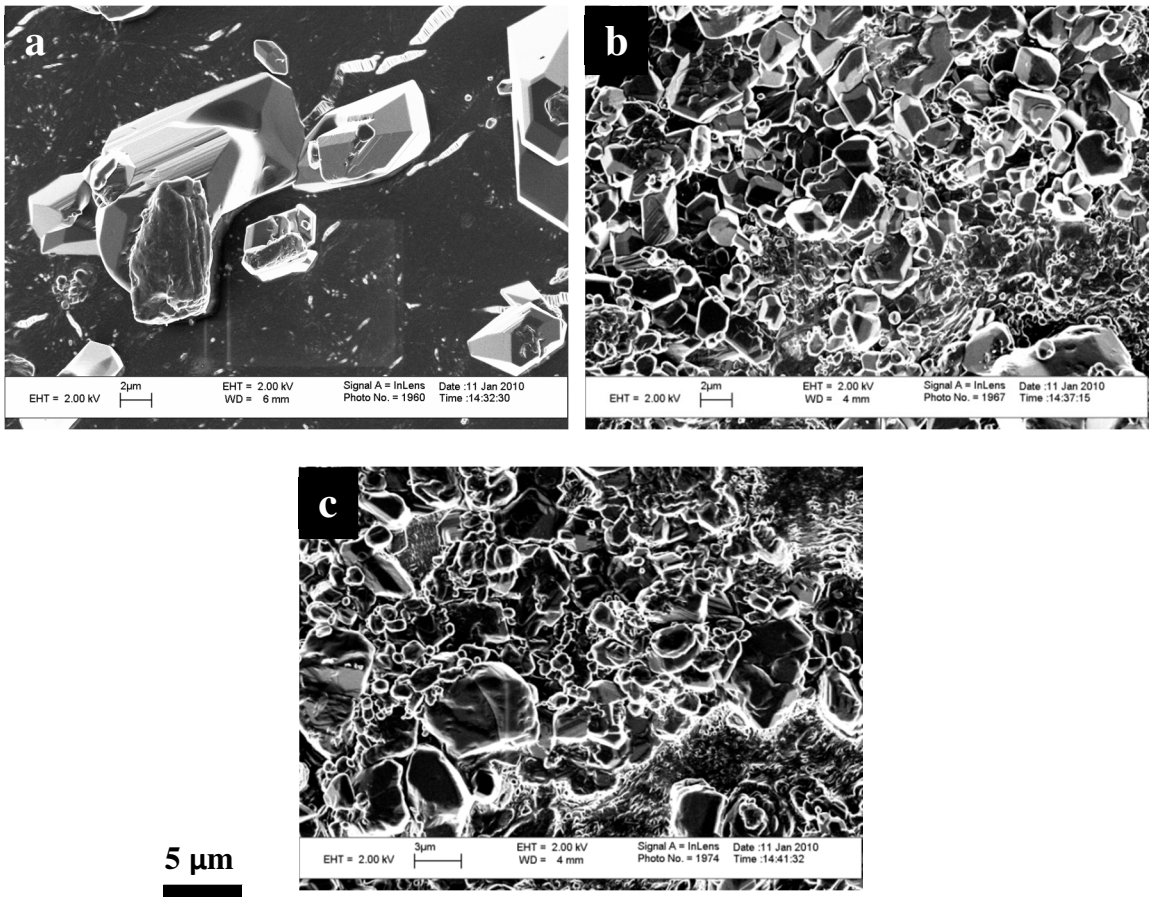

Figure 4.14 SEM images of the surface of (a) 10% (b) 20% and (c) 30%APAP-PEO after being stored for 6 months.

The morphology of the recrystallized APAP particles is of great importance since it may affect the drug's dissolution rate in an aqueous medium. For the APAP-PEO system cooled at room temperature, APAP crystalline particles formed from the recrystallization process have identical morphologies among samples with different drug loadings. The APAP particles are several micrometers in size and are richer in concentration at the sample surface (Figure 4.11c) than in the bulk (Figure 4.12a). Recently, other research groups have observed similar phenomena in that the recrystallization tends to happen at the material surface rather than in the bulk.[160, 161] Firstly, Wei et al. found that the surface tension of high density polyethylene, a semi-crystalline polymer, drops a stunning 20% in a small temperature region below the melting point.[160] They brought up a hypothesis that the initial small crystal regions would act as nanoparticles and locate at the polymer surface and reduce the surface tension. The hypothesis was later supported by the results of the statistical modeling of Thompson et al.[162] Their results showed that the nanoparticles locate robustly at the polymer surface, that is, the probability of finding a nanoparticle in the vicinity of the polymer surface is higher than the probability of finding a particle in the bulk. Zhu et al. found that the crystal growth at the surface of amorphous griseofulvin, a small molecule drug, to be 10- to 100-fold faster than that in the bulk, and they suggested the cause to be the molecules at the free surface having higher mobility than bulk molecules.[161]

The APAP loading does not affect the morphology of drug particles formed during recrystallization. The cooling rate is another parameter that may affect the morphology of recrystallized drug particles. To investigate the effect of the cooling rate on recrystallization, 20%APAP-PEO samples were cooled in two different cooling

media: open air (slow cooling) and liquid nitrogen (rapid quenching). Figure 4.15 suggests that different cooling rates lead to different morphologies of recrystallized drug particles. Dispersed drug particles, of several microns in size, are generated in the slowly-cooled samples. On the other hand, for the quenched sample, drug molecules grow into interconnected snowflake-like structures. The morphological difference may be traced to the different nucleation and growth rates of crystallization. The results suggest that the cooling rate does affect the drug particle morphologies and needs to be carefully considered in practice. In some drug-polymer systems, an extremely fast cooling rate may slow down the molecular mobility so much that the recrystallization becomes almost undetectably slow. Apparently this is not the case for the APAP-PEO system, a fact which may be due to the extremely low glass transition temperature of PEO (-56.6 ^{o}C).

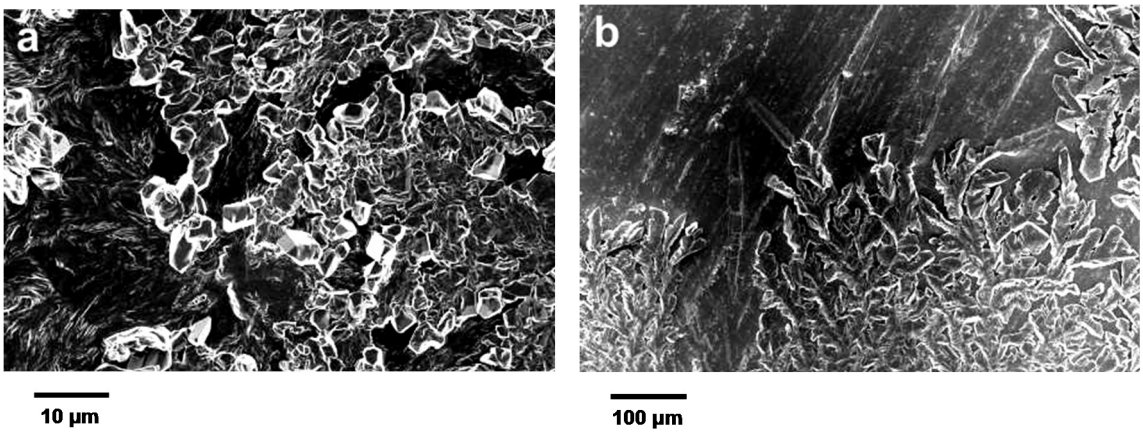

Figure 4.15 SEM images of 20%APAP-PEO cooled in different media: (a) Air and (b) Liquid N_2.

APAP recrystallization also happens in APAP-nanoclay-PEO ternary mixtures and the recrystallized APAP is of the same size range as in APAP-PEO binary mixtures (Figure 4.16). It is unknown at this point whether the ternary system forms a microcomposite, an intercalated nanocomposite, or an exfoliated nanocomposite due to the lack of characterization instruments such as small angle X-ray scattering (SAXS) and

transmission electron microscope (TEM). It is suspected that a microcomposite was formed since no significant change was observed in the X-ray diffraction (XRD) results as shown in Figure 4.17. TEM is often used to detect the size of the clay particles and the silica layers (Figure 2.18 and 2.19). It is difficult for SEM to perform the same duty and that is the reason why the morphologies of APAP-PEO and APAP-nanoclay-PEO show little difference.

In summary, SEM results are consistent with the DSC and DMTA results that above 10%, APAP will recrystallize from PEO. Thus, from a recrystallization point of view, the results indicate a maximum room temperature solubility of APAP in PEO of 10%. The size and the shape of the recrystallized APAP particles are independent of the drug loading. However, the cooling rate does affect the drug particles' morphology to some extent.

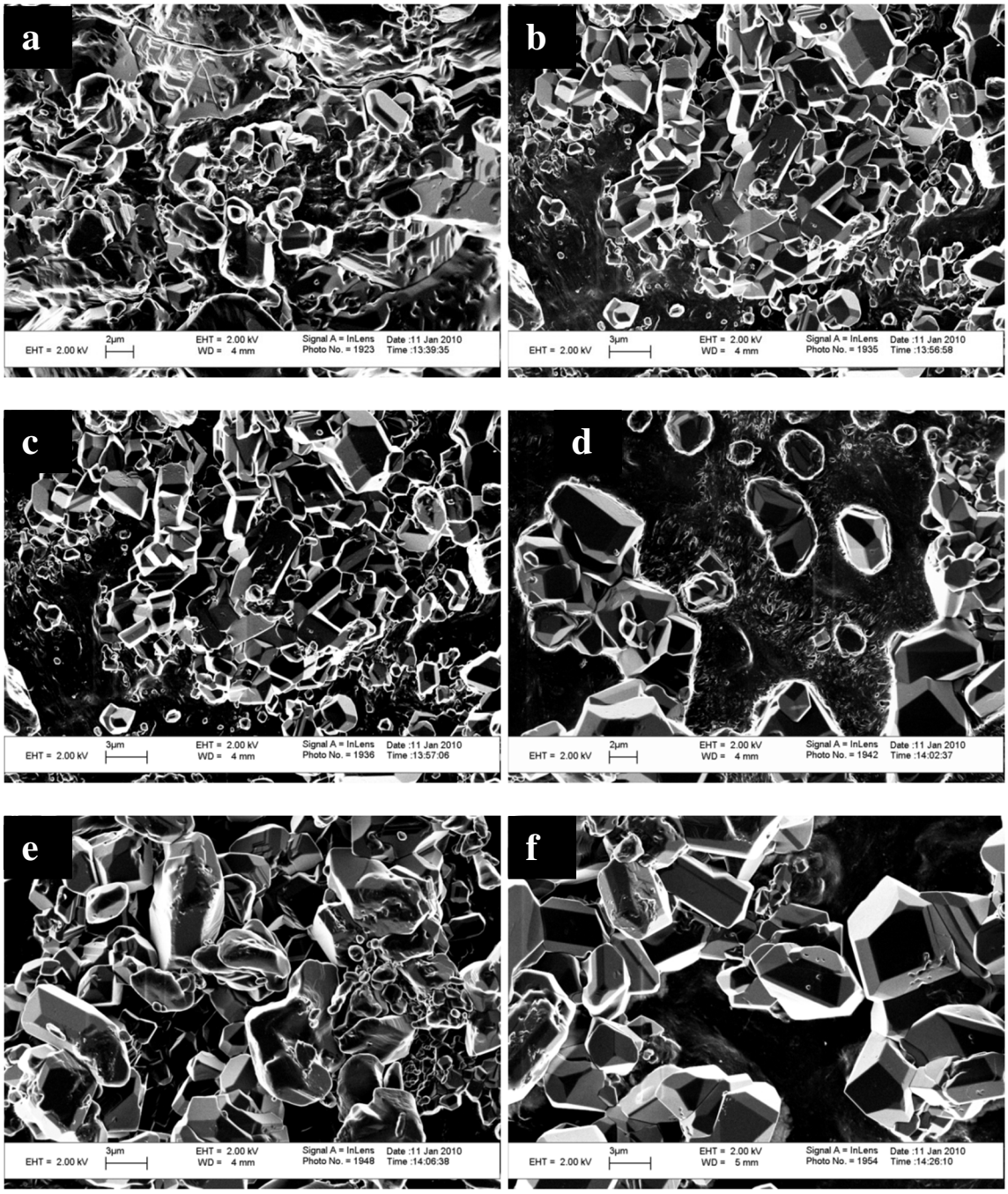

Figure 4.16 SEM images of the surface of (a)10%APAP-10%Cloisite15A (b) 10%APAP-10%Cloisite30B (c) 20%APAP-10%Cloisite15A (d) 20%APAP-10%Cloisite30B (e) 30%APAP-10%Cloisite15A and (f) 30%APAP-10%Cloisite30B-PEO ternary mixtures after being stored for 6 months.

4.2.3 Detection of Recrystallization via X-ray Diffraction (XRD)

Samples with 20 and 30 wt% APAP share the same XRD patterns. Figure 4.17 shows the XRD spectra of the binary and ternary APAP-PEO mixtures with 30% drug loading. The solid state of APAP has been intensively investigated.[112, 163] In this study, APAP exists in monoclinic form in all samples. Consistent with the SEM observations, APAP quickly recrystallizes within the first day of storage, after which the recrystallization becomes extremely slow, supporting the results discussed above on the second stage of recrystallization. APAP crystalline peaks in samples with 10 wt% APAP, on the other hand, are very weak and it is difficult to draw any conclusions regarding the recrystallization rate (spectra not shown). This, despite the fact that there is evidence of very slow recrystallization at that concentration, may be related to the sensitivity of the XRD. The detection limit of XRD is about 5% of crystalline material.

Adding nanoclays into the APAP-PEO mixture dramatically accelerates the recrystallization process of APAP (Figure 4.17b-c). Among all the modified Cloisite® series nanoclays, Cloisite® 15A is the most hydrophobic and Cloisite® 30B the most hydrophilic (Figure 2.15). Cloisite® 15A is often found to form intercalation nanocomposites (Figure 2.18) while Cloisite® 30B forms exfoliated nanocomposites (Figure 2.21). However, the hydrophobicity and structural difference do not appear to play a significant role since the nanoclays have essentially an identical effect on the APAP's recrystallization. Nanoclay particles act as nucleation agents and allow the APAP recrystallization process to complete within a much shorter time. No further change in APAP's solid state is observed during the next sixty days, based on the results from XRD and SEM. The finding suggests that nanoclays can potentially be employed to

prepare more stable tablets at the concentration which is dictated by the ambient temperature solubility.

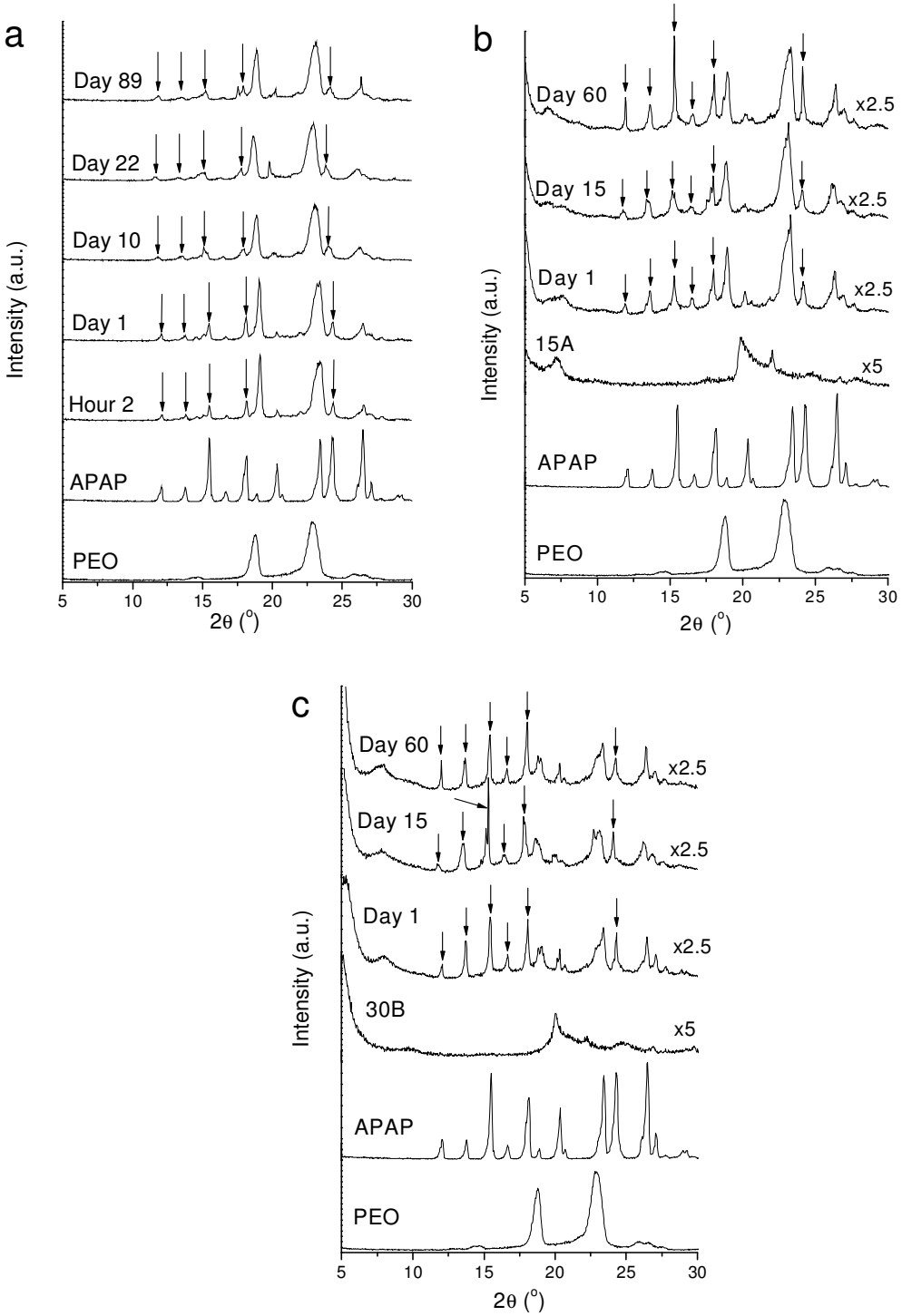

Figure 4.17 XRD spectra of (a) 30%APAP; (b) 30%APAP10%Cloisite15A and (c) 30%APAP10%Cloisite30B-PEO.

It should be mentioned that nanoclays can also affect the polymer's crystallization rate to various degrees, depending on the polymer-nanoclay system. For example, the addition of silicate layers can induce hetero-phase nucleation and promote the growth of polyamide crystallites.[164] Another study has shown that the crystallization kinetics of polyamide nanocomposites increase only when clay concentrations are very low, while high clay loadings retard the crystallization by restricting lamellae coarsening in PEO.[165] The clay particles act as a nucleating agent for maleic anhydride grafted polypropylene, but do not influence the linear growth rate of spherulites or overall crystallization rate significantly.[166] The APAP-nanoclay-PEO is a more complicated system comprising several phases, including layered silicate, amorphous APAP and PEO regions, crystalline PEO regions and crystalline APAP regions.

4.3 Room Temperature Solubility Prediction using the Flory-Huggins Theory

4.3.1 Theoretical Background

This section of the thesis work aims at the theoretical prediction of the drug's solubility in the polymer excipient and, especially, the understanding of the material parameters that influence the solubility. The polymer is regarded as a viscous solvent and the solubility of a solid drug in a polymer is described by the mixture phase equilibrium equation[167] below.

$$\ln x_1 a_1 = -\frac{\Delta_{fus} H}{RT}[1-\frac{T}{T_m}] - \frac{1}{RT}\int_{Tm}^{T} \Delta C_p dT + \frac{1}{R}\int_{Tm}^{T} \frac{\Delta C_p}{T} dT \qquad (4.3)$$

Here, x_1 is the saturation mole fraction of a solid drug in the polymer, a_1 is the activity coefficient of the drug in the polymer at the solubility limit, T_m is the drug's melting temperature, T is the designated temperature of interest (300 K, i.e., room

temperature, in the current study), $\Delta_{fus}H$ is the drug's heat of fusion at the melting point, R is the universal gas constant, and ΔC_p is the heat capacity difference between solid and liquid drug ($\Delta C_p = C_p^L - C_p^S$). Herein, liquid drug refers to the amorphous drug. ΔC_p is a function of temperature and the data can be found in the early literature.[11] Considering that ΔC_p does not change significantly in the temperature range of interest, it is assumed to be constant and Equation (4.3) can be rewritten as Equation (4.4).

$$\ln x_1 a_1 = -\frac{\Delta_{fus}H}{RT}[1-\frac{T}{T_m}] - \frac{\Delta C_p}{R}[1-\frac{T_m}{T}+\ln(\frac{T_m}{T})] \tag{4.4}$$

It is necessary to know the activity coefficient a_1 in order to calculate the molar solubility x_1. Based on the Flory-Huggins lattice theory, the activity coefficient of APAP is given by Equation (4.5).

$$\ln a_1 = \ln\frac{\phi_1}{x_1} + (1-\frac{1}{m})\phi_2 + \chi\phi_2^2 \tag{4.5}$$

Here, ϕ_1 is the volume fraction of the drug, ϕ_2 is the volume fraction of the polymer, m is the molar volume ratio of a polymer molecule to a drug molecule, and χ is the Flory-Huggins interaction parameter. Assuming the molar volume of the repeating unit in PEO is equal to the molar volume of APAP, that is, a drug molecule (○) occupies the same size of the grid as a segment of a polymer (●) does as in Figure 1.14, relationships between ϕ_1, ϕ_2 and x_1 are expressed by Equation (4.6)

$$\phi_1 = \frac{x_1}{x_1 + m(1-x_1)} \text{ and } \phi_2 = \frac{m(1-x_1)}{x_1 + m(1-x_1)} \tag{4.6}$$

The drug's solubility at a specific temperature can be calculated using Equations (4.3-4.5) when the value of χ is known. The interaction parameter χ can be calculated from melting point depression experiments, which have been widely applied to study

polymeric mixtures.[168-170] Similarly, the melting point of the drug in the presence of polymer can be described using Equation (4.7):

$$\frac{1}{T_m^{mix}} - \frac{1}{T_m} = \frac{-R}{\Delta_{fus}H}[\ln\phi_1 + (1-\frac{1}{m})\phi_2 + \chi\phi_2^2] \qquad (4.7)$$

T_m is the melting point of the pure drug, while T_m^{mix} is the melting point of the drug mixed with a polymer. The values of T_m^{mix} at different compositions have been determined from high temperature solubility measurements previously, thereby the interaction parameter χ can be obtained by fitting $[(\frac{1}{T_m^{mix}} - \frac{1}{T_m})\frac{\Delta_{fus}H}{-R} - \ln\phi_1 - (1-\frac{1}{m})\phi_2]$ linearly with ϕ_2^2.

4.3.2 Theoretical Calculation of APAP's Solubility in PEO

Figure 4.18 is a replot of Figure 4.8 showing the melting points of APAP at different polymer concentrations. It is worthwhile to point out that these APAP-PEO samples were melt-mixed using a Brabender mixer. As a result, the size of the undissolved dispersed APAP phase (Figure 4.14) becomes much smaller than the size of the original drug particles (Figure 2.5), which allows the sample to reach equilibrium much faster during heating in DSC. In other words, a faster heating rate, as compared to the typical slow scanning rate needed for T_m^{mix} determination,[70-73] can be used. Increasing the scanning rate not only saves experimental time, but also, more importantly, prevents the drug from thermal degradation. In this thesis work, a 10 ^{o}C/minute heating rate was used in DSC to determine the T_m^{mix} as explained in Chapter 4.1.3.

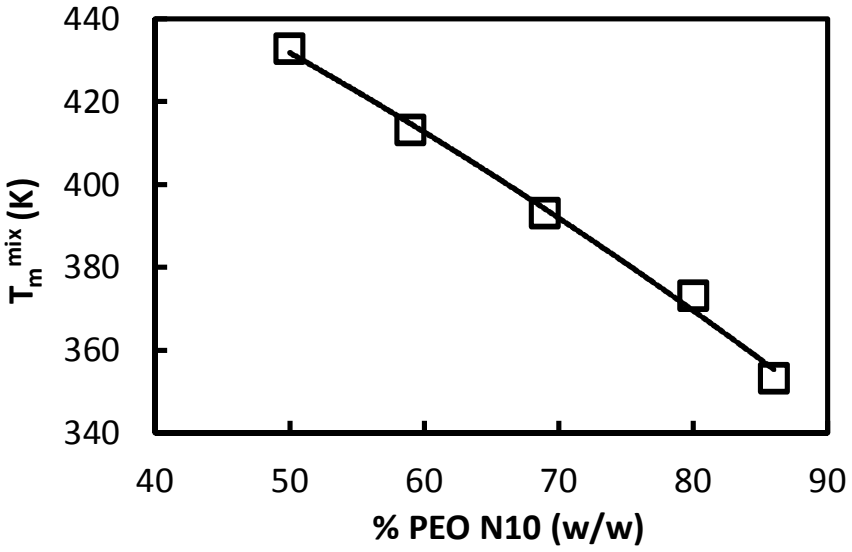

Figure 4.18 Melting point of APAP-PEO mixtures T_m^{mix} (□) with different weight percentage of PEO.

The T_m^{mix} of 86, 80, 69, 59, and 50 PEO wt% are 353, 373, 393, 413 and 432.74 K, respectively. The melting point and $\Delta_{fus}H$ values of pure APAP are determined from DSC and are 446.17 K and 29372.3 J/mol, respectively. The polymer-drug molar volume ratio *m* is 757 as calculated below:

$$m = \frac{\text{molar volume (PEO)}}{\text{molar volume (APAP)}} = \frac{\text{MW/density (PEO)}}{\text{MW/density (APAP)}} = \frac{100{,}000 g/mol / 1.13 g/cm^3}{151.17 g/mol / 1.293 g/cm^3} = 757$$

After substituting all the variables into Equation (4.7), $(\frac{1}{T_m^{mix}} - \frac{1}{T_m})\frac{\Delta_{fus}H}{-R} - \ln\phi_1 - (1-\frac{1}{m})\phi_2$ values were plotted against ϕ_2^2 (Figure 4.19). The slope of the linear-fitted curve gives the χ value of -1.65 with R^2 of 0.970. The drug's solubility at 300 K was calculated from Equations (4.4-4.6) by using χ = -1.65 and ΔC_p = 107 J/(mol·K).[11]

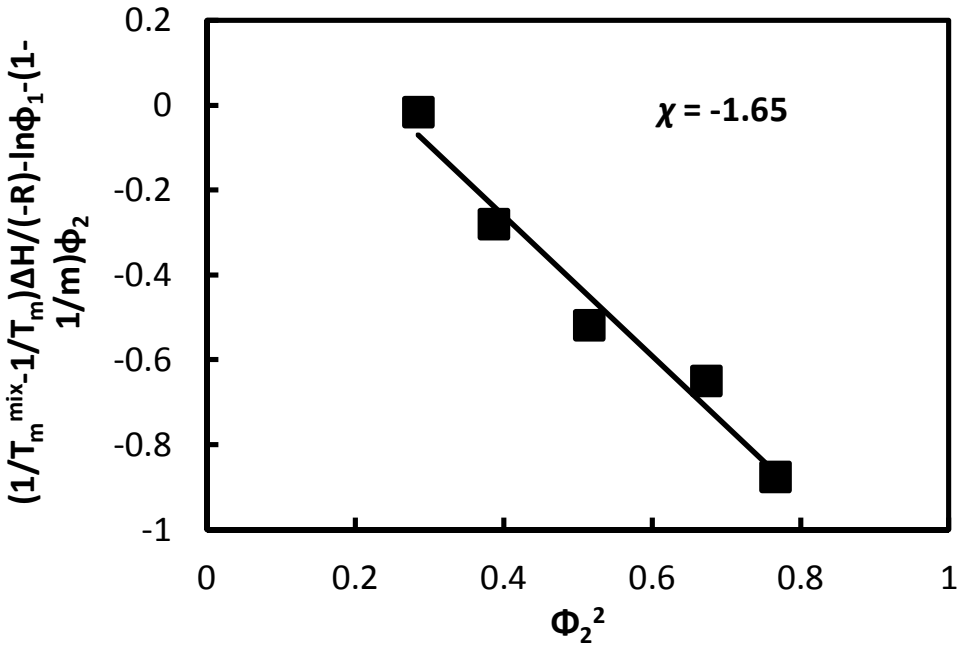

Figure 4.19 Plot of Equation (4.7) for the APAP-PEO system.

The APAP's mole solubility x_1 is calculated to be 98.9 mol% and the weight solubility w_1 is 11.7 wt% at 300 K. It should be emphasized that 11.7 wt% is the solubility in the amorphous portion of PEO. It is believed that much less APAP can be dissolved in crystalline PEO, if there is any, than in its amorphous portion.[171] For example, gas transport properties in a semi-crystalline polymer such as PEO are usually modeled by assuming that the crystals act as an impermeable dispersed phase imbedded in a permeable amorphous phase.[172] Assuming there is no APAP molecule dissolved in the crystalline regions of PEO, the overall solubility is reduced to 2.3% considering the fact that the crystallinity of PEO is around 80% for the PEO used, as determined experimentally using DSC. The apparent solubility after a month at room temperature was measured to be less than 10% based on previous DSC, DMTA, SEM and XRD results. Lower calculated theoretical solubility suggests that the system may still have not

reached equilibrium after one month. Nevertheless, the theoretical and apparent solubility from experiments are still close. The model was also used to calculate APAP's solubility in liquid PEG, which was compared to the obtained experimental data. The results will be presented in a later section.

4.3.3 Free Energy of Mixing: Entropic and Enthalpic Effects

The Flory-Huggins theory[78, 79] is a natural extension of regular solution theory for monomeric liquids to systems involving polymers in the amorphous state. It is a celebrated and successful molecularly-based model giving a convenient framework for describing the thermodynamic properties of polymer solutions and molten polymer mixtures. It represents the volume of a polymer system as a lattice which is divided into microscopic sites of the same volume (Figure 1.14). In the APAP-PEO system, one drug molecule is assumed to occupy one site, while a polymer molecule occupies *m* sites. The entropy of mixing of a drug-polymer system is smaller than that of a drug-small molecule system because there are fewer ways in which the same number of lattice sites can be occupied by polymer segments than by small molecules. In other words, mixing of large molecules involves smaller entropy of mixing, which is unfavorable for mixing. The free energy of mixing ΔG_m for a drug-polymer system can be described by Equation (4.8).

$$\frac{\Delta G_m}{RT} = N_1 \ln \phi_1 + N_2 \ln \phi_2 + \chi N_1 \phi_2 \tag{4.8}$$

Here, N_1 is the number of moles of the drug, N_2 is the number of moles of the polymer, ϕ_1 is the volume fraction of the drug, ϕ_2 is the volume fraction of the polymer, R is the universal gas constant and T is the designated temperature of interest. The first

two terms on the right hand side represent the entropy of mixing, while the third term stands for the enthalpy of mixing.

To investigate the entropic effect on the free energy of mixing, $\Delta G_m/RT$ *vs.* the composition at different m values were plotted (χ is fixed at -1.65) in Figure 4.20. The value m = 757 represents the PEO used, while m values of 48 and 3 are estimated using PEO's low molecular weight analog PEGs with MW of 6000 and 400 g/mol, respectively. The calculation results suggest that $\Delta G_m/RT$ varies only slightly with m, with $\Delta G_m/RT$ (m = 757) > $\Delta G_m/RT$ (m = 48) > $\Delta G_m/RT$ (m = 3). In other words, the change of ΔG_m is not significant when the MW of the polymer changes from 100,000 to 400 g/mol.

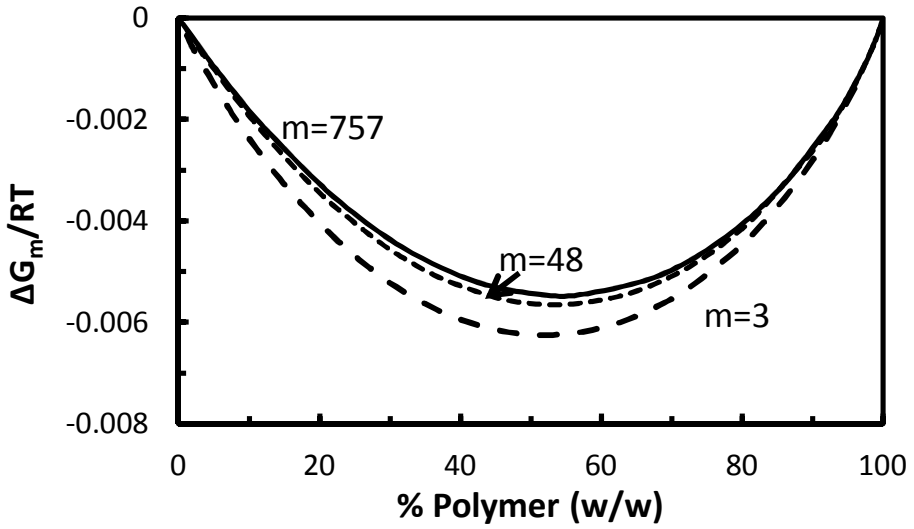

Figure 4.20 Free energy of mixing $\Delta G_m/RT$ *vs.* weight percentage of polymer as predicted using the Flory-Huggins theory with different polymer-drug volume ratios m. Curves from top to bottom are for m = 757 (PEO used), 48 (PEG 6000) and 3 (PEG 400) (χ = -1.65).

The Flory-Huggins interaction parameter χ characterizes the excess energy of interaction in solution per one molecule of the solvent. The curves of $\Delta G_m/RT$ *vs.* mixture composition at different χ value are plotted in Figure 4.21 (m is now fixed at 757). The

results show that the Gibbs free energy of mixing increase significantly with increasing χ. $\Delta G_m/RT$ is even positive in part of the $\chi = 2$ curve, suggesting poor miscibility of drug and polymer. Negative χ, on the other hand, leads to lower $\Delta G_m/RT$ and, consequently, better miscibility between the drug and polymer. By comparing Figure 4.20 with Figure 4.21, it seems that the polymer-drug interaction parameter plays a more important role in the polymer-drug miscibility compared to that of the polymer MW. However, it should be mentioned that the drug's solubility in the polymer cannot be determined directly from $\Delta G_m/RT$. Thus, a direct calculation of drug's solubility in polymers of different MW and χ will be given in a later section.

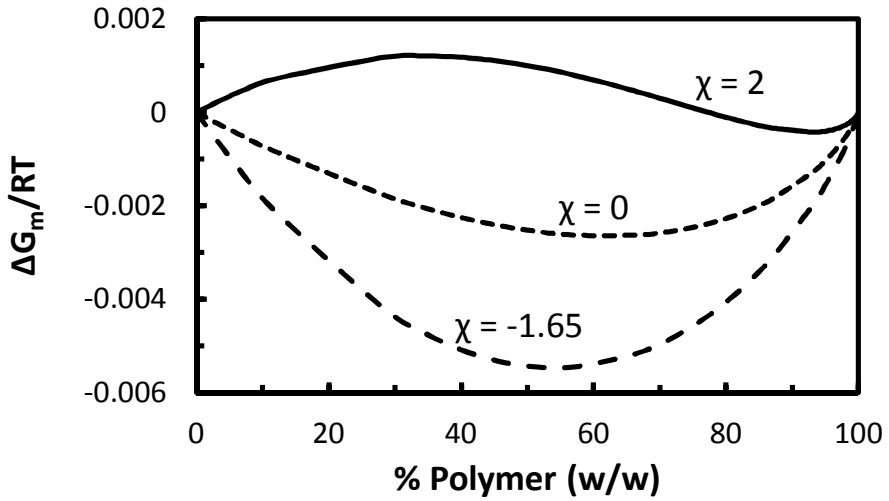

Figure 4.21 Free energy of mixing $\Delta G_m/RT$ *vs.* weight percentage of polymer as predicted using the Flory-Huggins theory with different interaction parameters χ. Curves from top to bottom are for $\chi = 2$, 0 and -1.65 ($m = 757$).

4.3.4 Enthalpic and Entropic Effect on the Drug's Melting Point Depression

As mentioned above, χ is a critical parameter which affects the miscibility of a polymer and a drug. However, it is difficult to theoretically predict its value. Hence, it is of interest to find out whether there are any simple experiments that help to compare the

interaction parameters of a drug with different polymers. Figure 4.22 shows the curves of the melting temperature of the drug *vs.* polymer loading at different interaction parameters based on Equation (4.7), which suggests that the melting point depression is sensitive to the χ value. In other words, the melting point depression may be used experimentally for determination of the χ value and use it as a practical indicator for polymer selection to a given API. Similarly to the impact on $\Delta G_m/RT$, the polymer MW shows only a small effect on the melting depression (Figure 4.23).

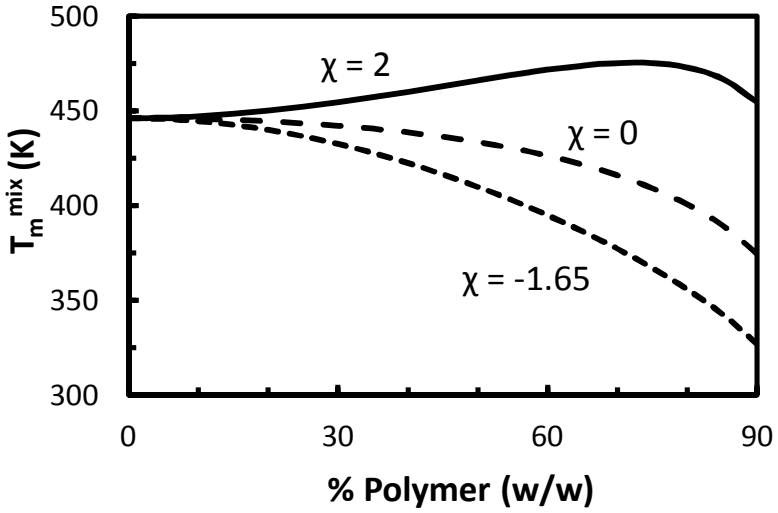

Figure 4.22 Melting point depression *vs.* weight percentage of polymer. The temperature curves are calculated using Equation (4.7) with χ = 2, 0 and -1.65 from top to bottom (*m* = 757).

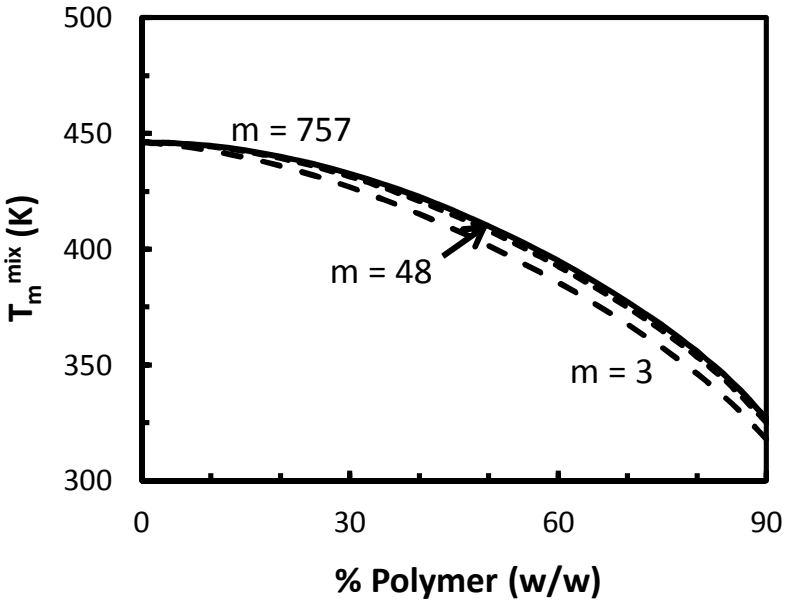

Figure 4.23 Melting point depression *vs.* weight percentage of polymer. The temperature curves are calculated using Equation (4.7) with *m*= 757 (PEO used), 48 (PEG 6000) and 3 (PEG 400) from top to bottom (χ = -1.65).

4.3.5 Effect of Polymer MW and χ on APAP's Solubility in PEO/PEG Excipients

Assuming that χ as measured from the melting point depression of APAP in PEO N10 could be extended to estimate the χ in PEG 400 because of the same molecular structure of the PEO and PEG, the APAP's solubility in PEG 400 (M_w = 400 g/mol) at 300K was calculated to be 14.6 wt% by using the same χ of -1.65. The predicted solubility of APAP in PEO N10 (M_w = 10^5 g/mol) is less than that in PEG 400, which is caused by the reduced entropic contribution to the mixing in the PEO N10 system. Therefore, attempts to estimate the solubility of a drug in a polymer by measuring solubility in a low molecular weight analogue of the polymer need to be corrected accordingly to avoid overestimating the solubility.[73] The analysis specifies how to avoid this.

In an attempt to verify the validity of this method, the solubility of APAP was measured in liquid PEG 400 and the result was 17.1%. Thus, the theoretical and

experimental solubilities are close, suggesting that the χ value calculated from the melting point depression method is a reasonable estimate.

To understand the broader impact of χ, which is represented by the polymer chemistry, and polymer MW on the drug's solubility, the drug's solubilities at different χ and *m* values were calculated and are given in Table 4.2. The χ values used here are from drug-polymer pairs, including indomethacin-PVP (χ = -1.83), nifedipine-PVP (χ = -0.81), and ketoconazole-PVP (χ = -0.12).[71] The results show that the solubility decreases by an order of magnitude when χ increases from -1.83 to -0.12, while the very low MW polymer (MW=400) only leads to 24-36% higher drug solubility as compared to large MW analogue (MW=100,000). It should be noted that process requirements often limit the usage of the MW of polymer excipients. Low MW PEG in this case is a liquid and cannot be used as the major excipient for solid dosage, while extremely high MW may cause difficulty for processing due to high viscosity. Hence, one should focus on the API-polymer excipient intermolecular interactions rather than the polymer MW to improve drug-polymer miscibility.

Table 4.2 Solubility in Drug-polymer Pairs Calculated Using Various Flory-Huggins Interaction Parameters χ at Different Polymer MW

χ	-1.83	-1.65	-0.81	-0.12
wt% in large MW polymer (m=757)	13.1	11.7	6.2	3.3
wt% in small MW polymer (m=3)	16.2	14.6	8.2	4.5

4.4 Dissolution Testing

The experimentally obtained dissolution rates of APAP-PEO and APAP-nanoclay-PEO are much slower than that of pure APAP powder in a capsule, as shown in Figures 4.24-4.26. It takes less than 30 minutes for powder-form APAP to be fully released into the buffer solution, while it takes melt-mixed APAP-PEO 90 minutes and APAP-nanoclay-PEO more than 360 minutes, an order of magnitude slower than powder form APAP, to be fully dissolved. Thus, the hot-melt mixed APAP-PEO samples are controlled-release formulations. The standard deviation for each release curve was less than 5% and therefore, is not shown.

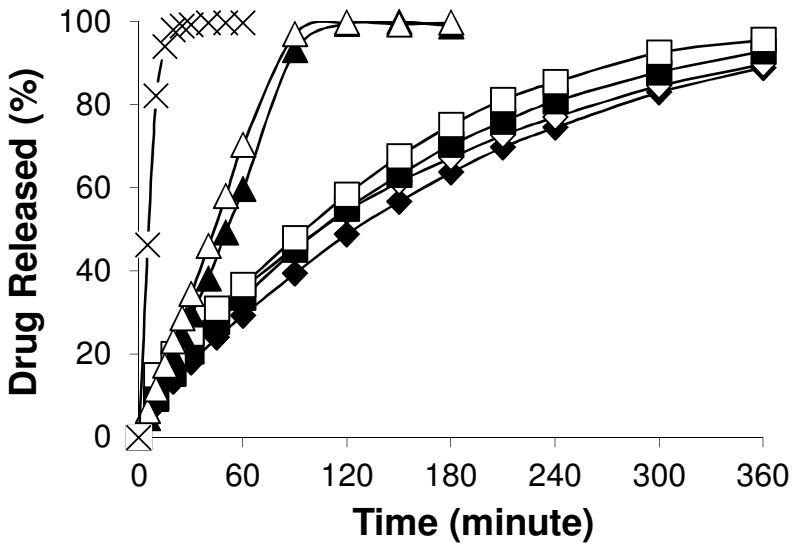

Figure 4.24 Dissolution profiles of (×) APAP powder in capsule, (▲) 10%APAP-PEO-day 1, (Δ) 10%APAP-PEO-day 169, (♦) 10%APAP-10%CL15A-PEO-hour 1, (◊) 10%APAP-10%CL15A-PEO-day 251, (■) 10%APAP-10%CL30B-PEO-hour 1, (□) 10%APAP-10%CL30B-PEO-day 251.

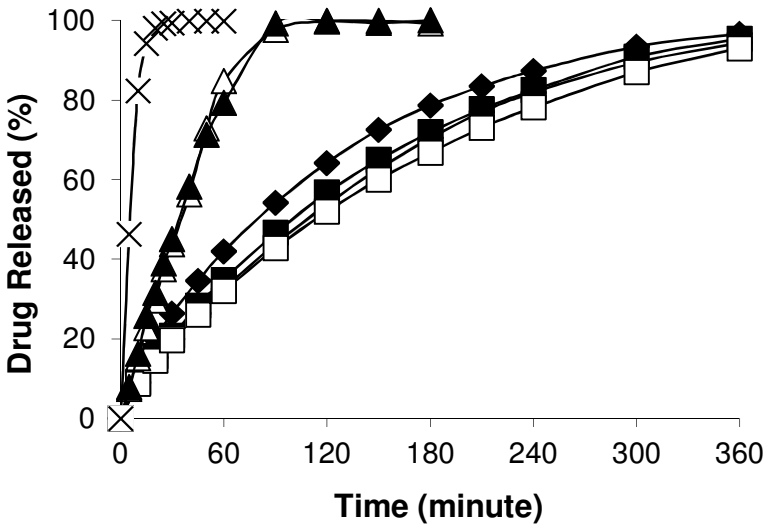

Figure 4.25 Dissolution profiles of (×) APAP powder in capsule, (▲) 20%APAP-PEO-hour 1, (Δ) 20%APAP-PEO-day 160, (♦) 20%APAP-10%CL15A-PEO-hour 1, (◊) 20%APAP-10%CL15A-PEO-day 212, (■) 20%APAP-10%CL30B-PEO-hour 1, (□) 20%APAP-10%CL30B-PEO-day 212.

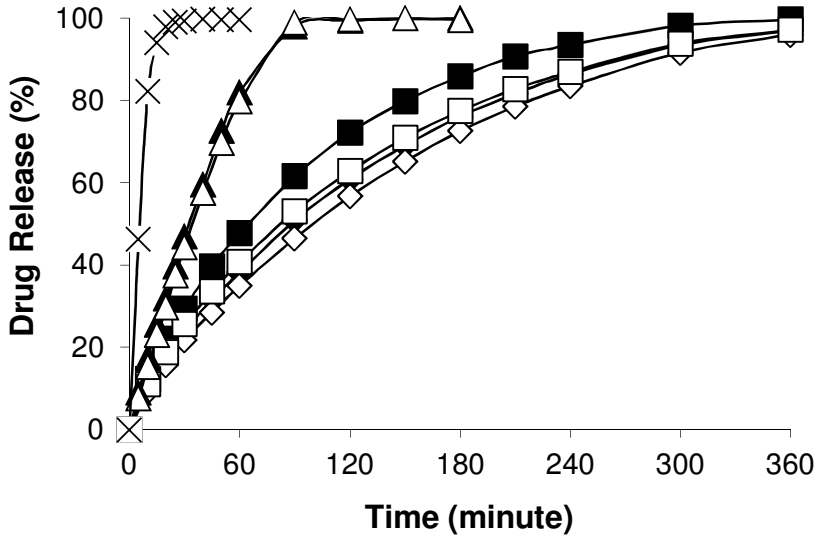

Figure 4.26 Dissolution profiles of (×) APAP powder in capsule, (▲) 30%APAP-PEO-hour 1, (Δ) 30%APAP-PEO-day 148, (◆) 30%APAP-10%CL15A-PEO-hour 1, (◊) 30%APAP-10%CL15A-PEO-day 213, (■) 30%APAP-10%CL30B-PEO-hour 1, (□) 30%APAP-10%CL30B-PEO-day 213.

Storage time shows little impact on the dissolution rate (Figures 4.24-26). For example, the Figure shows that the drug release profile on day 1 is essentially the same as that on day 169 for sample 10%APAP-PEO. A couple of facts should be mentioned in discussing this observation: firstly, in all cases, APAP particles never grow into more than several micrometers in size. In other words, the morphology does not change with the storage time. Secondly, PEO does not dissolve quickly but swells into a gel in the aqueous medium. Subsequently, the gel gradually dissolves and by the time it disappears, the drug is fully released. The slow dissolution rate of PEO may thus overshadow any changes in the APAP's dissolution rate during storage.

Diffusion, swelling and erosion are the most important rate-controlling mechanisms of commercially available controlled-release products.[173] In order to understand the mode of drug release from PEO matrices, the data (M_t/M_∞) are fitted using the following power law expression:[174-177]

$$\frac{M_t}{M_\infty} = kt^{n'} \tag{4.9}$$

M_t, M_∞, k and n' are, respectively, the amounts of drug released at time t, the absolute cumulative amount of drug released at infinite time, a constant incorporating the structural and geometric characteristics of the release device, and the exponent of the release kinetics. This semi-empirical equation was used to analyze the first 60% of a release curve ($M_t/M_\infty \leq 60\%$). The values of n' were obtained by fitting drug release data to Equation (4.9) using the ordinary least square regression (values ± 95% confidence limits) provided by software Polymath 5.1 (Polymath software, Willimantic, CT). It is widely accepted that for a disc, n' = 0.5 suggests a diffusion-controlled release

mechanism and, zero order drug release (n' = 1.0) indicates an erosion-controlled release mechanism. Anomalous transport leads to a value between 0.5 and 1.[175, 178]

Table 4.3 Fitting Results for Equations (4.9) and (4.10). In All Cases R^2 Is Greater Than 0.99

Sample	Power Law[174-177] $\frac{M_t}{M_\infty} = kt^{n'}$	Peppas and Sahlin[179, 180] $\frac{M_t}{M_\infty} = k_1 t^{0.5} + k_2 t$	
	n' ± 95% CI	k_1 (% $min^{-0.5}$) ± 95% CI	k_2 (% min^{-1}) ± 95% CI
10%APAP-PEO-day 1	1.02 ± 0.01	-0.16 ± 0.29	1.01 ± 0.05
20%APAP-PEO-hour 1	0.89 ± 0.06	1.40 ± 1.11	1.25 ± 0.21
30%APAP-PEO-hour 1	0.89 ± 0.03	1.57 ± 0.61	1.26 ± 0.12
10%APAP-10%CL15A-PEO-hour 1	0.71 ± 0.02	2.13 ± 0.26	0.21 ± 0.03
10%APAP-10%CL15A-PEO-day 251	0.56 ± 0.03	4.16 ± 0.29	0.07 ± 0.03
10%APAP-10%CL30B-PEO-hour 1	0.70 ± 0.01	2.63 ± 0.37	0.21 ± 0.04
20%APAP-10%CL15A-PEO-hour 1	0.67 ± 0.03	3.66 ± 0.61	0.21 ± 0.07
20%APAP-10%CL15A-PEO-day 212	0.71 ± 0.01	2.44 ± 0.24	0.22 ± 0.02
20%APAP-10%CL30B-PEO-hour 1	0.72 ± 0.02	2.63 ± 0.47	0.23 ± 0.05
30%APAP-10%CL15A-PEO-hour 1	0.68 ± 0.01	3.02 ± 0.42	0.24 ± 0.05
30%APAP-10%CL15A-PEO-day 213	0.71 ± 0.02	2.52 ± 0.42	0.25 ± 0.05
30%APAP-10%CL30B-PEO-hour 1	0.69 ± 0.06	3.52 ± 1.07	0.33 ± 0.14

The values of *n*' for APAP release are listed in Table 4.3. It is interesting that the exponent *n*' decreases from 1 for APAP-PEO system to about 0.7 for the APAP-nanoclay-PEO mixtures, indicating that drug release shifts from erosion dominant to anomalous by the addition of nanoclays.

Another power-law based expression developed by Peppas and Sahlin[179, 180] is Equation (4.10) and it can be used to estimate the contributions of drug diffusion and polymer erosion to the anomalous release.

$$\frac{M_t}{M_\infty} = k_1 t^{m'} + k_2 t^{2m'} \tag{4.10}$$

The first term on the right hand side represents the contribution of drug diffusion and the second term the contribution of polymer erosion. The coefficient *m*' is the diffusion exponent for a controlled release device of any geometrical shape exhibiting pure drug diffusion. The value of *m*' for the disc (or film) is 0.5 according to Peppas and Sahlin. Drug release data are fitted to Equation (4.10) using the software Polymath 5.1. k_1 and k_2 are the diffusion and relaxation constants, respectively.

The results show that the APAP diffusion has a much higher contribution to dissolution than polymer erosion ($k_1 >> k_2$) (Table 4.3) for the ternary mixtures. The difference in drug release mode between the binary and ternary mixtures is postulated to be caused by the decrease of wettability with the presence of nanoclays. It should be noted that the nanoclays are modified by the suppliers to improve their compatibility with polymers. The modified clays are more hydrophobic than the original montmorillonite. On the other hand, the contact angle of dissolution medium on the surface of 10%APAP-PEO is found to be 41°, ten degrees smaller than that on the surface of 10%APAP-10%CL15A-PEO or 10%APAP-10%CL30B-PEO. The decrease in wettability brought

by the presence of Cloisite® clays dramatically slows down the dissolution rate of the matrix: for the APAP-PEO system, the full release of APAP and the complete dissolution of matrix occur at the same time, roughly one hour since the sample was immersed in the solution. In comparison, the matrix of the ternary mixture remains intact even after six hours, when all APAP has been released.

4.5 Crystallization of PEO and APAP-PEO

4.5.1 Theoretical Background

4.5.1.1 Nucleation and Growth Kinetics Theories. Spherulitic nucleation and growth kinetics can be analyzed using the kinetic nucleation theory expounded by Hoffman et al.[181-185] Three regimes for nucleation and crystal growth are predicted by this theory caused by different degrees of supercooling. They are represented by the schematic drawings in Figure 4.27.[183, 184] In the Figure, G is the growth rate, L is the substrate length, b_0 is the thickness of the molecular layer, and a_0 is the stem width. The kinetics in each regime are being controlled by the competition between nucleation and growth. In regime I, a single nucleation site takes place on the substrate surface and leads to the substrate length being completely covered by a crystallization growth layer. At a lower temperature (i.e., higher supercooling, ΔT), regime II growth prevails where multiple nucleation sites take place on the substrate. At still larger supercooling ΔT, regime III is entered where nucleation on the substrate is so prolific that the distances between niches sites (S_n in Figure 4.27b) approximate a stem width. An example of three regime experimental crystal growth kinetics is presented in Figure 4.28, which shows growth rate data of polyethylene.[186]

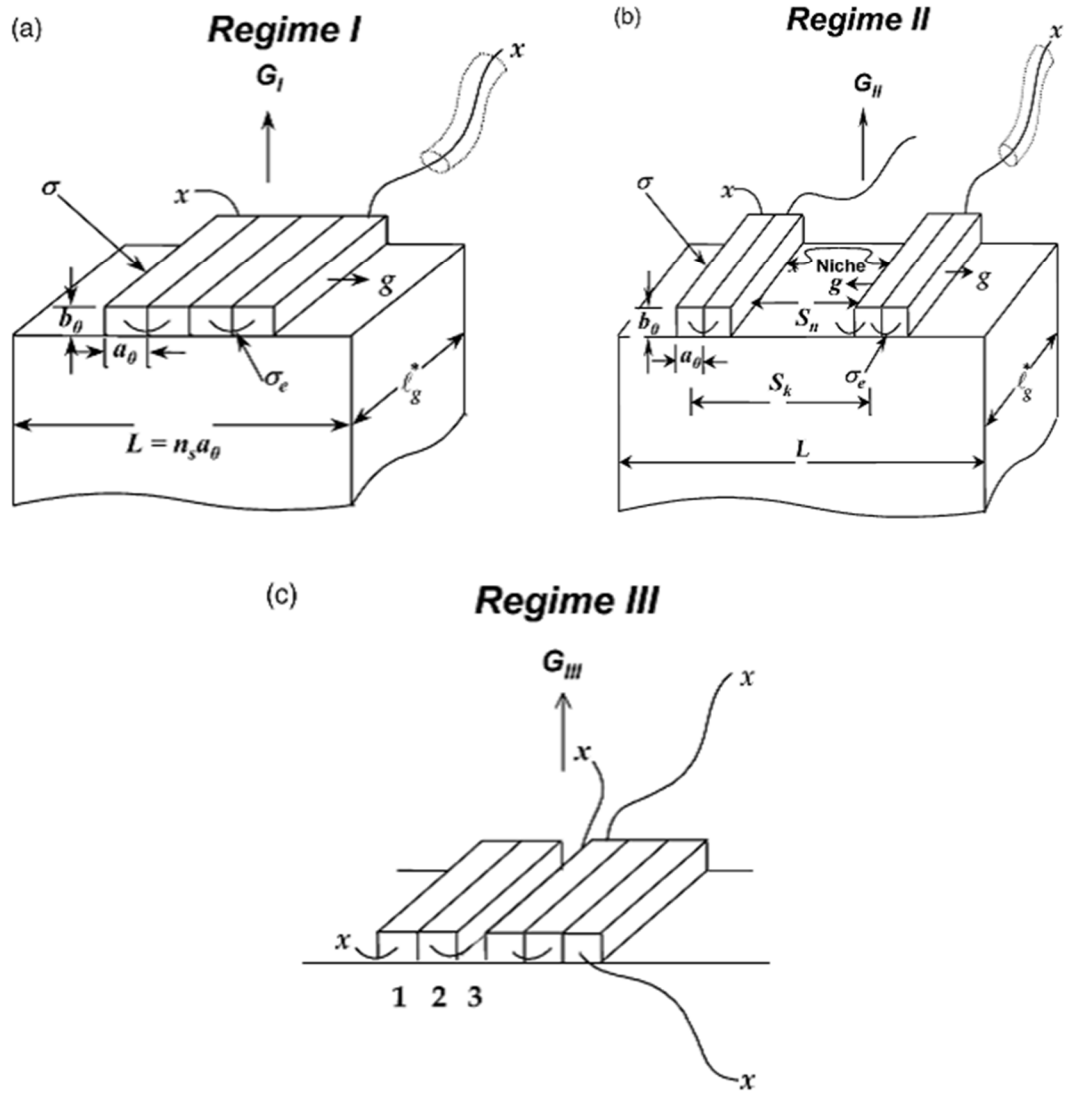

Figure 4.27 Schematic representation of how polymer crystal growth takes place in three regimes: (a) regime (I); (b) regime (II); (c) regime (III) occurring at increasing degree of supercooling.[183, 184]

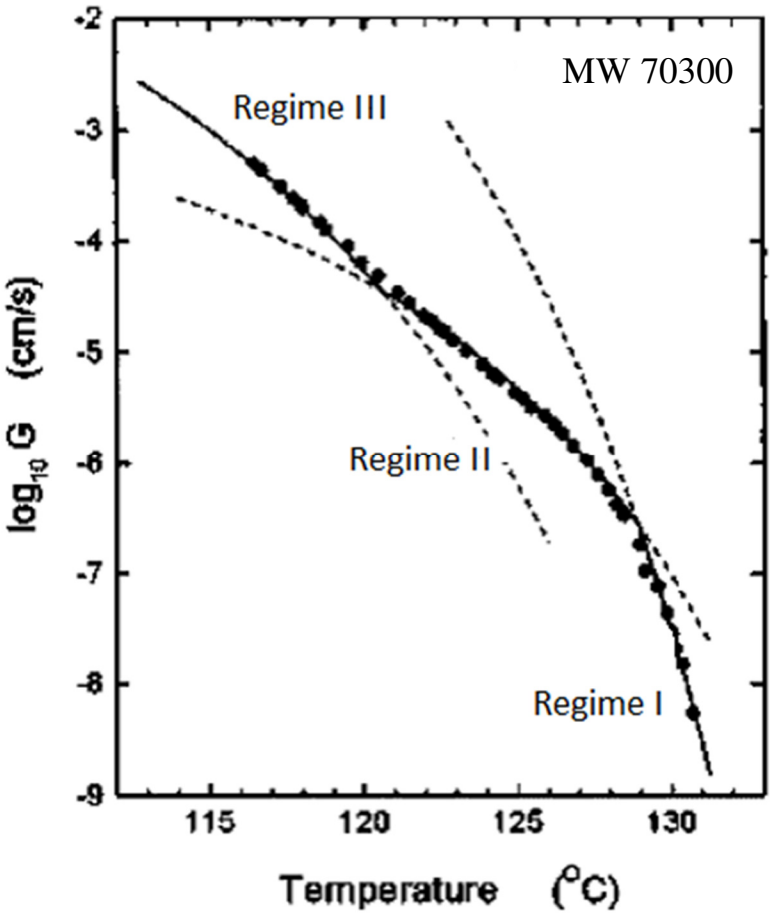

Figure 4.28 Experimentally measured linear crystal growth rate of polyethylene crystallized from the melt.[186]

For each of these regimes, the crystal growth rate is expressed by the following expression based on the Hoffman-Lauritzen (HL) model:

$$G(i) = G_0(\Delta T)\exp(\frac{-U^*}{R(T_c - T_\infty)})\exp(\frac{-K_g(i)}{T_c \Delta T f}) \tag{4.11}$$

where i = I, II or III denotes regimes, ΔT is the degree of supercooling ($T_m^0 - T_c$) with T_m^0 being the equilibrium melting temperature and T_c being the crystallization temperature, U^* is the activation energy needed for "reeling in" the polymer molecules (defined below) from their melt reptation tube,[187] R is the universal gas constant, T_∞ is the temperature below which this type of chain transport ceases (taken as T_g – 30 K), and f is

a temperature correction factor accounting for the change of melting enthalpy with temperature, given by $2T_c/(T_m^0+T_c)$. The pre-exponential term G_0 contains terms that are essentially temperature-independent. Each regime has a nucleation constant $K_g(i)$, and $K_g(\mathrm{I}) = 2\ K_g(\mathrm{II}) = K_g(\mathrm{III})$ with

$$K_g(\mathrm{I}) = \frac{4a_0\sigma\sigma_e T_m^0}{\Delta H_f k} \tag{4.12}$$

where σ is the lateral surface free energy, σ_e is the lamellar fold surface free energy which is related to the difficulty of the chain to perform folding during crystallization, a_0 is the stem width (the lattice distance between adjacent planes) as shown in Figure 4. 27, k is the Boltzmann constant, and ΔH_f is the heat of fusion per crystal unit volume.

Taking the logarithm of Equation (4.11) and rearranging, one obtains

$$\ln G - \ln(\Delta T) + \frac{U^*}{R(T_c - T_\infty)} = \ln G_0 - \frac{K_g}{fT_c\Delta T} \tag{4.13}$$

Kovacs et al.[188-192] have quoted a value of 29.3 kJ/mol for U^* while Hoffman et al.[181] have suggested that U^* has a universal value of 6.28 kJ/mol. Cheng et al. have tried both values for PEO and they preferred the former,[92] and consequently this value is here. The glass transition temperature T_gs of PEO, 2%, 10% and 20%APAP-PEO are -56.6, -45.9, -27.5 and -16.2 ºC, respectively. The equilibrium melting temperature T_m^0 of a polymer crystal is defined as the melting temperature of an "infinite stack" of extended chain crystals, large in directions perpendicular to the chain axis and where the chain ends have established an equilibrium state of pairing.[193] This quantity is one of the most important thermodynamic properties of crystallizable chain polymers, as it is the reference temperature from which the driving force for crystallization is defined. T_m^0 is

determined by extrapolation to the condition of $T_m = T_c$ according to the Hoffman-Weeks (HW) equation[194]

$$T_m = \frac{1}{\gamma'} T_c + (1 - \frac{1}{\gamma'}) T_m^0 \quad (4.14)$$

where γ' is the lamellar thickness factor, which is the ratio of the lamellar thickness to the critical nucleus thickness in the crystallization process. The HW equation is based on the assumption that the difference between crystallization and observed melting temperatures is solely due to the thickening of lamellae formed at the crystallization temperature. Because of its straightforward experimental implementation and its analytical simplicity, this method has been widely and successfully used for the determination of T_m^0 of semi-crystalline polymers.[193, 195-197]

4.5.1.2 Macroscopic Crystallization Kinetics (Avrami Theory). The celebrated Avrami analysis of isothermal crystallization kinetics was originally developed for metals[198-201] and later modified by others, for example, by Evans[202], for polymers. The resultant equation is

$$1 - X(t) = \exp(-K_n t^n) \quad (4.15)$$

where K_n is the overall rate constant for the crystallization process, n is the Avrami exponent and $X(t)$ is the crystallinity of the polymer at time t and is calculated from DSC isothermal exotherms as

$$X(t) = \frac{\Delta_{fus} H_t}{\Delta_{fus} H_\infty} \quad (4.16)$$

where $\Delta_{fus}H_\infty$ and $\Delta_{fus}H_t$ are the enthalpies of fusion on complete crystallization and at time t. n depends on the morphology of the growing crystalline regions, the nucleation

process, and whether growth is controlled by diffusion of polymer through the melt or by attachment to the growth surface. Based on Shultz's summary on the consequence of the Avrami theory (Table 4.4),[203, 204] the case $n = 4$ can only result from spherulitic growth from homogeneous nucleation. The analysis involves plotting $\log[-\ln(1-X(t)]$ as a function of $\log t$ and determining n from the initial slope and K_n from the intercept.

Table 4.4 Interpretation of Avrami Coefficients[204]

Avrami Exponent	Nucleation Type	Growth Geometry	Growth Velocity
½	Instantaneous	Rod	$t^{-1/2}$
1	Instantaneous	Rod	Constant
1	Instantaneous	Disc	$t^{-1/2}$
3/2	Instantaneous	Sphere	$t^{-1/2}$
	Homogeneous	Rod	$t^{-1/2}$
	Instantaneous	Disc	Constant
2	Homogeneous	Disc	$t^{-1/2}$
	Homogeneous	Rod	Constant
5/2	Homogeneous	Sphere	$t^{-1/2}$
3	Instantaneous	Sphere	Constant
	Homogeneous	Disc	Constant
4	Homogeneous	Sphere	Constant

4.5.2 Equilibrium Melting Temperature

The HW equation was used to determine the $T_m^0 s$ of pure PEO as well as the APAP-PEO mixtures prepared by solvent evaporation. The observed melting temperatures, T_m from the DSC 2nd heating are plotted against different crystallization temperatures T_c and shown in Figure 4.29. The values of $1/\gamma$', which are the slopes of the resulting linear curves, are 0.17, 0.18, 0.26, 0.20, 0.39, and 0.52 for PEO, 0.1%, 1%, 2%, 10% and 20%APAP-PEO, respectively. The value of $1/\gamma$' is between 0 ($T_m = T_m^0$ for all T_cs, the most stable crystal morphology) to 1 ($T_m = T_c$, for the case of inherently unstable crystals). The results show that the stability of the PEO crystals decreases dramatically with increasing APAP concentration. The equilibrium melting temperature T_m^0 also

increases with APAP concentration, from 67.1 °C of PEO to 68.0, 69.6, 69.3, 73.0 and 78.1 °C for 0.1%, 1%, 2%, 10% and 20%APAP-PEO, respectively. The shifting trend of T_m^0 is the opposite to that of the miscible polymer blends where T_m^0 decreases with increasing amount of the second polymer.[94, 205, 206] It is also possible that APAP, whose T_m is 170 °C, starts to recrystallize during the process and contributes to the T_m^0 increase.

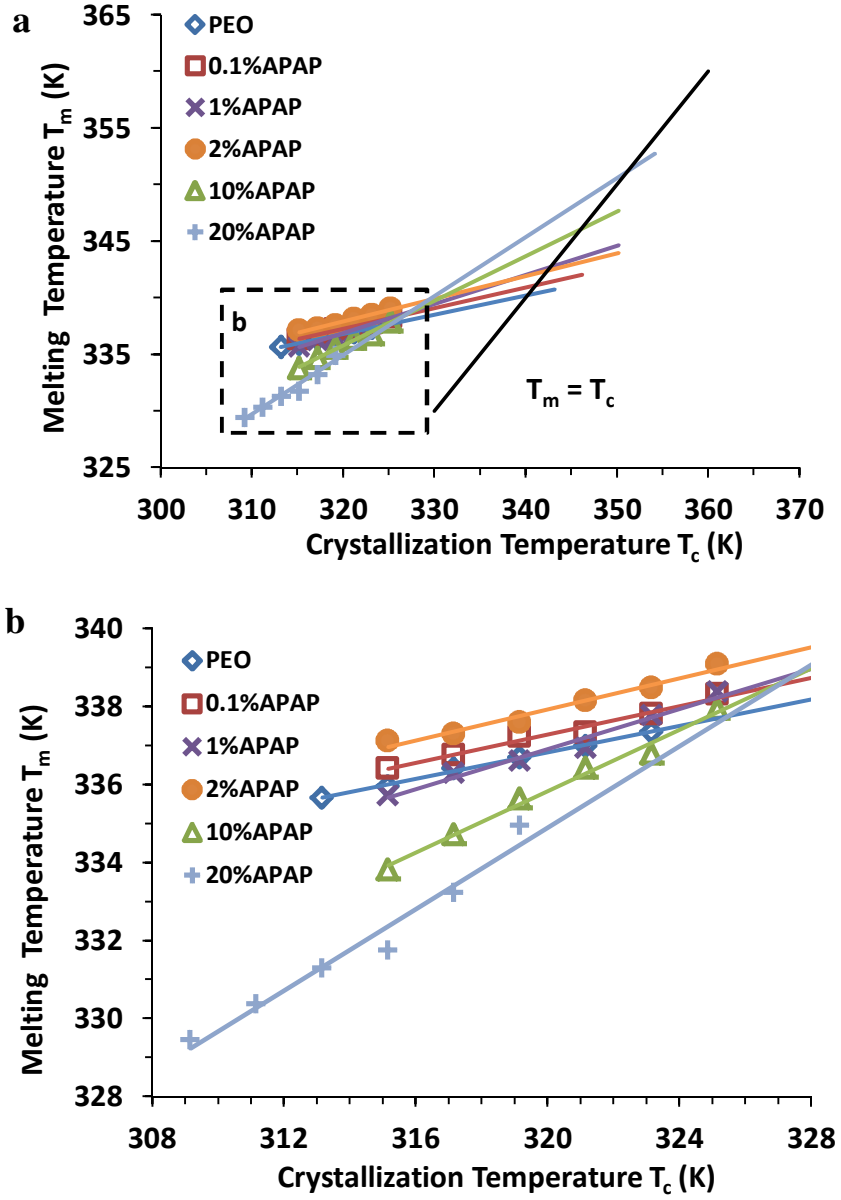

Figure 4.29 Hoffman-Weeks plots for PEO, 0.1%, 1%, 2%, 10% and 20%APAP-PEO. (b) is the zoom in of the rectangle area of (a).

4.5.3 Polarized Optical Microscopy (POM)

PEO, 0.1%, 1% and 10%APAP-PEO have spherulitic morphologies as evidenced by the Maltese cross patterns at T_x of 30 ^oC in Figure 4.30 below. As T_x increases and the supercooling ΔT decreases (T_xs of 40 and 50 ^oC), more amorphous content is formed in the crystals, which makes the texture more open and the Maltese cross patterns weaker. Similar phenomena were observed by previous investigations for PEO (MW = 10,500 g/mol)[92] and PEO (MW = 1,000 g/mol).[207] Figure 4.31 demonstrates the increasing "open" texture and weakening Maltese cross patterns of PEO with increasing crystallization temperature.[92] The apparent complete destruction of spherulite structure for 10%APAP-PEO at 50 ^oC is caused by either inclusion or exclusion of the APAP defects, which will discussed in details later.

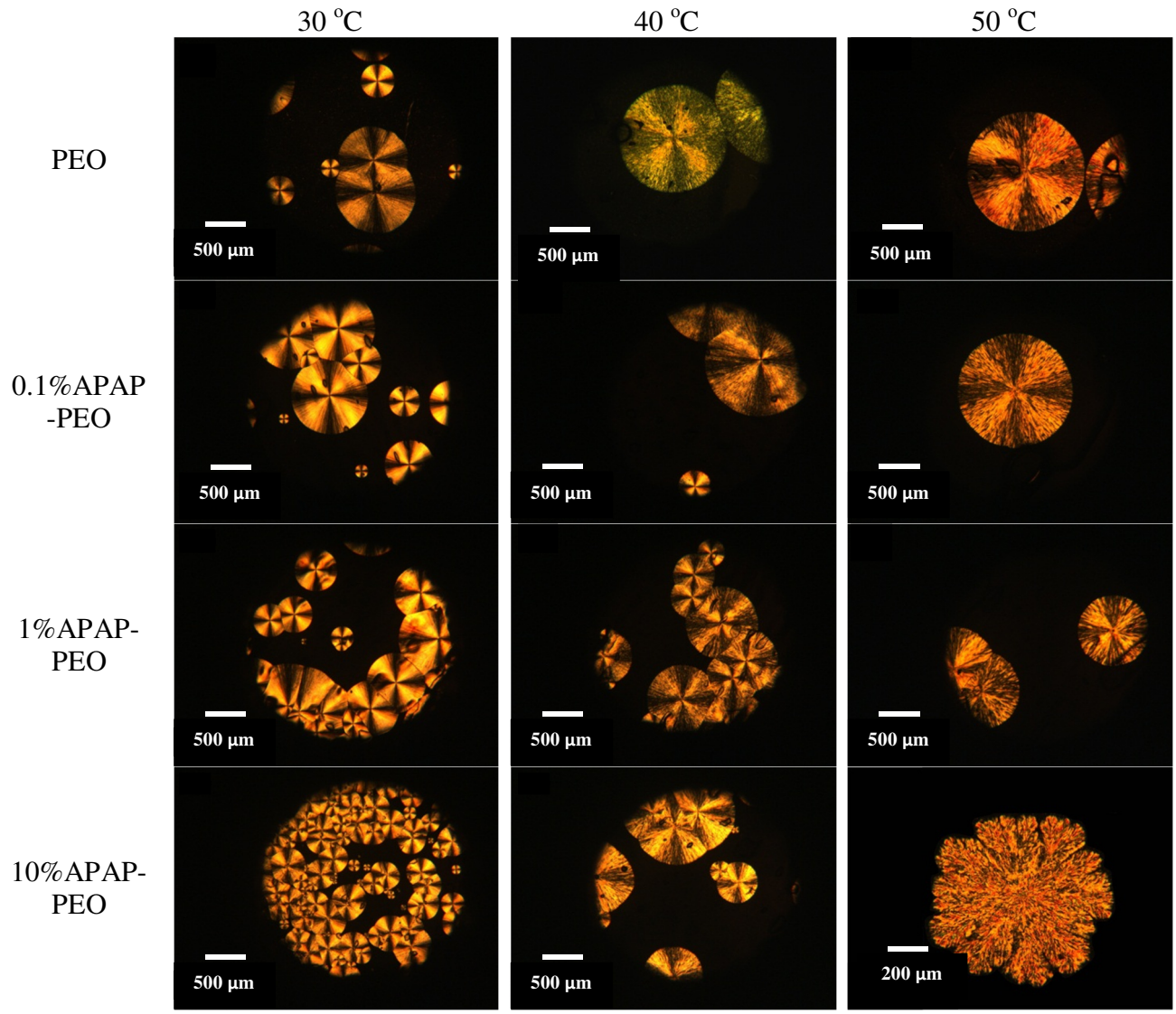

Figure 4.30 Polarized optical micrographs of spherulites at T_x of 30, 40 and 50 °C for PEO, 0.1%, 1% and 10% APAP-PEO. The POM field of view in pictures with 500 µm scale bar is a circle with diameter of 2.4 mm.

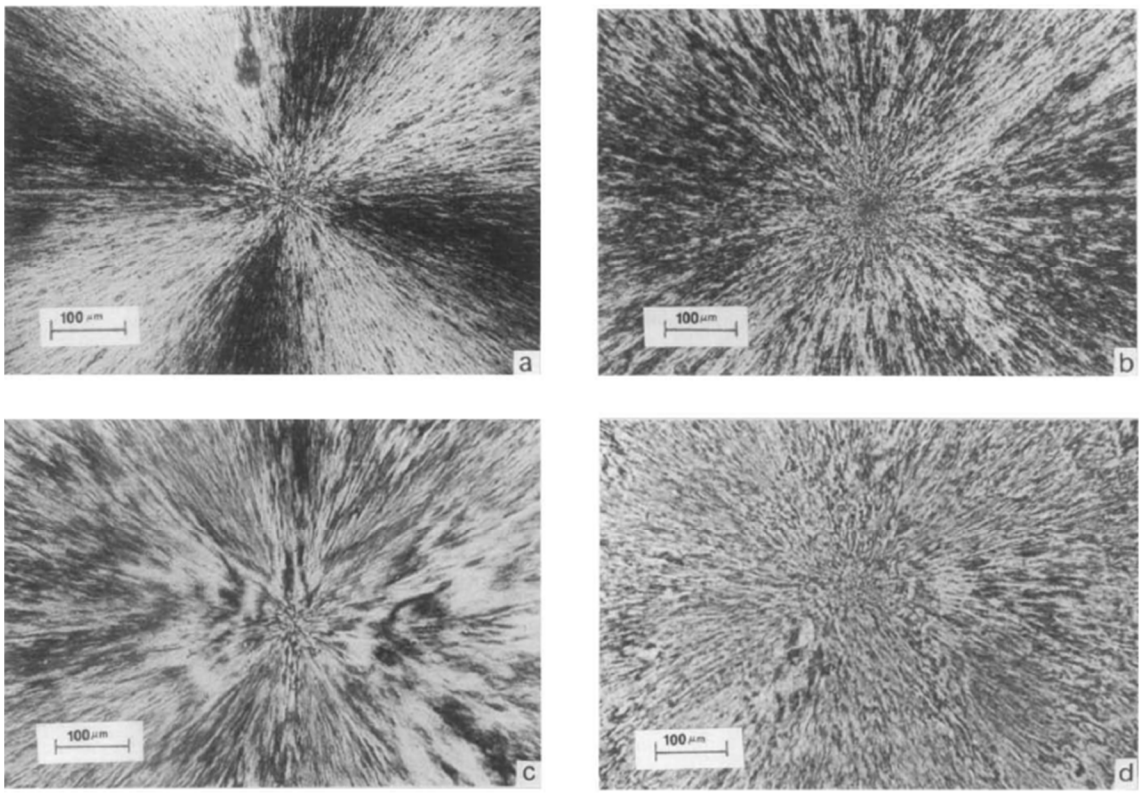

Figure 4.31 The spherulite morphology of PEO (MW 105,000) at different degrees of supercooling in the vicinities of regime transitions: (a) ΔT= 18.5K; (b) ΔT=16.5K; (c) ΔT=11 K; and (d) ΔT=9.5 K.[92]

It is seen from Figure 4.30 that the number of spherulitic nuclei in the 10%APAP-PEO mixture at T_x of 30 ^oC is substantially higher than that in the pure PEO, 0.1% and 1% APAP-PEO. The detailed results are summarized in Figure 4.32. At T_x of 30 ^oC, the number of nuclei in the 10%APAP-PEO samples is five times of that in PEO, indicating that APAP functions as a nucleating agent, denoting the existence/presence of tiny APAP crystalline regions, that reduce the free energy required to build new surfaces during crystallization. The results strongly suggest that APAP either recrystallizes or forms amorphous nanosize clusters[155] because it is oversaturated in the PEO at 30 ^oC. At T_x of 50 ^oC, the number of nuclei is the same for all samples regardless of the APAP concentration, suggesting that at this temperature, APAP and PEO are fully miscible. It

seems that 9% of APAP is dissolved when the temperature is raised from 30 to 40 °C, since the number of nuclei for 10%APAP-PEO and 1%APAP-PEO is the same. The fact that 1%APAP-PEO had more nuclei than PEO did at 40 °C hinted that the solubility was less than 1%. The reason for 1%APAP-PEO to have the same amount of nuclei as PEO at 30 °C was possibly due to the low molecular mobility at that temperature so that APAP did not recrystallize even though the solubility limit was exceeded. Based on these results, amorphous APAP could exist in the crystalline portion of PEO, possibly at a concentration between 0.1 and 1% at 30 °C.

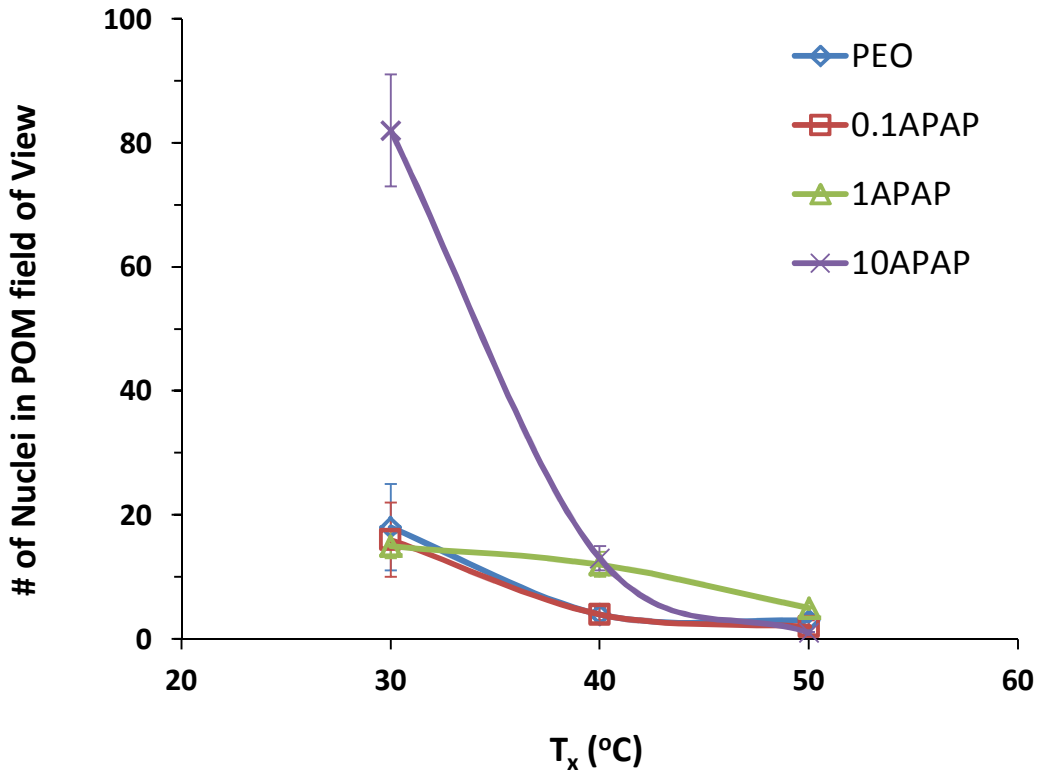

Figure 4.32 Number of nuclei in the POM field of view (a 4.5 mm^2 area) of PEO and APAP-PEO mixtures at different T_x.

Under isothermal crystallization conditions, spherulitic growth rates were calculated from the slope of the spherulite diameter versus time plots. The results obtained show a good linear increase of spherulite diameter with crystallization time for all samples. The spherulitic growth rate *G* is found to decrease with increasing APAP content as shown in Figure 4.33. The decrease is appreciable only for the 10%APAP concentration sample, where APAP solid regions are suspected to exist. When a polymer contains "defects", APAP in this case, these defects must be rejected from the crystals as long as they are sizable and cannot be accommodated by the lamellar folded chain growing crystallization regions.[208] Only small size defects may be included in the crystals. Thermodynamic descriptions of defect exclusion[209] and inclusion[210] in the crystal have been proposed. There are many case examples of steric reasons for exclusion[211-214] (short-chain branches formed by the comonomers of 1-butane, 1-hexane, or 1-octane in i-PP copolymers) as well as inclusion[215-217] (stereo-defect in i-PP) in the literature papers. Figure 4.34 shows the growth rate data for a series of i-PP with different isotacticities. With decreasing isotacticies, the growth rates are significantly reduced, while the structural analysis (small angle X-ray scattering and transmission electron microscopy, which will be discussed in more details later) indicates that the stero-defects of i-PP are included in the crystals.[216] In summary, both exclusion and inclusion mechanisms can slow down the growth rates as observed in the APAP-PEO system used in this work.

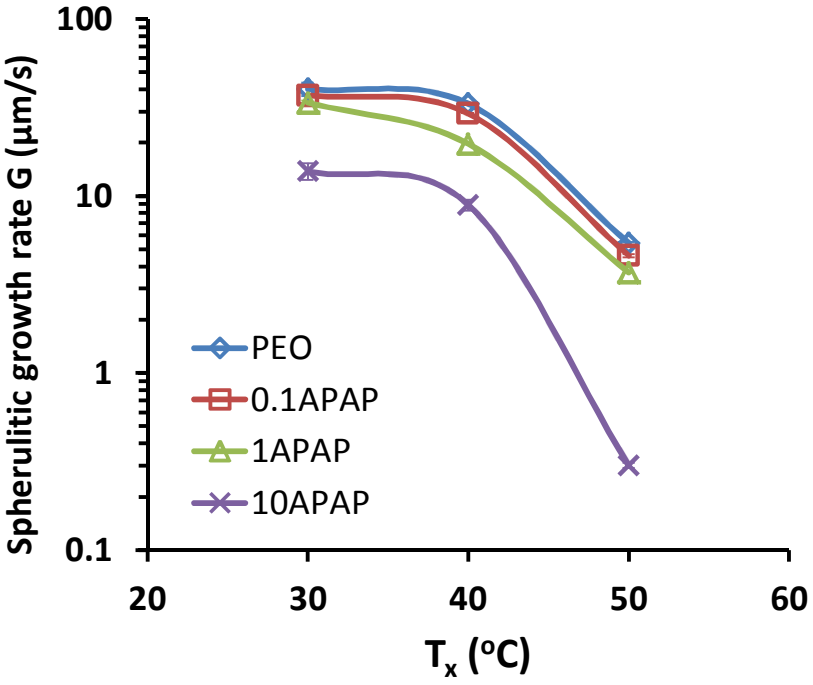

Figure 4.33 Isothermal spherulitic growth rate G (μm/s) of PEO and APAP-PEO at different T_x.

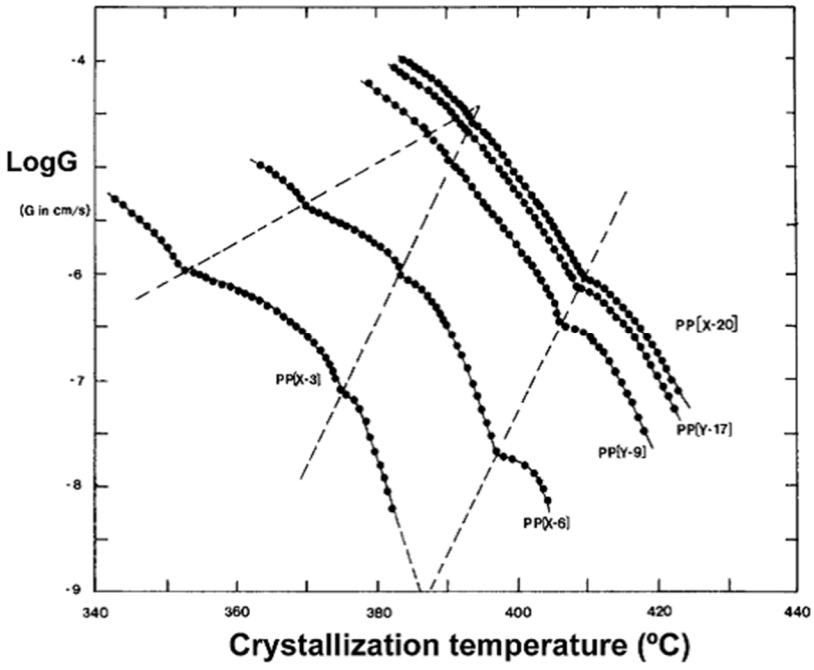

Figure 4.34 A set of linear growth rates of i-PP having five different extents of isotacticities over a wide crystallization temperature T_c range. From top to bottom, isotacticities of 98.8% PP(X-20), 97.8% PP(Y-17), 95.3% PP(Y-9), 88.2% PP(X-6) and 78.7%PP (X-3), respectively.[216]

For the case of a melt-miscible polymer blend of a semi-crystalline and an amorphous polymer, the length scale over which the diluent polymer diffuses during crystallization is determined by the relationship between the diffusion coefficient of the amorphous polymer in the semi-crystalline polymer and the crystallization rate.[218-221] The diluent polymer can reside in interlamellar regions (amorphous layers between crystalline lamellae), interfibrillar regions (amorphous regions between stacks of lamellae) and interspherulitic regions,[219] and the resulting segregation mechanisms are schematically illustrated in Figure 4.35. The difference between small molecular weight drugs and amorphous polymers is that the former, because of their size, are more favorable to be confined within the interlamellar regions, or even within the intralamellar regions. Having said this, the physical state of APAP is nevertheless unclear at this point. It might exist as amorphous clusters,[155] crystalline particles with the unit cell dimension of a monoclinic crystal being approximately 7.1 Å× 9.4 Å× 11.7 Å× sin(97.4^{o}) (0.77 nm^{3}),[111] or single molecules. Recently, Shekunov et al. reported that in the polymer synthesized from PEO crosslinked by polyurethane (PEO-PU), a hydrogel system, APAP was able to shift the SAXS peak (Figure 4.36) while the other model drug caffeine was not.[155] The reason for the difference is because APAP can form strong hydrogen bonds with the PEO, leading to a PEO-APAP complex, while the intermolecular interactions between caffeine and PEO-PU are much weaker and therefore their effect on the polymer structure is less pronounced. The size of APAP, derived from SAXS, was estimated to be between 7-10 nm.

At T_x of 30 ^{o}C when both PEO chain folding and APAP recrystallization rates are fast, the APAP may only affect the nucleation sites but not the isotropic three-dimensional

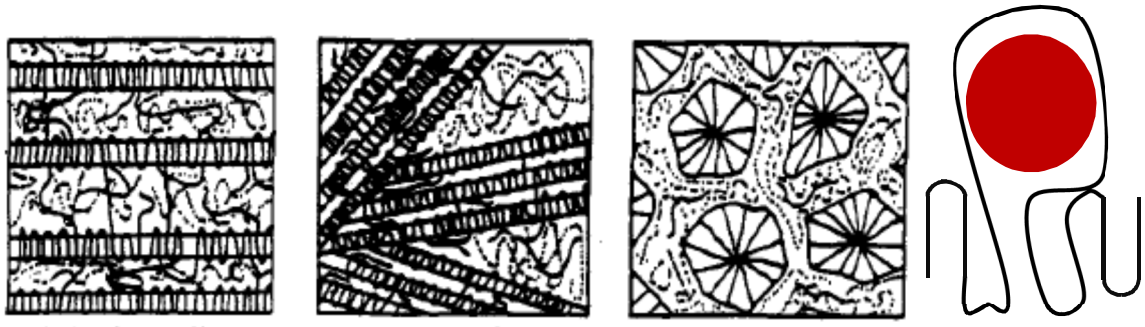

a. Interlamellar b. Interfibrillar c. Interspherulitic d. Intralamellar

Figure 4.35 Possible modes of segregation in a binary blend that is miscible in the amorphous state and contains one crystallizing component, (a-c) adapted from the literature paper;[219] (d) was proposed by the author, ● APAP.

shape or Maltese pattern. POM images show that the spherulites are space-filled with no evidence of APAP interspherulitic accumulation even for 10%APAP-PEO (Figure 4.37). At T_x of 50 ^oC, however, the morphology of 10%APAP-PEO is more dendritic than spherulitic with large unfilled space in between spherulites. To determine if APAP is located in the interspherulitic regions, one may use micro-Infrared (IR) spectroscopy coupled with POM for determination. The POM locates the microprobe to the area for IR measuring, the dark unfilled space in Figure 4.37 (b) for example, and the IR will determine if APAP exists in that particular space. The physical state of the APAP can also be determined by comparing the peak positions in the IR spectra.[32]

Since typical polymers are about 1000 nm long and the lamellar thickness is around 10 nm,[23] it is possible for APAP to locate either in the intralamellar, internlamellar, interfibrillar, or all these three regions. The most commonly used characterization techniques to determine the additive's location are SAXS and TEM. Recently, Zhu et al. have used SAXS to detect the increase of the long period, which is the sum of the thickness of the crystalline lamellae and amorphous layers, for the

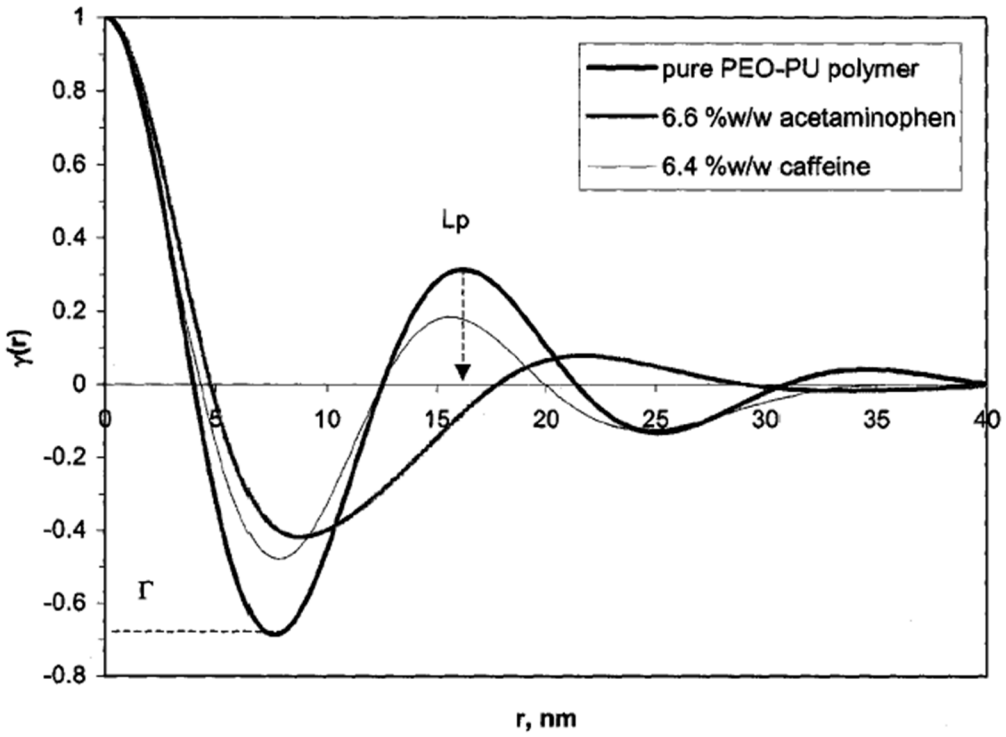

Figure 4.36 Characteristic SAXS correlation function obtained for the pure dry PEO-PU polymer; polymer saturated with 6.6% acetaminophen and saturated with 6.4% caffeine. The parameter L_p defines the long period (the sum of the thickness of the crystalline lamellae and amorphous layer).[155]

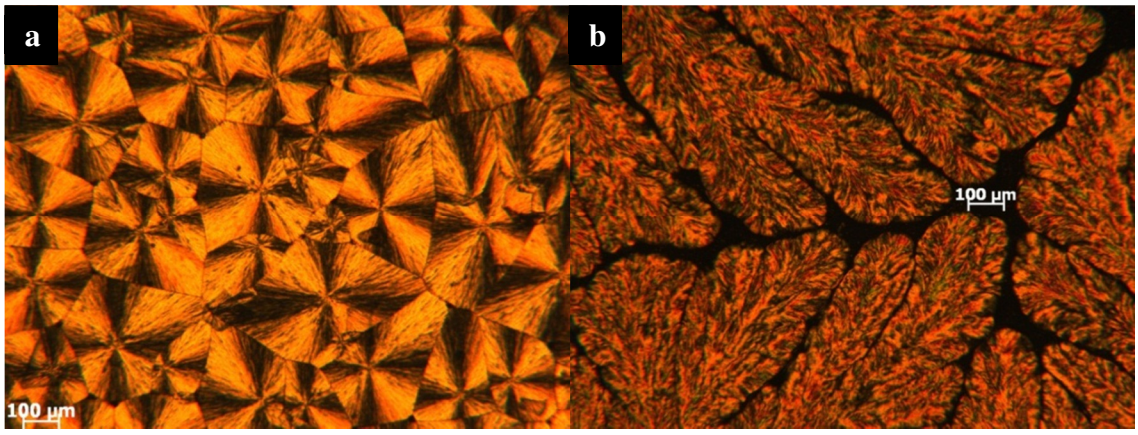

Figure 4.37 POM images of 10%APAP-PEO at T_x of (a) 30 ^{o}C and (b) 50 ^{o}C.

chlorpropamide(CPM)/PEG(MW 3350) solid dispersion system as compared to pure PEG.[222] As can be seen in Figure 4.38, the diffraction peak in the SAXS profile of 20%CPM/PEG shifted to a smaller scattering vector, which corresponded to a larger long period of 11.8nm. The long period of once-folded pure PEG was 11.0 nm. The diffraction peak shifted even further to a smaller scattering vector for the 40%CPM/PEG, where the long period increased to approximately 14 nm. TEM images also indicated more extensive amorphous regions between lamellae of PEO N10 after ketoprofen was melt-mixed into the matrix.[223] In Figure 4.39, the darker stained bands indicate the amorphous phase between crystallites. Although the morphology of the two types of samples resemble each other, the amorphous region of ketoprofen/PEO that lie between the crystalline regions are wider, suggesting that ketoprofen in the dispersion resides in the amorphous region.

It is important to determine APAP's location in the crystalline portion of PEO since the drug diffusion can be hindered due to the presence of crystallites.[85] The deeper APAP is buried in the PEO chains, the harder it is for APAP to be released during dissolution. Future work to determine the location and physical state of the APAP (amorphous or crystalline) and its physical size following the PEO chain folding will be very interesting. Unfortunately, the author's efforts to locate a SAXS have failed. As a result, this part of the work will be continued in 2012. Nevertheless, the number of spherulitic nuclei determined from the POM experiments is a good indication of drug-polymer miscibility. At 30 ^{o}C, the APAP's solubility in PEO is about 1% because the number of nuclei is the same for pure PEO, 0.1%APAP-PEO and 1%APAP-PEO. Based on the same criteria, the solubility at 50 ^{o}C is about 10%. Previous experimental work

concluded that the solubility at room temperature was less than 10% by using various characterization techniques such as SEM, XRD, DSC and DMTA. As compared to those techniques, the POM method has its advantage of being efficient because there is no need to wait for APAP's recrystallization from PEO, a phenomenon that could take days if not months to be detectable especially for samples with low APAP concentration. This is a simple and straight-forward way to estimate a drug's solubility in a semi-crystalline polymer at temperatures below the polymer's melting point.

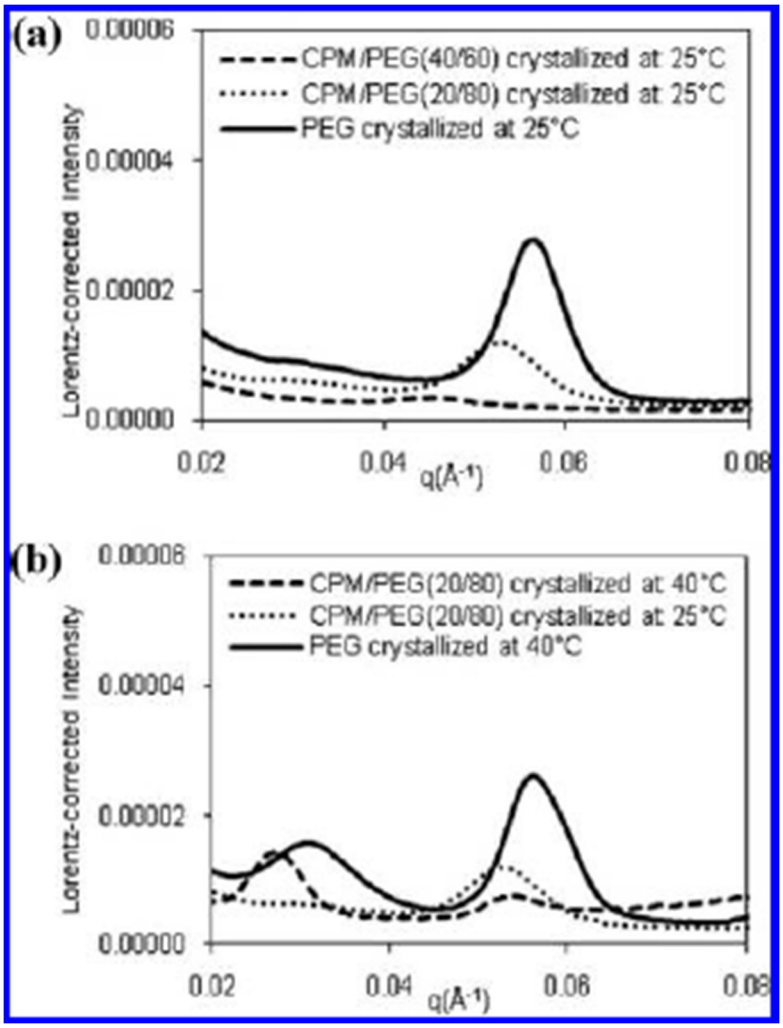

Figure 4.38 SAXS of different compositions of CPM/ PEG dispersions crystallized at different temperatures.[222]

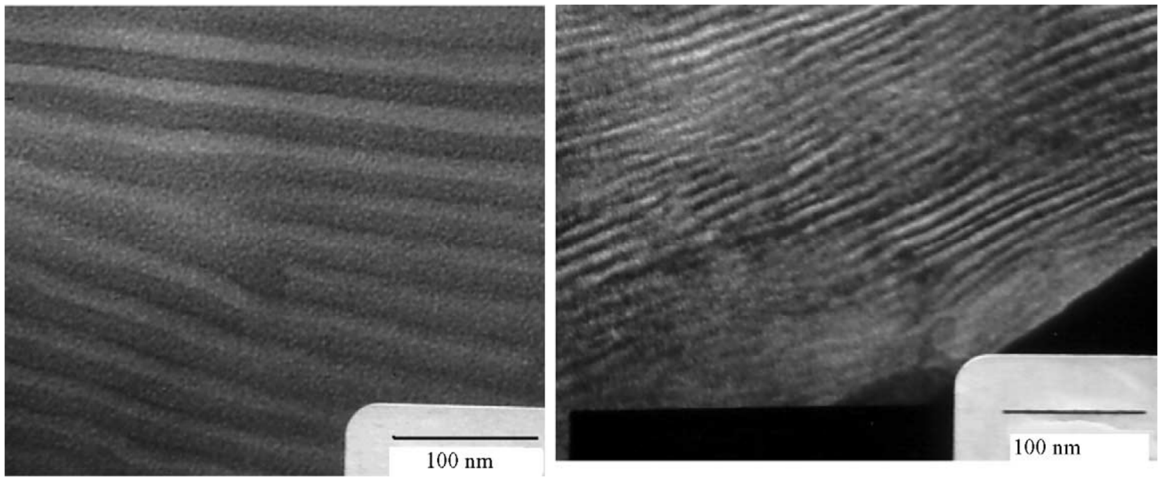

Figure 4.39 TEM micrographs of melt-processed neat PEO (right) and melt-processed 20%ketoprofen/PEO blend (left).[223]

To study the spherulitic growth kinetics, more spherulitic growth rates were measured and plotted in Figure 4.40. The Hoffman-Lauritzen (HL) theory was applied by utilizing Equation (4.13) and results were plotted in Figure 4.41. Only one regime of crystal growth is observed for each sample. Cheng et al. reported that for pure PEO regime III takes place for degrees of supercooling larger than 17.5 K, and regime II takes place for supercoolings between 10 and 17.5 K (Figure 4.42).[92] Regime I growth appears to be confined to a very narrow range of ΔT between 8.5 and 10 K. The supercooling ranges used here are 16.1 K < ΔT < 22.1 K for pure PEO, 19.3 K < ΔT < 25.3 K for 2%APAP-PEO, 23 K < ΔT < 29 K for 10%APAP-PEO, and 32.1 K < ΔT < 38.1 K for 20%APAP-PEO. The supercooling ranges for all samples are close to or larger than 17.5K, meaning that both PEO and APAP-PEO mixtures behave a regime III crystal growth.

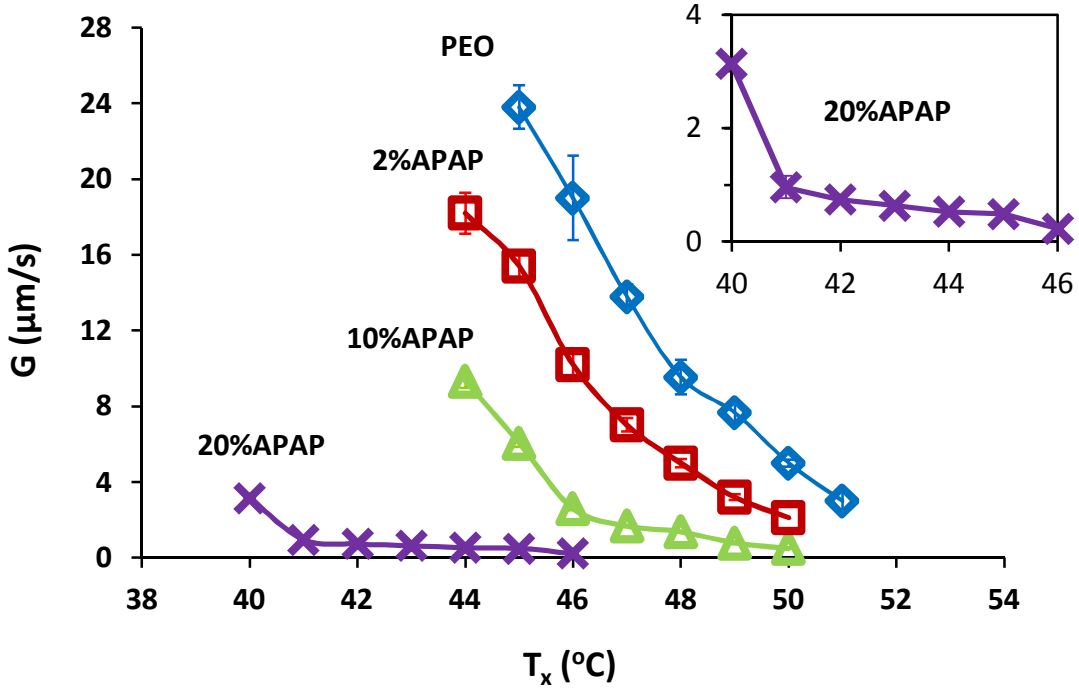

Figure 4.40 Isothermal spherulitic growth rate G (µm/s) vs. crystallization temperature (T_x, ºC) for PEO (◊), 2%APAP-PEO (□), 10%APAP-PEO (Δ) and 20%APAP-PEO (×).

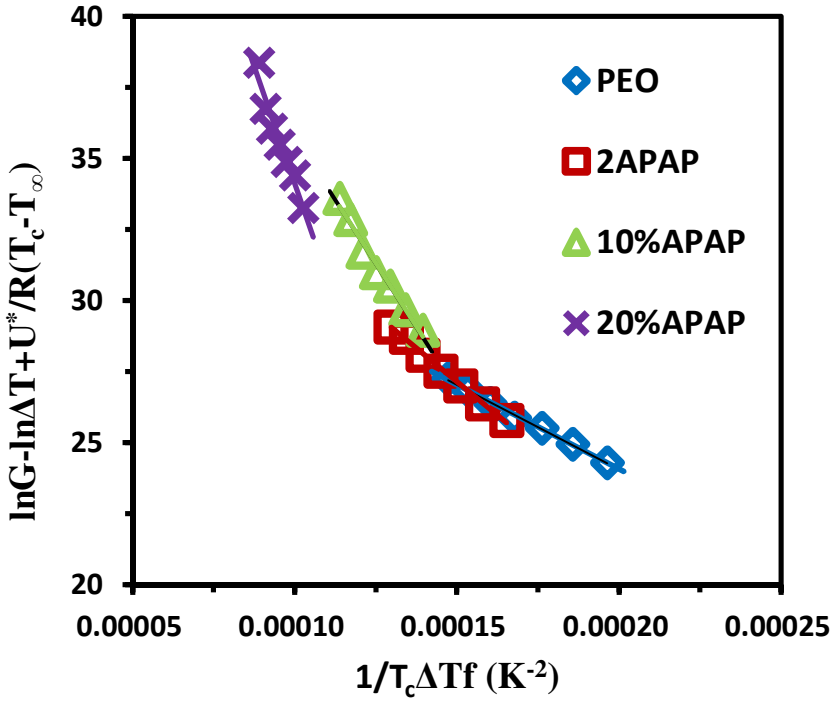

Figure 4.41 Hoffman-Lauritzen (HL) plots for PEO (◊), 2%APAP-PEO (□), 10%APAP-PEO (Δ) and 20%APAP-PEO (×) blends.

K_g is the slope of the linear HL function in Figure 4.41 and the obtained values for APAP-PEO systems are listed in Table 4.5. The nucleation constant K_g increases with APAP concentration, with 2%APAP-PEO being 1.6 times, 10%APAP-PEO being 3 times, and 20%APAP-PEO being 5.6 times of pure PEO. Using the stem width a_0 = 0.462 nm, and ΔH_f = 2.13 × 10^9 erg/cm^3 as previously determined by Godovsky et al.,[224] the products of lateral and folding surface free energies $\sigma\sigma_e$ are calculated based on Equation (4.12). The lateral surface free energy σ is estimated by the Thomas-Stavely relationship[225] and it is $\sigma = 0.1a_0(\Delta H_f)$ = 9.8 erg/cm^2. The folding surface free energy σ_e as well as the work of chain folding $q = 2\ \sigma_e A$,[181] where A is the molecular cross-sectional area and is 0.214 nm^2 for PEO, are then calculated and listed in Table 4.5. The σ_e value for pure PEO is in good agreement with the σ_e being 26-28 erg/cm^2 of PEO in regime III reported by Cheng.[92] Cheng et al. have observed that the folding surface free energy σ_e of phenoxy-end-capped PEO is about 1.3 times higher than that of PEO,[91] and Huang et al. have found the σ_e of single C_{60}(fullerene)-capped PEO is of about 1.8 times larger than that of PEO, while that of double C_{60}-capped PEO is about 2.5 times larger than that of PEO.[197] In this study, the σ_e values of 2%, 10% and 20%APAP-PEO are about 1.6 times, 2.9 times and 5.4 times those of pure PEO, respectively, indicating strongly that chain folding is much more difficult after APAP is incorporated into PEO. Since the APAP "defects" are either excluded or included in the PEO crystals, it is reasonable that extra work for chain folding is needed.

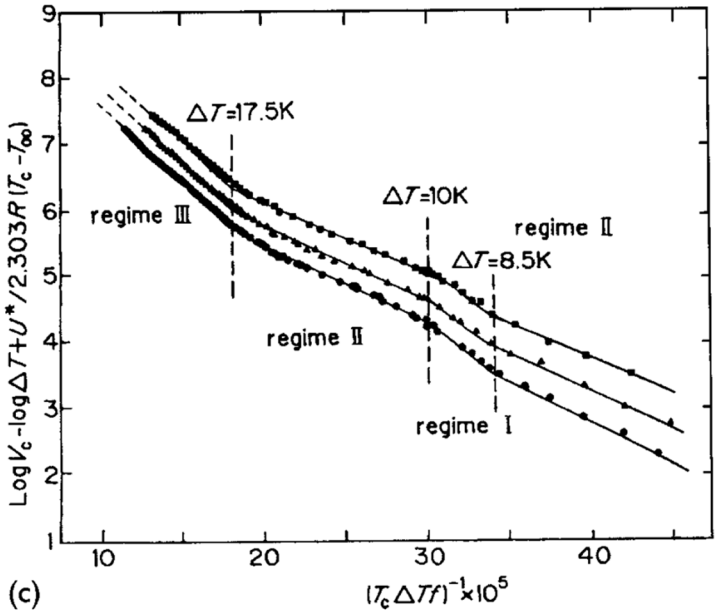

Figure 4.42 Hoffman-Lauritzen (HL) plots for PEO crystallized from the melt. From top to bottom, MW = ■ 23,000, ▲ 56,000, ● 105,000.[92]

Table 4.5 Kinetic Data of PEO and APAP-PEO Blends from POM Study

Sample	K_g (III)(10^4 K^{-2})	$\sigma\sigma_e$ (erg^2/cm^4)	σ_e (erg/cm^2)	q (kJ/mol)
PEO	5.9	278	28.2	7.3
2%APAP-PEO	9.4	435	44.2	11.4
10%APAP-PEO	17.8	818	83.1	21.4
20%APAP-PEO	33.1	1499	152.3	39.2

4.5.4 Macroscopic Properties – Differential Scanning Calorimetry (DSC)

An example of the isothermal DSC curves at various crystallization temperatures is presented in Figure 4.43. The Avrami parameter n values and the overall crystallization rate constants K_n are obtained from the double logarithmic plots of Equation (4.15). The log[-ln(1-$X(t)$)] versus log t plots are shown in Figure 4.44. The Avrami exponents n for PEO, 2%APAP, 10%APAP and 20%APAP-PEO are 2.0, 2.2, 2.1 and 1.7, respectively.

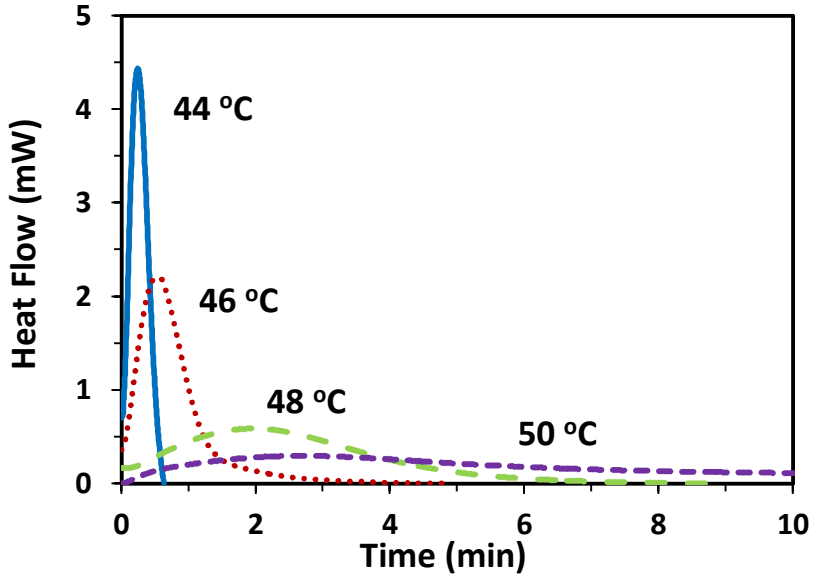

Figure 4.43 Isothermal DSC curves for 10%APAP-PEO at various T_cs.

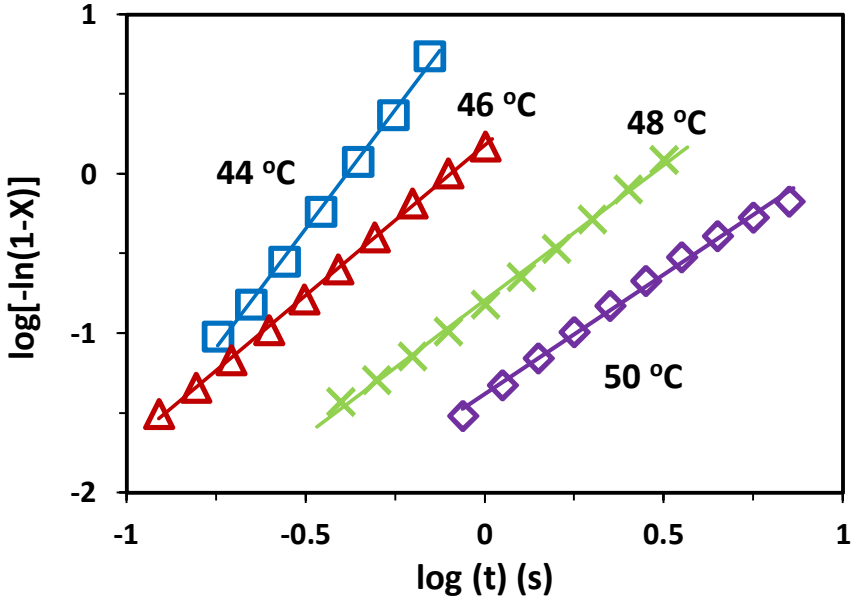

Figure 4.44 Avrami analysis of 10%APAP-PEO crystallized at various T_cs.

Since no systematic variation of *n* with composition or temperature is found, the crystal growth control mechanism is very likely to be the same for all samples. Based on Schultz's summary results in Table 4.4,[203, 204] n = 1.5 demonstrates spherulitic growth of

heterogeneous nucleation, with the rate limiting step being diffusion of polymer molecules to or from the growth surface.

The overall crystallization rate constant K_n is a combination of linear growth rate and nucleation density (rate). When the nucleation is instantaneous, the linear growth rate G is related to K_n by the simple relation $G \propto K_n^{1/n}$, as shown in the early work of Mandelkern, where n is the Avrami exponent.[226] Rewriting Equation (4.13), one gets the following relationship:

$$\frac{1}{n}\ln K_n - \ln(\Delta T) + \frac{U^*}{R(T_c - T_\infty)} = \ln A_0 - \frac{K_g}{fT_c\Delta T} \qquad (4.17)$$

K_n and n, calculated from Avrami analysis, are used in the plot of Figure 4.45 based on Equation (4.17). Since all supercooling ΔTs are larger than 17 K as shown earlier, regime III is used to analyze the kinetic data. Table 4.6 lists the values of K_g, folding surface free energies σ_e, and the work of chain folding q. The values are in good agreement from those obtained from the POM study. σ_e and q for the 2, 10% and 20%APAP-PEO are 1,4, 3.3 and 6.1 times that of pure PEO, respectively. In summary, incorporation of APAP makes the PEO chains behave in a "stiffer" fashion and makes it more difficult to fold in the process of crystallization.

The efficiency of nucleating agents is usually estimated from the changes of the crystallization temperature (T_{cp}) by cooling a polymer sample from the melt. Upon cooling, the sample will crystallize at a given temperature, and an effective nucleating agent will cause T_{cp} of the homopolymer to increase, with a higher temperature corresponding to an increased level of nucleation.[227-230] Figure 4.46 shows the T_{cp} of isotactic polypropylene (iPP) doped with three different nucleating agents, poly(vinylcyclohexane) (PVCH), 1,2,3,4-bis(3,4-dimethyl-benzidilene sorbitol (M 3988),

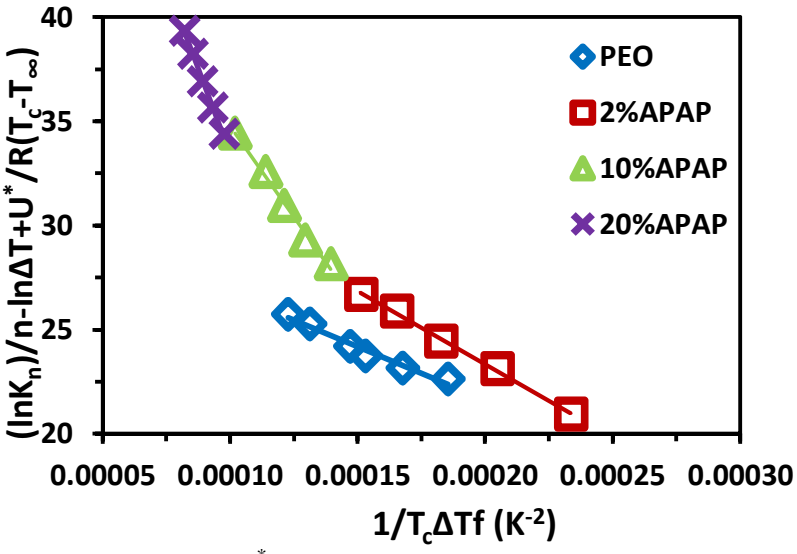

Figure 4.45 $(\ln K_n)/n - \ln\Delta T + U^*/R(T_c-T_\infty)$ vs. $1/T_c\Delta Tf$ for PEO (◊), 2%APAP-PEO (□), 10%APAP-PEO (Δ) and 20%APAP-PEO (×). K_n and n are calculated from Avrami analysis of isothermal DSC.

Table 4.6 Kinetic Data of PEO and APAP-PEO Blends from DSC Study

Sample	K_g (III)(10^4 K^{-2})	$\sigma\sigma_e$ (erg^2/cm^4)	σ_e (erg/cm^2)	q (kJ/mol)
PEO	5.1	240	24.3	6.3
2%APAP-PEO	7.0	325	33.1	8.5
10%APAP-PEO	17.3	796	80.9	20.9
20%APAP-PEO	32.4	1467	149.1	38.4

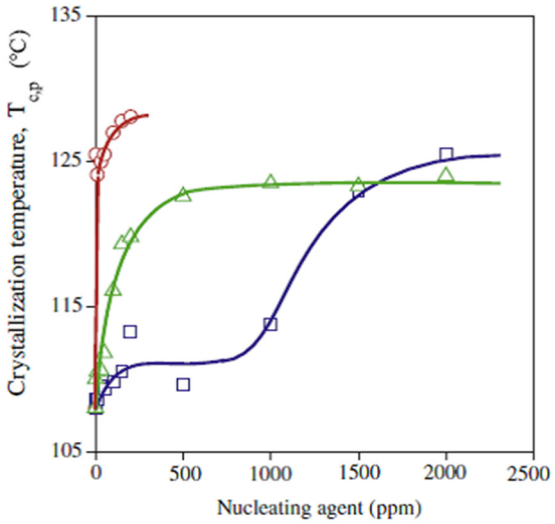

Figure 4.46 Comparison of the efficiency of the three nucleating agents. Effect of nucleating agent content on the peak temperature of crystallization of iPP. (○) PVCH, (□) M 3988, (Δ) NA21 E.[227]

and a traditional commercial nucleating agent NA21 E.[227] It is seen that all three agents can increase the T_{cp} and promote the nucleation of iPP. At a nucleating agent concentration of 200 ppm, the nucleating effect increases in the following order of M 3988 < NA21 E < PVCH judging from T_{cp} increase. The T_{cp} increase resulting from 200 ppm of M 3988 is only 3 ^{o}C while for the other two nucleating agents it is more pronounced and is around 13 ^{o}C and 20 ^{o}C. Thus, it is not surprising to see in their POM results, Figure 4.47, that M 3988 is a poor nucleating agent allowing for the few nucleated spherulites to grow to large sizes, which would render the i-PP opticality, not clear and more brittle than the i-PP nucleated by the other two agents.

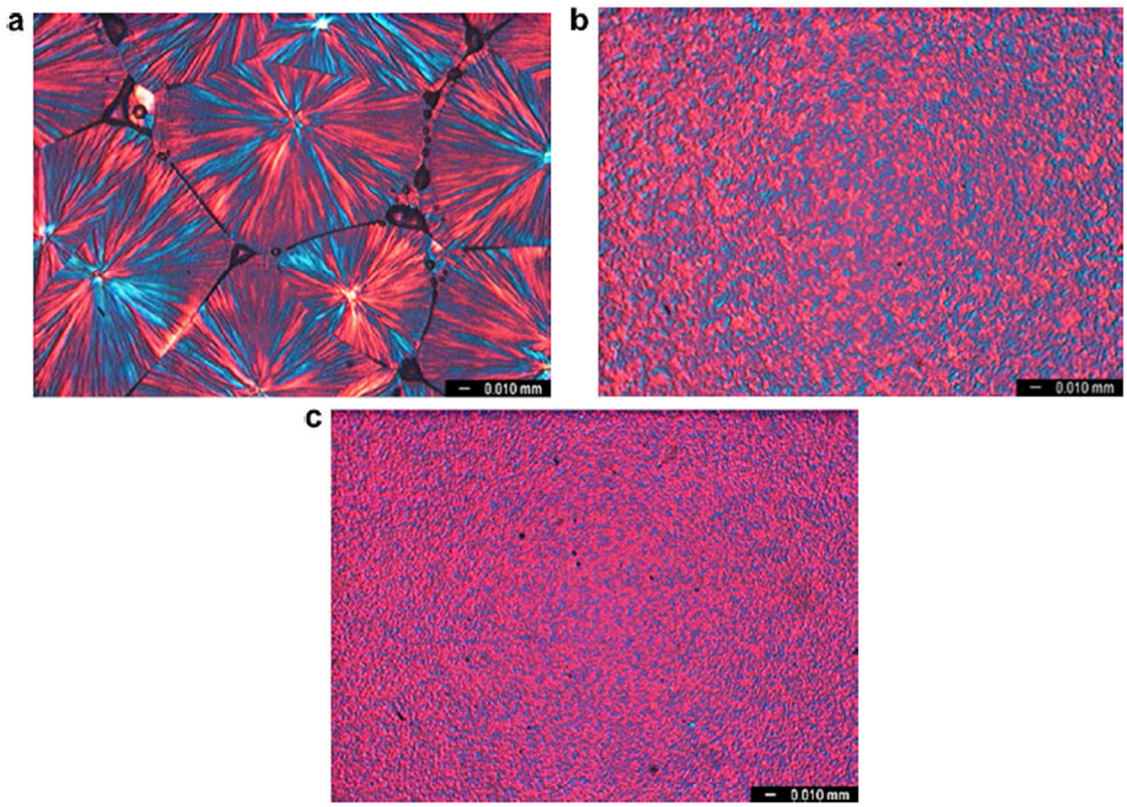

Figure 4.47 Structure development in the presence of 200 ppm of the three nucleating agents studied. Polarized microscope images taken at T_c = 130 ^{o}C on quenched samples; (a) M3988, (b) NA21E, (c) PVCH.[227]

The T_{cp}s and enthalpies of PEO containing different APAP concentration are plotted in Figure 4.48. The T_{cp}s are basically the same for PEO and low APAP concentration samples, which are 41.1, 41.4, 41.4 and 41.5 ^{o}C for PEO, 0.1%, 1% and 2%APAP-PEO, respectively. The T_{cp}s of 10% and 20%APAP-PEO samples, however, are 36.9 and 33.7 ^{o}C, respectively, substantially lower. Additionally, the crystallization enthalpy is reduced from 147.2 J/g for pure PEO to 134.8, 127.4 and 117.2 J/g for 0.1%, 10% and 20%APAP-PEO, respectively. The results show that APAP decreases the nucleation efficiency and inhibits the crystallization of PEO, which is consistent with previous kinetic result conclusions that the fold surface free energy σ_e is increased and the chain folding of PEO becomes more difficult with increasing APAP content.

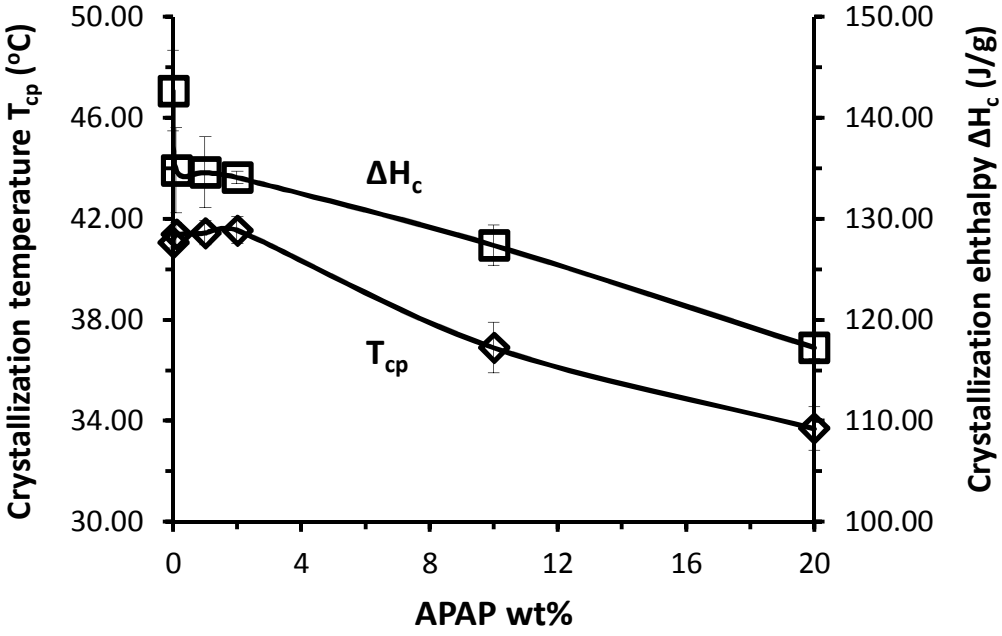

Figure 4.48 The crystallization temperature (T_{cp}) and enthalpy (ΔH_c) during non-isothermal cooling cycle at 10 ^{o}C/minute.

CHAPTER 5

CONTRIBUTIONS, CONCLUSIONS AND PROPOSED FUTURE WORK

The main objective and contribution of the thesis was to explore and develop novel and rather straight-forward experimental techniques for determining the solubility of APIs in polymer excipients at both hot-melt mixing processing temperatures, where the API solid dispersions/solutions are formed, and at ambient temperature, where the resulting oral dosages are stored and used. Knowledge of the increased temperature solubility, as well as the degree to which the API/excipient solid dispersion is able to remain this high solubility stably over its shelf life, is of paramount importance in understanding the emerging field of pharmaceutical hot-melt mixing/extrusion. Thus, developing novel and straight-forward solubility characterization methods at both processing and ambient temperatures, which are appropriate for such temperature sensitive material systems and which borrow techniques from the field of polymer rheology and thermomechanical properties characterization, have the potential of advancing this field more rapidly.

Solid dispersions of a model drug, acetaminophen (APAP), and a pharmaceutical grade polymer excipient poly(ethylene oxide) (PEO) of M_w= 100,000 g/mol, were prepared by hot-melt mixing. The main reason for choosing PEO, which is semi-crystalline (80% crystallinity), instead of a totally amorphous polymer excipient was to have the opportunity to explore the ambient temperature solubility of APAP in *both* the crystalline and amorphous phases of PEO.

5.1 Contributions

A novel rheological method measuring the viscosity of drug-polymer melts of different API concentrations at temperatures above the polymer's melting point or glass transition temperature, but below the drug's melting point has been developed to determine the drug's solubility in the polymer. Below that solubility limit, the viscosity of the molten mixture will decrease with increasing drug concentration denoting the plasticizing effect of the API. Above the solubility limit, the viscosity will increase with increasing drug concentration denoting the formation of a suspension created by API particles, which are able to dissolve at that temperature. Thus, the drug concentration corresponding to the minimum viscosity is the solubility at the specific temperature. The method is powerful, using accurate rheometers which do not expose the polymer excipient to high temperature for long time, is conducted under N_2, and which, therefore, can be applied to investigate many temperature sensitive drug-polymer systems. Furthermore, very few assumptions are made in the experimental study and results analysis. The solubility data determined rheologically can be used to optimize the HME processing temperature "window" in order to achieve a fully miscible drug-polymer system with the minimum risk of degradation.

As mentioned above, a semi-crystalline polymer was used as the excipient in this thesis work. Such a polymer allows for the use of polarized optical microscopy to study the polymer/drug spherulitic nucleation and growth rates, and morphology. As an example, the number of spherulitic nuclei can be used to determine a drug's solubility in the polymer at temperatures below the polymer's melting point, e.g., ambient temperature. When the drug concentration is below the solubility limit, the "quality" of

the spherulites will deteriorate with increasing drug concentration. Above the solubility limit, the number of spherulitic nuclei will increase dramatically with increasing drug concentration, due to the fact that the supercooled API acts as a nucleating agent. The method only requires a hot-stage polarized microscope, and thus it is easily accessible and straight-forward. It is the first method that can determine a drug's solubility in a semi-crystalline polymer accurately. As compared to other characterization techniques such as SEM, XRD, DSC and DMTA, the POM method has its advantage of being efficient because there is no need to wait for drug's recrystallization from the semi-crystalline polymer, a phenomenon that could take days if not months to be detectable especially for samples with low drug concentration.

5.2 Conclusions

Processing HMM conditions were optimized and fixed in order to focus the study on material properties. Rheological, microscopic and thermal methods were used to measure APAP's solubility in PEO at both hot-melt extrusion or hot-melt mixing processing temperatures and storage temperature. As mentioned above, the strain-controlled rheometer measured the viscosity of APAP-PEO and the solubility data were obtained from the critical point on the curve of viscosity *vs.* drug loading. The solubility of APAP in PEO was also obtained from measuring the glass transition temperature at different drug loadings. Results from the two methods agree with each other and are further confirmed by hot-stage optical microscopic observation. The $T_{\mathrm{m}}^{\mathrm{mix}}/T_m$(PEO) diagram developed in this work, which is essentially a "phase diagram", can be used to determine the optimal range of HME or HMM processing conditions and mixture composition.

The apparent drug solubility at room temperature was estimated through T_g measurements using DSC and DMTA, SEM observations, and XRD analysis. The APAP-PEO system was found to be a very difficult system because the miscibility of the two components is very poor at room temperature even though the components can achieve a fully miscible molten polymeric state at processing temperatures. One major reason is that PEO is a semi-crystalline polymer with a high tendency to recrystallize once the temperature drops below its melting point (62 ^{o}C). The apparent drug solubility after a month's storage was estimated to be between 5-10%. All samples with APAP concentration ≥ 10% showed extensive APAP recrystallization. For 20% and 30%APAP-PEO, APAP recrystallized almost instantaneously upon cooling to room temperature and the recrystallization process slowed down to an undetectable rate after one day. For the 10%APAP-PEO system, the recrystallization process was found to be slower. However, the size and shape of the APAP crystalline particles formed by recrystallization were independent of the drug loading and did not change with increasing storage time. APAP's recrystallization was found to be sensitive to the presence of the nanoclays melt-mixed into the APAP-PEO system during HMM. XRD spectra showed that nanoclays facilitated APAP's recrystallization.

A model using Flory-Huggins lattice theory and thermodynamic mixture phase equilibria was utilized to predict APAP's solubility in PEO. The interaction parameter χ was calculated to be -1.65 from the depression of drug's melting point determined from the $T_{\mathrm{m}}^{\mathrm{mix}}/T_m$(PEO) diagram. The drug's solubility in amorphous PEO was estimated to be 11.7% at 300 K. Since PEO is a semi-crystalline polymer with crystallinity of 80%, the actual solubility is around 2.3%, assuming no APAP molecules dissolve in the crystalline

part of PEO. The solubility of APAP in PEG 400 was calculated to be 14.6% by using the same χ of -1.65, while the experimental measurement was 17.1%. The good match between the experimental and calculated data suggests that the χ for APAP-PEO calculated from the melting point depression method is a reasonable estimate.

The nucleation and crystallization behavior of PEO was altered by the incorporation of APAP. At high crystallization temperature (50 ^{o}C), pure PEO, 0.1%APAP-PEO, 1%APAP-PEO and 10%APAP-PEO had the same low number of spherulitic nuclei, indicating that APAP and PEO were fully miscible for all the compositions. At low crystallization temperature (30 ^{o}C), the number of nuclei for 10%APAP-PEO was dramatically higher, suggesting that APAP was oversaturated and, therefore, recrystallized and acted as a nucleating agent. The fact that 1%APAP-PEO had more nuclei than PEO did at 40 ^{o}C hinted that the solubility was less than 1%. The reason for 1%APAP-PEO to have the same amount of nuclei as PEO at 30 ^{o}C was attributed to the low molecular mobility at that temperature so that APAP did not recrystallize even though the solubility limit was exceeded. Based on the results, amorphous APAP could exist in the crystalline portion of PEO, possibly between the concentration of 0.1 and 1% at 30 ^{o}C.

The impact of the interaction parameter and the polymer MW on the Gibbs free energy of mixing ΔG_m was investigated. The χ, which is controlled by the drug-polymer interaction, was found to play an important role while the polymer MW showed negligible effect on ΔG_m. The drug's solubility could be altered noticeably by the change of both χ and MW. The study also suggests that the depression of drug's melting point is

a good indicator for preliminary polymer screening. The polymer that reduces the melting point the most, is likely to be most miscible with the drug.

The releasing rate of APAP was slowed down significantly after melt-mixing with PEO. Nanoclay-containing samples presented much slower dissolution rates compared to both the drug powder and melt-mixed APAP-PEO. Data analysis of the dissolution results suggests that the drug's release mechanism changes from an erosion dominant mode to a diffusion dominant one, due to the addition of nanoclays. The results suggest that nanoclays may be utilized to tailor the drug's releasing rate.

The crystallization behavior of pure PEO and APAP-PEO mixtures was studied by using polarized optical microscopy, isothermal DSC and nonisothermal DSC. Solvent evaporation method was utilized to prepare clean APAP-PEO and PEO films. The equilibrium melting temperature T_m^0 was found to increase with APAP concentration by using the Hoffman-Weeks equation. At high crystallization temperature (50 ^oC), the Maltese cross pattern and symmetry of the PEO spherulites were disrupted in the presence of 10%APAP. At low crystallization temperature (30 ^oC), 10%APAP-PEO had significantly more spherulitic nuclei as compared to pure PEO, 0.1%APAP-PEO and 1%APAP-PEO. The morphological, spherulitic growth and number of spherulitic nuclei analysis appears to be a promising, simple and novel method to determine a drug's solubility in a semi-crystalline polymer at temperatures below polymer's melting point and close to ambient.

An extensive spherulitic nucleation and growth kinetics study using the classical theoretical relationships, e.g., the Hoffman-Lauritzen (HL) and Avrami theories, was conducted. The spherulitic growth rates G of PEO were suppressed with increasing

APAP concentration. HL theory was used to calculate the kinetic parameters. Both POM and DSC analysis yielded similar values for the nucleation constant K_g as well as the fold surface free energy σ_e and work of chain folding q. The values of σ_e and q increased with APAP concentration, indicating that the chain folding of PEO became much more difficult because of hindering by APAP. Non-isothermal DSC showed that APAP reduced the nucleation efficiency and inhibited the crystallization of PEO, which is consistent with the kinetic results that the chain folding of PEO became more difficult with increasing APAP concentration.

5.1 Proposed Future Work

The spherulitic nucleation and growth kinetics study suggests that APAP is mostly likely working as a chemical defect and is either rejected from or included in the PEO crystals during chain folding. However, the physical state (amorphous, crystalline) and the size of the APAP are unknown due to the detection limit of the instruments for the crystallization study. SAXS, TEM and micro-IR spectroscopy coupled with POM can be utilized in the future to analyze the location of the APAP in PEO spherulites, namely interspherulitic, interfibrillar, interlamellar or intralamellar. By determining the location of APAP, it is thereby possible to estimate the size, physical state and role of APAP.

REFERENCES

1. Lipinski CA, Lombardo F, Dominy BW, Feeney PJ. Experimental and computational approaches to estimate solubility and permeability in drug discovery and development settings. Adv Drug Delivery Rev. 2001; 46: 3-26.

2. Fahr A, Liu X. Drug delivery strategies for poorly water-soluble drugs. Expert Opin Drug Deliv. 2007; 4: 403-16.

3. Ranzani LS, Font J, Galimany F, Santanach A, Gomez-Gomar AM, Casadevall G, Gryczke A. Enhanced in vivo absorption of CB-1 antagonist in rats via solid solutions prepared by hot-melt extrusion. Drug Dev Ind Pharm. 2011; 37: 694-701.

4. Jijun F, Lishuang X, Xiaoli W, Shu Z, Xiaoguang T, Xingna Z, Haibing H, Xing T. Nimodipine (NM) tablets with high dissolution containing NM solid dispersions prepared by hot-melt extrusion. Drug Dev Ind Pharm. 2011; 37: 934-44.

5. Yassin AEB, Alanazi FK, El-Badry M, Alsarra IA, Barakat NS. Preparation and Characterization of Spironolactone-Loaded Gelucire Microparticles Using Spray-Drying Technique. Drug Dev Ind Pharm. 2009; 35: 297-304.

6. Wu K, Li J, Wang W, Winstead DA. Formation and characterization of solid dispersions of piroxicam and polyvinylpyrrolidone using spray drying and precipitation with compressed antisolvent. J Pharm Sci. 2009; 98: 2422-31.

7. Lakshman JP, Cao Y, Kowalski J, Serajuddin ATM. Application of Melt Extrusion in the Development of a Physically and Chemically Stable High-Energy Amorphous Solid Dispersion of a Poorly Water-Soluble Drug. Mol Pharmaceutics. 2008; 5: 994-1002.

8. Chiou WL, Riegelman S. Pharmaceutical applications of solid dispersion systems. J Pharm Sci. 1971; 60: 1281-302.

9. Van den Mooter G, Wuyts M, Blaton N, Busson R, Grobet P, Augustijns P, Kinget R. Physical stabilisation of amorphous ketoconazole in solid dispersions with polyvinylpyrrolidone K25. Eur J Pharm Sci. 2001; 12: 261-9.

10. Chokshi RJ, Zia H, Sandhu HK, Shah NH, Malick WA. Improving the dissolution rate of poorly water soluble drug by solid dispersion and solid solution—Pros and cons. Drug Deliv. 2007; 14: 33-45.

11. Zhou D, Zhang GGZ, Law D, Grant DJW, Schmitt EA. Physical stability of amorphous pharmaceuticals: Importance of configurational thermodynamic quantities and molecular mobility. J Pharm Sci. 2002; 91: 1863-72.

12. DiNunzio JC, Brough C, Hughey JR, Miller DA, Williams Iii RO, McGinity JW. Fusion production of solid dispersions containing a heat-sensitive active ingredient by hot melt extrusion and Kinetisol® dispersing. Eur J Pharm Biopharm. 2010; 74: 340-51.

13. Coppens KA, Hall MJ, Mitchell SA, Read MD. Hypromellose, ethylcellulose, and polyethylene oxide use in hot melt extrusion. Pharm Technol. 2006; 30: 62-70.

14. Biswal S, Sahoo J, Murthy P, Giradkar R, Avari J. Enhancement of Dissolution Rate of Gliclazide Using Solid Dispersions with Polyethylene Glycol 6000. AAPS PharmSciTech. 2008; 9: 563-70.

15. Al-Obaidi H, Buckton G. Evaluation of Griseofulvin Binary and Ternary Solid Dispersions with HPMCAS. AAPS PharmSciTech. 2009; 10: 1172-7.

16. Curatolo W, Nightingale J, Herbig S. Utility of Hydroxypropylmethylcellulose Acetate Succinate (HPMCAS) for Initiation and Maintenance of Drug Supersaturation in the GI Milieu. Pharm Res. 2009; 26: 1419-31.

17. Koester LS, Mayorga P, Bassani VL. Carbamazepine/βCD/HPMC Solid Dispersions. I. Influence of the Spray-Drying Process and βCD/HPMC on the Drug Dissolution Profile. Drug Dev Ind Pharm. 2003; 29: 139-44.

18. Albers J, Alles R, Matthée K, Knop K, Nahrup JS, Kleinebudde P. Mechanism of drug release from polymethacrylate-based extrudates and milled strands prepared by hot-melt extrusion. Eur J Pharm Biopharm. 2009; 71: 387-94.

19. Liu H, Wang P, Zhang X, Shen F, Gogos CG. Effects of extrusion process parameters on the dissolution behavior of indomethacin in Eudragit® E PO solid dispersions. Int J Pharm. 2010; 383: 161-9.

20. Crowley MM, Zhang F, Repka MA, Thumma S, Upadhye SB, Kumar Battu S, McGinity JW, Martin C. Pharmaceutical Applications of Hot-Melt Extrusion: Part I. Drug Dev Ind Pharm. 2007; 33: 909-26.

21. Janssens S, Van den Mooter G. Review: physical chemistry of solid dispersions. J Pharm Pharmacol. 2009; 61: 1571-86.

22. Rottendorf Pharma. accessed November 17, 2011 Available from: http://www.rottendorf.de/index.php/hot-melt-extrusion.html.

23. Tadmor Z, Gogos CG. Principles of Polymer Processing. Wiley-Interscience; 2006.

24. Dobry DE, Bend Research Inc., Dextran-Based Amorphous Dispersions as a Platform Technology in Pre-clinical Screening for Inhaled Dry Powders, 2011; accessed November 17, 2011 http://www.xtalks.com/xto428bendres.ashx

25. Janssens S, de Armas HN, Remon JP, Van den Mooter G. The use of a new hydrophilic polymer, Kollicoat IR®, in the formulation of solid dispersions of Itraconazole. Eur J Pharm Sci. 2007; 30: 288-94.

26. Six K, Verreck G, Peeters J, Brewster M, Mooter GVd. Increased physical stability and improved dissolution properties of itraconazole, a class II drug, by solid dispersions that combine fast- and slow-dissolving polymers. J Pharm Sci. 2004; 93: 124-31.

27. Mididoddi PK, Repka MA. Characterization of hot-melt extruded drug delivery systems for onychomycosis. Eur J Pharm Biopharm. 2007; 66: 95-105.

28. Sun Y, Rui Y, Wenliang Z, Tang X. Nimodipine semi-solid capsules containing solid dispersion for improving dissolution. Int J Pharm. 2008; 359: 144-9.

29. Zheng X, Yang R, Tang X, Zheng L. Part I: Characterization of Solid Dispersions of Nimodipine Prepared by Hot-melt Extrusion. Drug Dev Ind Pharm. 2007; 33: 791-802.

30. Patterson J, James M, Forster A, Rades T. Melt Extrusion and Spray Drying of Carbamazepine and Dipyridamole with Polyvinylpyrrolidone/Vinyl Acetate Copolymers. Drug Dev Ind Pharm. 2008; 34: 95-106.

31. Qi S, Belton P, Nollenberger K, Clayden N, Reading M, Craig D. Characterisation and Prediction of Phase Separation in Hot-Melt Extruded Solid Dispersions: A Thermal, Microscopic and NMR Relaxometry Study. Pharm Res. 2010; 27: 1869-83.

32. Qi S, Gryczke A, Belton P, Craig DQM. Characterisation of solid dispersions of paracetamol and Eudragit(R) E prepared by hot-melt extrusion using thermal, microthermal and spectroscopic analysis. Int J Pharm. 2008; 354: 158-67.

33. Zhang F, McGinity J. Properties of sustained-release tablets prepared by hot-melt extrusion. Pharm Dev Tech. 1999; 4: 241-50.

34. Repka MA, Gerding TG, Repka SL, McGinity JW. Influence of Plasticizers and Drugs on the Physical-Mechanical Properties of Hydroxypropylcellulose Films Prepared by Hot Melt Extrusion. Drug Dev Ind Pharm. 1999; 25: 625-33.

35. Miller D, DiNunzio J, Yang W, McGinity J, Williams R. Targeted Intestinal Delivery of Supersaturated Itraconazole for Improved Oral Absorption. Pharm Res. 2008; 25: 1450-9.

36. Bruce CD, Fegely KA, Rajabi-Siahboomi AR, McGinity JW. The influence of heterogeneous nucleation on the surface crystallization of guaifenesin from melt extrudates containing Eudragit® L10055 or Acryl-EZE®. Eur J Pharm Biopharm. 2010; 75: 71-8.

37. Zhu Y, Shah NH, Waseem Malick A, Infeld MH, McGinity JW. Controlled Release of a Poorly Water-Soluble Drug from Hot-Melt Extrudates Containing Acrylic Polymers. Drug Dev Ind Pharm. 2006; 32: 569-83.

38. Repka MA, Prodduturi S, Stodghill SP. Production and characterization of hot-melt extruded films containing clotrimazole. Drug Dev Ind Pharm. 2003; 29: 757-65.

39. Schilling SU, Shah NH, Waseem Malick A, McGinity JW. Properties of melt extruded enteric matrix pellets. Eur J Pharm Biopharm. 2010; 74: 352-61.

40. Aitken-Nichol C, Zhang F, McGinity JW. Hot Melt Extrusion of Acrylic Films. Pharm Res. 1996; 13: 804-8.

41. Crowley MM, Fredersdorf A, Schroeder B, Kucera S, Prodduturi S, Repka MA, McGinity JW. The influence of guaifenesin and ketoprofen on the properties of hot-melt extruded polyethylene oxide films. Eur J Pharm Sci. 2004; 22: 409-18.

42. De Brabander C, Van den Mooter G, Vervaet C, Remon JP. Characterization of ibuprofen as a nontraditional plasticizer of ethyl cellulose. J Pharm Sci. 2002; 91: 1678-85.

43. Verreck G, Decorte A, Heymans K, Adriaensen J, Liu D, Tomasko D, Arien A, Peeters J, Van den Mooter G, et al. Hot stage extrusion of p-amino salicylic acid with EC using CO_2 as a temporary plasticizer. Int J Pharm. 2006; 327: 45-50.

44. Hercules Incorporated, Aqualon Division, Physical and Chemical Properties, Klucel®, Hydroxypropylcellulose. 1997.

45. Crowley MM, Zhang F, Koleng JJ, McGinity JW. Stability of polyethylene oxide in matrix tablets prepared by hot-melt extrusion. Biomaterials. 2002; 23: 4241-8.

46. Repka MA, McGinity JW. Influence of Vitamin E TPGS on the properties of hydrophilic films produced by hot-melt extrusion. Int J Pharm. 2000; 202: 63-70.

47. Qian F, Huang J, Zhu Q, Haddadin R, Gawel J, Garmise R, Hussain M. Is a distinctive single Tg a reliable indicator for the homogeneity of amorphous solid dispersion? Int J Pharm. 2010; 395: 232-5.

48. Cassagnau P, Courmont M, Melis F, Puaux JP. Study of mixing of liquid/polymer in twin screw extruder by residence time distribution. Polym Eng Sci. 2005; 45: 926-34.

49. Gao J, Walsh GC, Bigio D, Briber RM, Wetzel MD. Mean residence time analysis for twin screw extruders. Polym Eng Sci. 2000; 40: 227-37.

50. Breitenbach J, Magerlein M. Melt-extruded molecular dispersions. In: Ghebre-Sellassie I, Martin C, editors. Pharmaceutical Extrusion Technology. New York: Marcel Dekker; 2003. 183-208.

51. Hardung H, Djuric D, Ali S. Combining HME & solubilization: Soluplus® - The solid solution. Drug Delivery Technol. 2010; 10: 20-7.

52. Miller DA, McConville JT, Yang W, Williams ROI, McGinity JW. Hot-melt extrusion for enhanced delivery of drug particles. J Pharm Sci. 2007; 96: 361-76.

53. Andrews GP, AbuDiak OA, Jones DS. Physicochemical characterization of hot melt extruded bicalutamide-polyvinylpyrrolidone solid dispersions. J Pharm Sci. 2010; 99: 1322-35.

54. Fukuda M, Peppas NA, McGinity JW. Floating hot-melt extruded tablets for gastroretentive controlled drug release system. J Controlled Release. 2006; 115: 121-9.

55. Yang R, Wang Y, Zheng X, Meng J, Tang X, Zhang X. Preparation and evaluation of ketoprofen hot-melt extruded enteric and sustained-release tablets. Drug Dev Ind Pharm. 2008; 34: 83-9.

56. Verhoeven E, De Beer TRM, Schacht E, Van den Mooter G, Remon JP, Vervaet C. Influence of polyethylene glycol/polyethylene oxide on the release characteristics of sustained-release ethylcellulose mini-matrices produced by hot-melt extrusion: in vitro and in vivo evaluations. Eur J Pharm Biopharm. 2009; 72: 463-70.

57. Özgüney I, Shuwisitkul D, Bodmeier R. Development and characterization of extended release Kollidon® SR mini-matrices prepared by hot-melt extrusion. Eur J Pharm Biopharm. 2009; 73: 140-5.

58. Ghalanbor Z, Körber M, Bodmeier R. Improved Lysozyme Stability and Release Properties of Poly(lactide-co-glycolide) Implants Prepared by Hot-Melt Extrusion. Pharm Res. 2010; 27: 371-9.

59. Prodduturi S, Manek RV, Kolling WM, Stodghill SP, Repka MA. Solid-state stability and characterization of hot-melt extruded poly(ethylene oxide) films. J Pharm Sci. 2005; 94: 2232-45.

60. Repka MA, Gutta K, Prodduturi S, Munjal M, Stodghill SP. Characterization of cellulosic hot-melt extruded films containing lidocaine. Eur J Pharm Biopharm. 2005; 59: 189-96.

61. Fukuda M, Peppas NA, McGinity JW. Properties of sustained release hot-melt extruded tablets containing chitosan and xanthan gum. Int J Pharm. 2006; 310: 90-100.

62. Hancock BC, Zografi G. Characteristics and significance of the amorphous state in pharmaceutical systems. J Pharm Sci. 1997; 86: 1-12.

63. Khougaz K, Clas S-D. Crystallization inhibition in solid dispersions of MK-0591 and poly(vinylpyrrolidone) polymers. J Pharm Sci. 2000; 89: 1325-34.

64. Miyazaki T, Yoshioka S, Aso Y, Kojima S. Ability of polyvinylpyrrolidone and polyacrylic acid to inhibit the crystallization of amorphous acetaminophen. J Pharm Sci. 2004; 93: 2710-7.

65. Miyazaki T, Yoshioka S, Aso Y. Physical stability of amorphous acetanilide derivatives improved by polymer excipients. Chem Pharm Bull. 2006; 54: 1207-10.

66. Janssens S, Armas HNd, Roberts CJ, Mooter GVd. Characterization of ternary solid dispersions of itraconazole, PEG 6000, and HPMC 2910 E5. J Pharm Sci. 2008; 97: 2110-20.

67. Prodduturi S, Urman K, Otaigbe J, Repka M. Stabilization of hot-melt extrusion formulations containing solid solutions using polymer blends. AAPS PharmSciTech. 2007; 8: E152-E61.

68. Bruce C, Fegely KA, Rajabi-Siahboomi AR, McGinity JW. Crystal growth formation in melt extrudates. Int J Pharm. 2007; 341: 162-72.

69. DiNunzio J, Hoffmann-La Roche, Inc., Pharmaceutical Melt Extrusion Process Development, 2011; accessed November 17, 2011 http://eudragit.evonik.com/product/eudragit/en/workshops/webinars/pages/default.aspx

70. Sun Y, Tao J, Zhang GGZ, Yu L. Solubilities of crystalline drugs in polymers: An improved analytical method and comparison of solubilities of indomethacin and nifedipine in PVP, PVP/VA, and PVAc. J Pharm Sci. 2010; 99: 4023-31.

71. Marsac P, Li T, Taylor L. Estimation of drug–polymer miscibility and solubility in amorphous solid dispersions using experimentally determined interaction parameters. Pharm Res. 2009; 26: 139-51.

72. Tao J, Sun Y, Zhang G, Yu L. Solubility of small-molecule crystals in polymers: D -mannitol in PVP, indomethacin in PVP/VA, and nifedipine in PVP/VA. Pharm Res. 2009; 26: 855-64.

73. Marsac P, Shamblin S, Taylor L. Theoretical and practical approaches for prediction of drug–polymer miscibility and solubility. Pharm Res. 2006; 23: 2417-26.

74. Zhao Y, Inbar P, Chokshi HP, Malick AW, Choi DS. Prediction of the thermal phase diagram of amorphous solid dispersions by flory–huggins theory. J Pharm Sci. 2011; 100: 3196-207.

75. Taylor LS, Zografi G. Spectroscopic characterization of interactions between PVP and indomethacin in amorphous molecular dispersions. Pharm Res. 1997; 14: 1691-8.

76. Matsumoto T, Zografi G. Physical properties of solid molecular dispersions of indomethacin with poly(vinylpyrrolidone) and poly(vinylpyrrolidone-co-vinyl-acetate) in relation to indomethacin crystallization. Pharm Res. 1999; 16: 1722-8.

77. Chokshi RJ, Shah NH, Sandhu HK, Malick AW, Zia H. Stabilization of low glass transition temperature indomethacin formulations: Impact of polymer-type and its concentration. J Pharm Sci. 2008; 97: 2286-98.

78. Flory PJ. Thermodynamics of High Polymer Solutions. J Chem Phys. 1942; 10: 51-61.

79. Huggins ML. Solutions of Long Chain Compounds. J Chem Phys. 1941; 9: 440.

80. Mather PT, Liu C, Campo CJ, inventors; University of Connecticut, Farmington, CT, USA, assignee. Blends of Amorphous and Semicrystalline Polymers Having Shape Memory Properties, 2010.

81. Trollsas MO, Gale DC, Wang Y, inventors; Abbott Cardiovascular Systems Inc. (Santa Clara, CA, US), assignee. Implantable medical devices comprising semi-crystalline poly(ester-amide), 2010.

82. Middleton JC, Tipton AJ. Synthetic biodegradable polymers as orthopedic devices. Biomaterials. 2000; 21: 2335-46.

83. Joshi HN, Tejwani RW, Davidovich M, Sahasrabudhe VP, Jemal M, Bathala MS, Varia SA, Serajuddin ATM. Bioavailability enhancement of a poorly water-soluble drug by solid dispersion in polyethylene glycol-polysorbate 80 mixture. Int J Pharm. 2004; 269: 251-8.

84. Law D, Wang W, Schmitt EA, Qiu Y, Krill SL, Fort JJ. Properties of rapidly dissolving eutectic mixtures of poly(ethylene glycol) and fenofibrate: The eutectic microstructure. J Pharm Sci. 2003; 92: 505-15.

85. Peterlin A. Transport phenomena and polymer morphology. Die Makromolekulare Chemie. 1979; 3: 215-32.

86. Michaels AS, Vieth WR, Bixler HJ. Gas permeability of highly oriented dibutyl maleate–ethylene copolymer films. J Appl Polym Sci. 1964; 8: 2735-50.

87. Harland RS, Peppas NA. Solute diffusion in swollen membranes VII. Diffusion in semicrystalline networks. Colloid Polym Sci. 1989; 267: 218-25.

88. Langer R, Peppas N. Chemical and Physical Structure of Polymers as Carriers for Controlled Release of Bioactive Agents: A Review. J Macromol Sci, Rev Macromol Chem Phys. 1983; 23: 61-126.

89. Cheng SZD, Wunderlich B. Molecular segregation and nucleation of poly(ethylene oxide) crystallized from the melt. I. Calorimetric study. J Polym Sci, Part B: Polym Phys. 1986; 24: 577-94.

90. Cheng SZD, Wunderlich B. Molecular segregation and nucleation of poly(ethylene oxide) crystallized from the melt. II. Kinetic study. J Polym Sci, Part B: Polym Phys. 1986; 24: 595-617.

91. Cheng SZD, Wu SS, Chen J, Zhuo Q, Quirk RP, von Meerwall ED, Hsiao BS, Habenschuss A, Zschack PR. Isothermal thickening and thinning processes in low-molecular-weight poly(ethylene oxide) fractions crystallized from the melt. 4. End-group dependence. Macromolecules. 1993; 26: 5105-17.

92. Cheng SZD, Chen J, Janimak JJ. Crystal growth of intermediate-molecular-mass poly(ethylene oxide) fractions from the melt. Polymer. 1990; 31: 1018-24.

93. Buckley CP, Kovacs AJ. Melting behaviour of low molecular weight poly (ethylene-oxide) fractions. Colloid Polym Sci. 1976; 254: 695-715.

94. Kuo S-W, Huang W-J, Huang C-F, Chan S-C, Chang F-C. Miscibility, Specific Interactions, and Spherulite Growth Rates of Binary Poly(acetoxystyrene)/Poly(ethylene oxide) Blends. Macromolecules. 2004; 37: 4164-73.

95. Lisowski MS, Liu Q, Cho J, Runt J, Yeh F, Hsiao BS. Crystallization Behavior of Poly(ethylene oxide) and Its Blends Using Time-Resolved Wide- and Small-Angle X-ray Scattering. Macromolecules. 2000; 33: 4842-9.

96. Mucha M. Poly(ethylene oxide) blends with crosslinking polyester resin. Colloid Polym Sci. 1994; 272: 1090-7.

97. Qiu Z, Ikehara T, Nishi T. Miscibility and crystallization of poly(ethylene oxide) and poly(ε-caprolactone) blends. Polymer. 2003; 44: 3101-6.

98. Talibuddin S, Runt J, Liu L-Z, Chu B. Microstructure Development and Crystallization of Poly(ethylene oxide) and Melt-Miscible PEO Blends. Macromolecules. 1998; 31: 1627-34.

99. Wu L, Lisowski M, Talibuddin S, Runt J. Crystallization of Poly(ethylene oxide) and Melt-Miscible PEO Blends. Macromolecules. 1999; 32: 1576-81.

100. Khan J, Harton SE, Akcora P, Benicewicz BC, Kumar SK. Polymer Crystallization in Nanocomposites: Spatial Reorganization of Nanoparticles. Macromolecules. 2009; 42: 5741-4.

101. Sun L, Ertel EA, Zhu L, Hsiao BS, Avila-Orta CA, Sics I. Reversible De-Intercalation and Intercalation Induced by Polymer Crystallization and Melting in a Poly(ethylene oxide)/Organoclay Nanocomposite. Langmuir. 2005; 21: 5672-6.

102. Sun L, Zhu L, Ge Q, Quirk RP, Xue C, Cheng SZD, Hsiao BS, Avila-Orta CA, Sics I, et al. Comparison of crystallization kinetics in various nanoconfined geometries. Polymer. 2004; 45: 2931-9.

103. AHFS Consumer Medication Information. Acetaminophen. updated March 2011; accessed November 17, 2011 Available from: http://www.ncbi.nlm.nih.gov/pubmedhealth/PMH0000521/.

104. Prescott LF. Paracetamol: Past, Present, and Future. Am J Ther. 2000; 7: 143-8.

105. Martindale: The complete drug reference. London UK: Pharmaceutical press: Greenwood Village Colorado: Thomson MICROMEDEX; 2004.

106. Haisa M, Kashino S, Kawai R, Maeda H. The Monoclinic Form of p-Hydroxyacetanilide. Acta Crystallogr, Sect B: Struct Sci. 1976; 32: 1283-5.

107. Haisa M, Kashino S, Maeda H. The orthorhombic form of p-hydroxyacetanilide. Acta Crystallogr, Sect B: Struct Sci. 1974; 30: 2510-2.

108. Sacchetti M. Thermodynamic Analysis of DSC Data for Acetaminophen Polymorphs. J Therm Anal Calorim. 2000; 63: 345-50.

109. Sohn YT. Study on the polymorphism of acetaminophen. J Korean Pharm Sci. 1990; 20: 97-104.

110. Di Martino P, Guyot-Hermann AM, Conflant P, Drache M, Guyot JC. A new pure paracetamol for direct compression: The orthorhombic form. Int J Pharm. 1996; 128: 1-8.

111. Nichols G, Frampton CS. Physicochemical characterization of the orthorhombic polymorph of paracetamol crystallized from solution. J Pharm Sci. 1998; 87: 684-93.

112. Lang M, Grzesiak AL, Matzger AJ. The Use of Polymer Heteronuclei for Crystalline Polymorph Selection. J Am Chem Soc. 2002; 124: 14834-5.

113. Granberg RA, Rasmuson AC. Solubility of paracetamol in pure solvents. J Chem Eng Data. 1999; 44: 1391-5.

114. Etman MA, Naggar VF. Thermodynamics of paracetamol solubility in sugar-water cosolvent systems. Int J Pharm. 1990; 58: 177-84.

115. Amidon GL, Lennernäs H, Shah VP, Crison JR. A Theoretical Basis for a Biopharmaceutic Drug Classification: The Correlation of in Vitro Drug Product Dissolution and in Vivo Bioavailability. Pharm Res. 1995; 12: 413-20.

116. Kalantzi L, Reppas C, Dressman JB, Amidon GL, Junginger HE, Midha KK, Shah VP, Stavchansky SA, Barends DM. Biowaiver monographs for immediate release solid oral dosage forms: Acetaminophen (paracetamol). J Pharm Sci. 2006; 95: 4-14.

117. Grattan T, Hickman R, Darby-Dowman A, Hayward M, Boyce M, Warrington S. A five way crossover human volunteer study to compare the pharmacokinetics of paracetamol following oral administration of two commercially available paracetamol tablets and three development tablets containing paracetamol in combination with sodium bicarbonate or calcium carbonate. Eur J Pharm Biopharm. 2000; 49: 225-9.

118. Strickley R. Solubilizing Excipients in Oral and Injectable Formulations. Pharm Res. 2004; 21: 201-30.

119. Wunderlich B. Macromolecular Physics. New York: Academic Press; 1980.

120. Scheirs J, Bigger SW, Delatycki O. Characterizing the solid-state thermal oxidation of poly(ethylene oxide) powder. Polymer. 1991; 32: 2014-9.

121. Duval C, Poelman MC. Scavenger effect of vitamin E and derivatives on free radicals generated by photoirradiated pheomelanin. J Pharm Sci. 1995; 84: 107-10.

122. Southern Clay Products, INC. http://www.nanoclay.com/selection_chart.asp. accessed November 17, 2011.

123. Alexandre M, Dubois P. Polymer-layered silicate nanocomposites: preparation, properties and uses of a new class of materials. Mater Sci Eng, R. 2000; 28: 1-63.

124. Camargo PHC, Satyanarayana KG, Wypych F. Nanocomposites: synthesis, structure, properties and new application opportunities. Mater Res. 2009; 12: 1-39.

125. Homminga D, Goderis B, Dolbnya I, Reynaers H, Groeninckx G. Crystallization behavior of polymer/montmorillonite nanocomposites. Part I. Intercalated poly(ethylene oxide)/montmorillonite nanocomposites. Polymer. 2005; 46: 11359-65.

126. Homminga D, Goderis B, Dolbnya I, Groeninckx G. Crystallization behavior of polymer/montmorillonite nanocomposites. Part II. Intercalated poly(ε-caprolactone)/montmorillonite nanocomposites. Polymer. 2006; 47: 1620-9.

127. Loyens W, Jannasch P, Maurer FHJ. Effect of clay modifier and matrix molar mass on the structure and properties of poly(ethylene oxide)/Cloisite nanocomposites via melt-compounding. Polymer. 2005; 46: 903-14.

128. Park JK, Choy YB, Oh J-M, Kim JY, Hwang S-J, Choy J-H. Controlled release of donepezil intercalated in smectite clays. Int J Pharm. 2008; 359: 198-204.

129. AR 2000, Rheometrics Series Operator's Manual TA Instruments, 2006.

130. Meyers MA, Chawla KK. Mechanical behavior of materials. Prentice Hall; 1999.

131. Zhang X, Burgar I, Do MD, Lourbakos E. Intermolecular interactions and phase structures of plasticized wheat proteins materials. Biomacromolecules. 2005; 6: 1661-71.

132. Hodge RM, Bastow TJ, Edward GH, Simon GP, Hill AJ. Free volume and the mechanism of plasticization in water-swollen poly(vinyl alcohol). Macromolecules. 1996; 29: 8137-43.

133. Heijboer J. Secondary loss peaks in glassy amorphous polymers. In: Meier DJ, editor. Molecular basis of transitions and relaxations. New York: Gordon and Breach; 1978. 75-102.

134. Einstein A. A new determination of molecular dimensions. Annals of Physics. 1909; 19: 289-306.

135. Kaully T, Siegmann A, Shacham D. Rheology of highly filled natural $CaCO_3$ composites: IV. Effect of surface treatment. Polym Adv Technol. 2007; 18: 696-704.

136. Inn YW, Wang SQ. Molecular interfacial slip between solid and liquid in polymer suspensions of hard spheres. Langmuir. 1995; 11: 1589-94.

137. Kitano T, Kataoka T, Shirota T. An empirical equation of the relative viscosity of polymer melts filled with various inorganic fillers. Rheol Acta. 1981; 20: 207-9.

138. Guth E. Theory of filler reinforcement. J Appl Phys. 1945; 16: 20-5.

139. Mutel AT, Kamal MR. The effect of glass fibers on the rheological behavior of polypropylene melts between rotating parallel plates. Polym Compos. 1984; 5: 29-35.

140. Rasiah IJ, Ho PS, Manoharan M, Ng CL, Chau M, editors. Rheological analysis of an underfill material. Electronics Packaging Technology Conference, 1998 Proceedings of 2nd; 1998 8-10 Dec 1998.

141. Kairn T, Daivis PJ, Ivanov I, Bhattacharya SN. Molecular-dynamics simulation of model polymer nanocomposite rheology and comparison with experiment. J Chem Phys. 2005; 123: 194905.

142. Fox TG. Influence of diluent and of copolymer composition on the glass transition temperature of a polymer system. Bull Am Phys Soc. 1956; 1: 123.

143. Gordon M, Taylor JS. Ideal copolymers and the second-order transitions of synthetic rubbers. I. Non-crystalline copolymers. J Appl Chem. 1952; 2: 493-500.

144. Tang M, Dong Y, Stevens MM, Williams CK. Tailoring Polylactide Degradation: Copolymerization of a Carbohydrate Lactone and S,S-Lactide. Macromolecules. 2010; 43: 7556-64.

145. Liu F, Urban MW. New thermal transitions in stimuli-responsive copolymer films. Macromolecules. 2009; 42: 2161-7.

146. Wei Z, Liu L, Qu C, Qi M. Microstructure analysis and thermal properties of L-lactide/ε-caprolactone copolymers obtained with magnesium octoate. Polymer. 2009; 50: 1423-9.

147. Gutierrez-Villarreal MH, Rodríguez-Velazquez J. The effect of citrate esters as plasticizers on the thermal and mechanical properties of poly(methyl methacrylate). J Appl Polym Sci. 2007; 105: 2370-5.

148. Blasi P, Schoubben A, Giovagnoli S, Perioli L, Ricci M, Rossi C. Ketoprofen poly(lactide-co-glycolide) physical interaction. AAPS PharmSciTech. 2007; 8: E10-E8.

149. Pillin I, Montrelay N, Grohens Y. Thermo-mechanical characterization of plasticized PLA: Is the miscibility the only significant factor? Polymer. 2006; 47: 4676-82.

150. Qian F, Huang J, Hussain MA. Drug-polymer solubility and miscibility: Stability consideration and practical challenges in amorphous solid dispersion development. J Pharm Sci. 2010; 99: 2941-7.

151. Haddadin R, Qian F, Desikan S, Hussain M, Smith RL. Estimation of drug solubility in polymers via differential scanning calorimetry and utilization of the Fox equation. Pharm Dev Technol. 2009; 14: 19-27.

152. Tong P, Zografi G. A study of amorphous molecular dispersions of indomethacin and its sodium salt. J Pharm Sci. 2001; 90: 1991-2004.

153. Chokshi RJ, Sandhu HK, Iyer RM, Shah NH, Malick AW, Zia H. Characterization of physico-mechanical properties of indomethacin and polymers to assess their suitability for hot-melt extrusion processs as a means to manufacture solid dispersion/solution. J Pharm Sci. 2005; 94: 2463-74.

154. Schneider HA. Glass transition behaviour of compatible polymer blends. Polymer. 1989; 30: 771-9.

155. Shekunov BY, Chattopadhyay P, Tong HHY, Chow AHL, Grossmann JG. Structure and drug release in a crosslinked poly(ethylene oxide) hydrogel. J Pharm Sci. 2007; 96: 1320-30.

156. Shekunov BY, Taylor P, Grossmann JG. Structural phenomena in hydrogel-drug systems. J Cryst Growth. 1999; 198-199: 1335-9.

157. Wen H, Morris K, Park K. Synergic effects of polymeric additives on dissolution and crystallization of acetaminophen. Pharm Res. 2008; 25: 349-58.

158. Wen H, Morris KR, Park K. Hydrogen bonding interactions between adsorbed polymer molecules and crystal surface of acetaminophen. J Colloid Interface Sci. 2005; 290: 325-35.

159. Cheremisinoff NP. Polymer characterization: laboratory techniques and analysis. Westwood, NJ: William Andrew Publishing; 1996.

160. Wei H, Thompson RB, Park CB, Chen P. Surface tension of high density polyethylene (HDPE) in supercritical nitrogen: Effect of polymer crystallization. Colloids Surf, A. 2010; 354: 347-52.

161. Zhu L, Jona J, Nagapudi K, Wu T. Fast Surface Crystallization of Amorphous Griseofulvin Below T_g. Pharm Res. 2010; 27: 1558-67.

162. Thompson RB, Park CB, Chen P. Reduction of polymer surface tension by crystallized polymer nanoparticles. J Chem Phys. 2010; 133: 144913.

163. De Wet FN, Gerber JJ, Lotter AP, Van Der Watt JG, Dekker TG. A Study of the Changes During Heating of Paracetamol. Drug Dev Ind Pharm. 1998; 24: 447-53.

164. Liu X, Wu Q. Non-isothermal crystallization behaviors of polyamide 6/clay nanocomposites. Eur Polym J. 2002; 38: 1383-9.

165. Fornes TD, Paul DR. Crystallization behavior of nylon 6 nanocomposites. Polymer. 2003; 44: 3945-61.

166. Maiti P, Nam PH, Okamoto M, Hasegawa N, Usuki A. Influence of crystallization on intercalation, morphology, and mechanical properties of polypropylene/clay nanocomposites. Macromolecules. 2002; 35: 2042-9.

167. Sandler SI. Chemical, Biochemical, and Engineering Thermodynamics. Hoboken, New Jersey: Wiley; 2006.

168. Scott RL. The Thermodynamics of High Polymer Solutions. V. Phase Equilibria in the Ternary System: Polymer 1---Polymer 2---Solvent. J Chem Phys. 1949; 17: 279-84.

169. Flory PJ. Principles of Polymer Chemistry. Ithaca, NY: Cornell University Press; 1953.

170. Nishi T, Wang TT. Melting Point Depression and Kinetic Effects of Cooling on Crystallization in Poly(vinylidene fluoride)-Poly(methyl methacrylate) Mixtures. Macromolecules. 1975; 8: 909-15.

171. Goodship V, Ogur E. Polymer Processing with Supercritical Fluids. Shawbury, UK: Smithers Rapra Press; 2005.

172. Lin H, Freeman BD. Gas solubility, diffusivity and permeability in poly(ethylene oxide). J Membr Sci. 2004; 239: 105-17.

173. Langer R, Peppas NA. Chemical and physical structure of polymers as carriers for controlled release of bioactive agents: a review. Rev Macromol Chem Phys. 1983; 23: 61-126.

174. Siepmann J, Peppas NA. Modeling of drug release from delivery systems based on hydroxypropyl methylcellulose (HPMC). Adv Drug Delivery Rev. 2001; 48: 139-57.

175. Peppas NA, Korsmeyer RW. Hydrogels Med. Pharm. In: Peppas NA, editor. Dynamically swelling hydrogels in controlled release applications. Boca Raton: CRC Press; 1986.

176. Ritger P, Peppas N. A simple equation for description of solute release II. Fickian and anomalous release from swellable devices. J Controlled Release. 1987; 5: 37-42.

177. Crank J. The mathematics of diffusion, 2nd ed. Clarendon Press, Oxford; 1975.

178. Peppas NA. Analysis of Fickian and non-Fickian drug release from polymers. Pharm Acta Helv. 1985; 60: 110-1.

179. Peppas NA, Sahlin JJ. A simple equation for the description of solute release. III. Coupling of diffusion and relaxation. Int J Pharm. 1989; 57: 169-72.

180. Hopfenberg HB, Hsu KC. Swelling-controlled, constant rate delivery systems. Polym Eng Sci. 1978; 18: 1186-91.

181. Hoffman JD, Davis GT, Lauritzen JI. The rate of crystallization of linear polymers with chain folding. In: Hannay NB, editor. Treatise on solid state chemistry. New York: Plenum Press; 1976. 497-614.

182. Point JJ, Rault J, Hoffman JD, Kovacs AJ, Mandelkern L, Wunderlich B, DiMarzio EA, de Gennes PG, Klein J, et al. Faraday Discuss Chem Soc: The Royal Society of Chemistry; 1979.

183. Hoffman JD. Role of reptation in the rate of crystallization of polyethylene fractions from the melt. Polymer. 1982; 23: 656-70.

184. Hoffman JD. Regime III crystallization in melt-crystallized polymers: The variable cluster model of chain folding. Polymer. 1983; 24: 3-26.

185. Hoffman JD, Miller RL. Test of the reptation concept: crystal growth rate as a function of molecular weight in polyethylene crystallized from the melt. Macromolecules. 1988; 21: 3038-51.

186. Armistead JP, Hoffman JD. Direct Evidence of Regimes I, II, and III in Linear Polyethylene Fractions As Revealed by Spherulite Growth Rates. Macromolecules. 2002; 35: 3895-913.

187. deGennes PG. Reptation of a Polymer Chain in the Presence of Fixed Obstacles. J Chem Phys. 1971; 55: 572.

188. Kovacs AJ, Gonthier A. Crystallization and fusion of self-seeded polymers. Colloid Polym Sci. 1972; 250: 530-52.

189. Kovacs AJ, Gonthier A, Straupe C. Isothermal growth, thickening, and melting of poly(ethylene oxide) single crystals in the bulk. J Polym Sci Polym Symp. 1975; 50: 283-325.

190. Kovacs AJ, Straupe C, Gonthier A. Isothermal growth, thickening, and melting of polyethylene oxide) single crystals in the bulk. II. J Polym Sci Polym Symp. 1977; 59: 31-54.

191. Kovacs AJ, Straupe C. Isothermal growth, thickening and melting of poly(ethylene oxide) single crystals in the bulk. Part 4. - Dependence of pathological crystal habits on temperature and thermal history. Faraday Discuss Chem Soc. 1979; 68: 225-38.

192. Kovacs AJ, Straupe C. Isothermal growth, thickening and melting of poly(ethylene-oxide) single crystals in the bulk : III. Bilayer crystals and the effect of chain ends. J Cryst Growth. 1980; 48: 210-26.

193. Marand H, Xu J, Srinivas S. Determination of the Equilibrium Melting Temperature of Polymer Crystals: Linear and Nonlinear Hoffman–Weeks Extrapolations. Macromolecules. 1998; 31: 8219-29.

194. Hoffman JD, Weeks JJ. Melting process and equilibrium melting temperature of poly(chlorotrifluoroethylene). J Res Natl Bur Stand, Sect A. 1962; 66A: 13-28.

195. Organ SJ, Barham PJ. On the equilibrium melting temperature of polyhydroxybutyrate. Polymer. 1993; 34: 2169-74.

196. Mezghani K, Anderson Campbell R, Phillips PJ. Lamellar Thickening and the Equilibrium Melting Point of Polypropylene. Macromolecules. 1994; 27: 997-1002.

197. Huang XD, Goh SH. Crystallization of C_{60}-End-Capped Poly(ethylene oxide)s. Macromolecules. 2001; 34: 3302-7.

198. Johnson WA, Mehl RF. Reaction kinetics in processes of nucleation and growth. Trans Am Inst Min, Metall Pet Eng. 1939; 135: 416-58.

199. Avrami M. Kinetics of Phase Change. I General Theory. J Chem Phys. 1939; 7: 1103-12.

200. Avrami M. Kinetics of Phase Change. II Transformation-Time Relations for Random Distribution of Nuclei. J Chem Phys. 1940; 8: 212-24.

201. Avrami M. Granulation, Phase Change, and Microstructure Kinetics of Phase Change. III. J Chem Phys. 1941; 9: 177-84.

202. Evans UR. The laws of expanding circles and spheres in relation to the lateral growth of surface films and the grain-size of metals. Trans Faraday Soc. 1945; 41: 365-74.

203. Shultz JM. Polymer Materials Science. Englewood Cliffs, NJ: Prentice Hall; 1974.

204. Schultz JM. Polymer Crystallization: The Development of Crystalline Order in Thermoplastic Polymers 1st ed. New York: An American Chemical Society Publication; 2001.

205. Richardson PH, Richards RW, Blundell DJ, MacDonald WA, Mills P. Differential scanning calorimetry and optical microscopy investigations of the isothermal crystallization of a poly(ethylene oxide)-poly(methyl methacrylate) block copolymer. Polymer. 1995; 36: 3059-69.

206. Huang J, Marand H. Kinetics of Spherulitic Growth of Poly(pivalolactone) in Blends with Poly(vinylidene fluoride-co-tetrafluoroethylene): Effect of Specific Interactions on the Thermodynamic and Kinetic Secondary Nucleation Parameters. Macromolecules. 1997; 30: 1069-73.

207. Machado JC, Silva GG, Oliveira FCd, Lavall RL, Rieumont J, Licinio P, Windmöller D. Free-volume and crystallinity in low molecular weight poly(ethylene oxide). J Polym Sci, Part B: Polym Phys. 2007; 45: 2400-9.

208. Cheng SZD, Lotz B. Enthalpic and entropic origins of nucleation barriers during polymer crystallization: the Hoffman-Lauritzen theory and beyond. Polymer. 2005; 46: 8662-81.

209. Flory PJ. Theory of crystallization in copolymers. Trans Faraday Soc. 1955; 51: 848-57.

210. Helfand E, Lauritzen JI. Theory of Copolymer Crystallization. Macromolecules. 1973; 6: 631-8.

211. Alamo RG, Blanco JA, Agarwal PK, Randall JC. Crystallization Rates of Matched Fractions of MgCl2-Supported Ziegler Natta and Metallocene Isotactic Poly(Propylene)s. 1. The Role of Chain Microstructure. Macromolecules. 2003; 36: 1559-71.

212. Hosier IL, Alamo RG, Esteso P, Isasi JR, Mandelkern L. Formation of the α and γ Polymorphs in Random Metallocene–Propylene Copolymers. Effect of Concentration and Type of Comonomer. Macromolecules. 2003; 36: 5623-36.

213. Dai PS, Cebe P, Capel M, Alamo RG, Mandelkern L. In Situ Wide- and Small-Angle X-ray Scattering Study of Melting Kinetics of Isotactic Poly(propylene). Macromolecules. 2003; 36: 4042-50.

214. Hosier IL, Alamo RG, Lin JS. Lamellar morphology of random metallocene propylene copolymers studied by atomic force microscopy. Polymer. 2004; 45: 3441-55.

215. Cheng SZD, Janimak JJ, Zhang A, Hsieh ET. Isotacticity effect on crystallization and melting in polypropylene fractions: 1. Crystalline structures and thermodynamic property changes. Polymer. 1991; 32: 648-55.

216. Janimak JJ, Cheng SZD, Giusti PA, Hsieh ET. Isotacticity effect on crystallization and melting in polypropylene fractions. II. Linear crystal growth rate and morphology study. Macromolecules. 1991; 24: 2253-60.

217. Janimak JJ, Cheng SZD, Zhang A, Hsieh ET. Isotacticity effect on crystallization and melting in polypropylene fractions: 3. Overall crystallization and melting behaviour. Polymer. 1992; 33: 728-35.

218. Keith HD, Padden FJ. A Phenomenological Theory of Spherulitic Crystallization. J Appl Phys. 1963; 34: 2409-21.

219. Crevecoeur G, Groeninckx G. Binary blends of poly(ether ether ketone) and poly(ether imide): miscibility, crystallization behavior and semicrystalline morphology. Macromolecules. 1991; 24: 1190-5.

220. Hudson SD, Davis DD, Lovinger AJ. Semicrystalline morphology of poly(aryl ether ether ketone)/poly(ether imide) blends. Macromolecules. 1992; 25: 1759-65.

221. Talibuddin S, Wu L, Runt J, Lin JS. Microstructure of Melt-Miscible, Semicrystalline Polymer Blends. Macromolecules. 1996; 29: 7527-35.

222. Zhu Q, Taylor LS, Harris MT. Evaluation of the Microstructure of Semicrystalline Solid Dispersions. Mol Pharmaceutics. 2010; 7: 1291-300.

223. Schachter DM, Xiong J, Tirol GC. Solid state NMR perspective of drug-polymer solid solutions: a model system based on poly(ethylene oxide). Int J Pharm. 2004; 281: 89-101.

224. Godovsky YK, Slonimsky GL, Garbar NM. Effect of molecular weight on the crystallization and morphology of poly (ethylene oxide) fractions. J Polym Sci, Part C: Polym Symp. 1972; 38: 1-21.

225. Thomas DG, Staveley LAK. A study of the supercooling of drops of some molecular liquids. J Chem Soc. 1952; 4569-77.

226. Mandelkern L. Crystallization in Polymers. New York: McGraw-Hill; 1964.

227. Menyhárd A, Gahleitner M, Varga J, Bernreitner K, Jääskeläinen P, Øysæd H, Pukánszky B. The influence of nucleus density on optical properties in nucleated isotactic polypropylene. Eur Polym J. 2009; 45: 3138-48.

228. Anderson KS, Hillmyer MA. Melt preparation and nucleation efficiency of polylactide stereocomplex crystallites. Polymer. 2006; 47: 2030-5.

229. Schmidt SC, Hillmyer MA. Polylactide stereocomplex crystallites as nucleating agents for isotactic polylactide. J Polym Sci, Part B: Polym Phys. 2001; 39: 300-13.

230. Fillon B, Thierry A, Lotz B, Wittmann J. Efficiency scale for polymer nucleating agents. J Therm Anal Calorim. 1994; 42: 721-31.